LARGE-SCALE BIOLOGY ARTICLE

The transcriptional landscape of plant infection by the rice blast fungus *Magnaporthe oryzae* reveals distinct families of temporally co-regulated and structurally conserved effectors

Xia Yan, Bozeng Tang, Lauren S. Ryder, Dan MacLean, Vincent M. Were, Alice Bisola Eseola, Neftaly Cruz-Mireles, Andrew J. Foster, Miriam Osés-Ruiz[1] and Nicholas J. Talbot[2]

The Sainsbury Laboratory, University of East Anglia, Norwich Research Park, NR4 7UH, United Kingdom

[1]Present address: Universidad Pública de Navarra, Pamplona, Navarra, Spain.

[2]To whom correspondence should be addressed (Nick.Talbot@tsl.ac.uk)

ORCID IDs:

Xia Yan, https://orcid.org/0000-0003-4509-0137

Bozeng Tang , https://orcid.org/0000-0002-3986-9622

Lauren S. Ryder, https://orcid.org/0000-0003-0370-5746

Dan MacLean, https://orcid.org/0000-0003-1032-0887

Vincent M. Were, https://orcid.org/0000-0002-9885-4877

Alice Bisola Eseola, https://orcid.org/0000-0001-5698-8204

Neftaly Cruz-Mireles, https://orcid.org/0000-0003-1031-1470

Andrew J. Foster, https://orcid.org/0000-0002-8459-7590

Miriam Osés-Ruiz, https://orcid.org/0000-0002-3989-9071

Nicholas J. Talbot, https://orcid.org/0000-0001-6434-7757

The rice blast fungus *Magnaporthe oryzae* causes a devastating disease which threatens global rice production. In spite of intense study, the biology of plant tissue invasion during blast disease remains poorly understood. Here we report a high resolution, transcriptional profiling study of the entire plant-associated development of the blast fungus. Our analysis revealed major temporal changes in fungal gene expression during plant infection. Pathogen gene expression could be classified into 10 modules of temporally co-expressed genes, providing evidence of induction of pronounced shifts in primary and secondary metabolism, cell signalling and transcriptional regulation. A set of 863 genes encoding secreted proteins are differentially expressed at specific stages of infection, and 546 were predicted to be effectors and named *MEP* (*Magnaporthe* effector protein) genes. Computational prediction of structurally-related *MEPs*, including the MAX effector family, revealed their temporal co-regulation in the same co-expression modules. We functionally characterised 32 *MEP* genes and demonstrate that Mep effectors are predominantly targeted to the cytoplasm of rice cells via the biotrophic interfacial complex (BIC), and use a common unconventional secretory pathway. Taken together, our study reveals major changes in gene expression associated with blast disease and identifies a diverse repertoire of effectors critical to successful infection.

INTRODUCTION

Rice blast disease is one of the most significant constraints on rice production worldwide. Each year, despite deployment of rice varieties carrying numerous resistance genes and the extensive use of fungicides, between 10 and 30% of the rice harvest is lost to rice blast disease (Yamaguchi, 2004; Wang and Valent, 2017; Stam and McDonald, 2018; Poloni et al., 2020). Given that rice provides 23% of the calories to humankind and is a staple food for half of the world's population, controlling rice blast in a sustainable way, would constitute a major contribution to global food security. Rice blast is caused by the filamentous fungus *Magnaporthe oryzae* (synonym of *Pyricularia oryzae*) (Zhang et al., 2016) which has evolved the ability to breach the tough outer cuticle of rice leaves and invade living plant tissue. *M. oryzae* can also infect a wide range of grass hosts causing diseases such as wheat blast, for instance, an emerging threat to wheat production (Urashima. et al., 1993; Islam et al., 2016; Inoue et al., 2017; Latorre et al., 2022).

The blast fungus undergoes a series of morphogenetic transitions during plant infection, involving cellular differentiation to develop infection cells called appressoria on the leaf surface, followed by penetration and rapid proliferation of invasive hyphae within rice cells, facilitated by active suppression of plant immunity. Like many of the most important crop pathogens, rice blast fungus is a hemibiotroph, which means that it actively grows in living plant tissue during its initial biotrophic phase of development, but later causes plant cell death when it develops necrotrophically, utilising nutrients released from dead plant cells to enable the fungus to sporulate from necrotic disease lesions.

So far, more than 1600 *M. oryzae* genes have been functionally characterised by targeted gene deletion or mutagenesis– greater than 10% of the rice blast genome (Foster et al., 2021). These studies have provided insight into the biology of blast disease, especially the ability of the fungus to form appressoria on the leaf surface, but there are many aspects of the biology of blast disease that are not well understood, even after such intense study. We do not know, for example, how the blast fungus is able to invade living plant tissue so rapidly, overcoming host defences, colonising new plant cells, and spreading long distances throughout rice leaves. To be such an efficient invader of plant cells, *M. oryzae* must be able to adapt successfully to the host environment– sequestering carbon and nitrogen sources to fuel its growth –while evading recognition by the host, but how this is achieved is not clear. The blast fungus also induces profound changes in the organisation of plant cells, including extensive membrane biogenesis, changes in cytoskeletal configuration and perturbation of cell-to-cell communication. How these processes are orchestrated and regulated by the invading fungus also remains largely unknown. One of the principal reasons for our current lack of understanding is that there have been very few investigations which have taken a holistic view of plant infection– in contrast to gene functional studies –attempting to understand the progression of blast disease and the major temporal changes in pathogen physiology.

84 In this study, we set out to define the transcriptional landscape of rice blast infection. Our aim was to
85 identify major changes in pathogen gene expression from the moment of initial inoculation of plants
86 until development of disease symptoms and, in particular, to use this information to identify the full
87 repertoire of fungal effector proteins deployed by the fungus.

88 Effectors are secreted proteins that target components of the plant immune system to suppress
89 host defense and enable proliferation of the pathogen (Jones and Dangl, 2006; Kamoun, 2006; Lo Presti
90 et al., 2015). In addition to suppression of plant immunity, effectors may target cell signalling and
91 metabolic processes to help facilitate fungal invasive growth (Zhai et al., 2022). In *M. oryzae,* effectors
92 target extracellular processes such as chitin-triggered immunity that operate in the apoplast (Mentlak et
93 al., 2012), or intracellular processes such as perturbation of reactive oxygen species generation (Liu and
94 Zhang, 2021), targeted protein degradation (Park et al., 2012) or re-programming host transcription
95 (Kim et al., 2020). Intracellular effectors accumulate in a membrane-rich plant structure called the
96 biotrophic interfacial complex (BIC), which appears necessary for their delivery into plant cells
97 (Kankanala et al., 2007), and four cytoplasmic effectors have been shown to be secreted by an unusual
98 Golgi-independent mechanism (Giraldo et al., 2013). A sub-set of *M. oryzae* effectors are recognised
99 by rice immune receptors leading to disease resistance. The interaction of such avirulence effectors
100 (Avrs) with cognate NLR receptors has also helped reveal their likely intracellular targets, especially in
101 cases where specific effector-binding domains have become integrated into NLRs (Cesari et al., 2013;
102 Maqbool et al., 2015; De la Concepcion et al., 2018). Several sequence-un-related Avr effectors possess
103 a conserved protein fold and are termed MAX effectors (de Guillen et al., 2015). Structural modelling
104 of the predicted secreted proteome of *M. oryzae* has recently identified large sets of structurally-related
105 proteins (Seong and Krasileva, 2021a), although their role in blast disease is not yet known.

106 We reasoned that comprehensive transcriptional profiling would provide a means by which the
107 landscape of blast disease could be systematically analysed at a holistic level and the true effector
108 repertoire of *M. oryzae* revealed. Transcriptomic studies have, for instance, provided key insights into
109 physiologically complex states, such as tumorigenesis (Wingrove et al., 2019), embryonic development
110 (He et al., 2020) and host immunity (Bjornson et al., 2021), as well as fungal-plant interactions (Copley
111 et al., 2017; Zeng et al., 2017; Lanver et al., 2018). We recognised that in the *M. oryzae*-rice interaction
112 there have been previous attempts to define global patterns of gene expression, using methods such as
113 microarrays and super-SAGE analysis or, more recently, by RNA-seq (Mosquera et al., 2009; Chen et
114 al., 2012; Kawahara et al., 2012; Soanes et al., 2012; Dong et al., 2015; Sharpee et al., 2017; Shimizu
115 et al., 2019). These studies have, however, suffered from the lower resolution of previous
116 methodologies, failing to detect gene expression from the low fungal biomass during early stages of
117 plant infection. Relatively poor coverage of fungal gene expression changes have therefore been
118 reported, with only the most abundantly expressed fungal genes identified. More recent studies using
119 RNA-seq analysis have benefited from the dynamic range and resolution of deep sequencing, but these
120 investigations have focused, almost exclusively, on a single time point during infection, leading to

121 assumptions regarding the progress of disease that have severe limitations. Moreover, most
122 transcriptomic studies of *M. oryzae* have generated only superficial coverage of fungal gene expression
123 changes, because of the type of inoculation methods carried out and the relatively poor rates of blast
124 infection observed.

125 In this project, we set out to overcome the major limitations of previous studies by carrying out
126 a comprehensive time-course of rice blast disease using different infection protocols and rice hosts to
127 enhance the efficiency of blast infection. We reasoned that by infecting rice cultivars of varying blast
128 susceptibility, coupled with using different inoculation methods, we could optimise the number of
129 fungal genes analysed and thereby generate deeper insights into the transcriptional landscape of plant
130 infection. We performed RNA-seq analysis of *M. oryzae* strain Guy11 infecting two rice cultivars of
131 different susceptibility, either in spray infections or using leaf drop inoculation of attached rice leaves.
132 We report the global pattern of fungal gene expression at 8 time-points from 0h (the time of spore
133 inoculation) until full blast symptom expression at 144h. In this way we were able to define 10 modules
134 of temporally co-expressed fungal genes and define physiological, metabolic, and gene regulatory
135 networks represented by each module. We identified 863 secreted protein-encoding genes that are
136 differentially-regulated during plant infection, many of which are predicted to encode effectors. The
137 effector repertoire of *M. oryzae* and its temporal expression dynamics are therefore much greater in
138 complexity than previously recognised. Strikingly, we also found that effector candidates predicted to
139 be structurally conserved (Seong and Krasileva, 2021) are temporally co-expressed during the
140 biotrophic growth. Using live cell imaging and gene functional analysis, we report the cell biological
141 features of these effectors and their specific positioning during infection. When considered together,
142 our findings provide new insight into the biology of blast disease and the complexity of the deployed
143 effector repertoire.
144

145 **RESULTS**

146 To determine the transcriptional landscape of rice blast disease, we first selected two rice cultivars
147 differing in their susceptibility to blast. CO39 is a dwarf *indica* variety of rice, moderately susceptible
148 to blast, that has been used as a host in many gene functional studies of *M. oryzae* (Talbot et al., 1993a;
149 Chauhan et al., 2002; Zhu et al., 2004). Moukoto, meanwhile, is a *japonica* rice variety, highly
150 susceptible to blast disease and resulting in large, coalescing disease lesions (Yoshida et al., 2009). We
151 inoculated 21-day-old rice seedlings by spray infection with 1 x 10^5 conidia mL^{-1}, as well as carrying
152 out leaf drop infections in which a 20 µl drop of a suspension of 1 x 10^6 conidia mL^{-1} was placed on the
153 surface of a rice leaf which remained attached to a 21-day-old rice seedling. The compatible
154 *Magnaporthe oryzae* strain Guy11 was used for all infections and rapid invasion of new rice cells could
155 be observed in using live cell imaging of a GFP-expressing strain of Guy11, between 40-48h after
156 inoculation, as shown in Figure 1A and Supplemental Movie 1. All infection experiments were repeated
157 three times with *M. oryzae* cultures and rice seedlings of the same age and always inoculated at the

158 same time of day to control for circadian effects (Figure 1B). The inoculated leaf area was collected for
159 sample extraction at 8 different times which are key stages for disease development; 0h (uninfected),
160 8h, 16h, 24h, 48h, 72h, 96h and 144h post-infection as depicted in Figure 2. These time points cover
161 all morphogenetic transitions associated with appressorium development, appressorium-mediated
162 penetration, biotrophic growth, transpressorium-dependent cell-to-cell movement, fungal proliferation
163 in rice tissue, the switch to necrotrophic growth and fungal sporulation (Cruz-Mireles et al., 2021).
164 Using Illumina sequencing of mRNA libraries extracted from rice tissue, we generated 4.37 billion
165 reads from all samples (Supplemental Dataset 1). All data is freely accessible through ENA Accession
166 Number PRJEB45007. Kraken 2 was used to identify *M. oryzae* and rice reads from the mixed
167 transcriptome (Wood et al., 2019). We classified reads either as rice or the rice blast fungus and focus
168 here on reads mapping to the annotated *M. oryzae* reference genome (Dean et al., 2005). By utilizing
169 the highly susceptible Moukoto, we were able to show a greater number of *M. oryzae* sequence reads
170 at earlier stage of infection and throughout disease progression compared with CO39 infections, as
171 shown in Figure 1C. We observed, however, that leaf drop infections were significantly enriched in
172 fungal reads in the mixed transcriptome analysis. The greater number of fungal reads probably reflects
173 a higher proportion of rice cells infected by the fungus in leaf drop samples compared to spray
174 inoculations, so the transcriptome data are likely to be more representative of the infected state. By
175 contrast, in spray inoculations many rice cells remain uninfected throughout and will only respond at a
176 distance from the site of infection (Figure 1C and Supplemental Figure 1A). During infection, we
177 observed a 3-fold increase in the proportion of *M. oryzae* reads between 24 hpi and 48 hpi in leaf drop
178 infections (Supplemental Dataset 1), consistent with the steep increase in fungal biomass that
179 accompanies invasion of neighbouring cells during this 24h period (Figure 1C and Figure 2B). Principal
180 Component Analysis (PCA) using Transcripts Per Kilobase Million (TPM) highlighted the
181 reproducibility between biological replicates of each sample (Supplemental Figure 1B) and also
182 provided evidence of a significant change in gene expression between early stages (8 hpi-24 hpi) of
183 infection and later stages (48 hpi-144 hpi), which occurs irrespective of inoculation method
184 (Supplemental Figure 2A).
185
186 **Temporal dynamics of gene expression during rice blast disease**
187 To define the temporal sequence of fungal gene expression changes during rice infection, we analysed
188 gene expression across the time course using weighted gene co-expression network analysis (WGCNA)
189 (Zhang and Horvath, 2005; Langfelder and Horvath, 2008). This analysis identified 10 modules of co-
190 expressed genes, for which the expression pattern of a representative eigengene is shown in Figure 2.
191 Modules ranged in size from 216 to 3792 temporally co-expressed genes (Figure 2A and Supplemental
192 Dataset 2). Genes in color-coded modules are highly expressed at the developmental stages shown in
193 Figure 2B. Module (M) 1, for example, represents 3792 genes that show peak expression in conidia and
194 are then down-regulated following appressorium-mediated penetration. These include genes involved

195 in fungal growth, conidiation and spore germination, such as *LEU1* (Tang et al., 2019; Que et al., 2020),
196 *SOM1*(Yan et al., 2011) and *YPT7* (Liu et al., 2015), all previously reported to be necessary for
197 sporulation, as well as genes implicated in appressorium morphogenesis, such as the osmosensor-
198 encoding gene *SHO1* (Liu et al., 2011), the appressorium turgor sensor kinase gene *SLN1* (Zhang et al.,
199 2010; Ryder et al., 2019), and the *RGS* family of genes that regulate G-protein signalling (Zhang et al.,
200 2011). The septins are also predominantly classified in M1 (*SEP3*, *SEP4* and *SEP6*) and M2 (*SEP5*)
201 consistent with their vital role in appressorium re-polarisation (Dagdas et al., 2012).
202 Genes associated with appressorium-mediated infection were predominantly represented by
203 M2, which shows peak expression at 8hpi (Figure 2B), and contains 1039 genes highly expressed during
204 the pre-penetration phase of fungal growth. These include *PTH11* (Sweigard et al., 1998), *BUF1*
205 (Valent et al., 1991), *MAGB* (Liu and Dean, 1997) and *ZNF1* (Cao et al., 2016; Yue et al., 2016), all
206 necessary for appressorium development and function. Initial biotrophic colonisation of rice tissue is
207 represented by genes in M3, M4 and M5, which show peaks of gene expression at 16hpi, 24hpi and
208 48hpi, respectively. M3 contains *MSB2* (Liu et al., 2011), *HOX7* (Kim et al., 2009; Oses-Ruiz et al.,
209 2021) and *MET13* (Yan et al., 2013) implicated in appressorium function, and *SEC6,* which encodes a
210 component of the octameric exocyst complex, that assembles in a septin-dependent manner during plant
211 infection (Gupta et al., 2015). M4 consists of 634 genes including gene functions expected during early
212 biotrophic growth, such as *RBF1* which encodes a protein required for BIC formation (Nishimura et al.,
213 2016), as well as many effectors (see below). M5 contains 835 genes associated with invasive growth,
214 such as *NOXD*, the NADPH oxidase sub-unit-encoding gene (Galhano et al., 2017) as well as the *MPS1*
215 MAPK (Xu et al., 1998), *SSB1*, *SSZ1* and *ZUO1* which are all involved in the cell wall integrity pathway
216 (Yang et al., 2018). This is consistent with a substantial change in cell wall organisation occurring
217 during invasive growth. M6 contains genes up-regulated in association with the increase in fungal
218 biomass that occurs during invasive growth. The module is also enriched in genes encoding
219 transcription factors and signalling proteins (Supplemental Data Set 2), which are predominantly
220 uncharacterised, and may reflect the dramatic reprogramming in fungal physiology that occurs at the
221 switch from biotrophic growth to necrotrophic growth. M7 shows genes which peak in expression
222 during appressorium development at 8 h and then again during transpressorium development at 48h.
223 This observation is consistent with the developmental conservation of these two infection structures, as
224 recently highlighted (Cruz-Mireles et al., 2021). M7 contains *MST12*, for example, which encodes a
225 transcription factor required for appressorium-mediated penetration (Park et al., 2002), *CPKA* encoding
226 the catalytic sub-unit of cAMP-dependent protein kinase A, another key regulator of appressorium
227 development (Mitchell and Dean, 1995), as well as the cell cycle regulator *NIM1* (Saunders et al., 2010)
228 and peroxin-encoding gene *PEX1* (Deng et al., 2016). Their bi-modal expression profile in M7 is
229 consistent with these functions being implicated in transpressorium morphogenesis. Finally, the switch
230 to necrotrophic growth by *M. oryzae* is represented by M8, M9 and M10, which peak in expression
231 after 72hpi (Figure 2B). These modules include gene functions associated with conidiogenesis, such as

232 *SMO1*, encoding a Ras GTPase-Activating Protein, the fatty acid synthase beta subunit dehydratase
233 *FAS1* (Sangappillai and Nadarajah, 2020) and the necrosis- and ethylene-inducing protein 1-encoding
234 gene *NLP1* (Park et al., 2006; Fang et al., 2017; Kershaw et al., 2019).
235
236 **Invasive growth of *M. oryzae* involves specific physiological transitions**
237 To identify physiological processes within each WGCNA module of co-expressed genes, we next
238 carried out metabolic pathway enrichment analysis, as shown in Figure 2C. As the temporal progression
239 of rice blast infection proceeds, several waves of gene expression could be identified. Over-
240 representation of genes associated with regulated proteolysis, for example, are a feature of M1,
241 consistent with the role of autophagy in appressorium maturation. There is also a switch from the
242 tricarboxylic acid cycle (M1), to sucrose metabolism (M2, M6, M9) and the pentose phosphate pathway
243 during invasive growth (M8). This is consistent with the Nut1/Pas1 /Asd4-regulated NADPH-
244 dependent metabolic regulation previously reported in *M. oryzae* (Wilson et al., 2010) and the metabolic
245 transitions that occur during fungal invasive growth (Fernandez et al., 2014). The physiological
246 signature of biotrophy also includes evidence of rapid fungal proliferation, exhibited by cell division-
247 associated functions in M2 and M3, as well as protein processing and export in M4, and ribosomal
248 biogenesis in M5. There is also a very pronounced switch that is clear in M6, associated with the
249 appearance of disease symptoms, which occurs at 72h, and the onset of necrotrophy. M6 shows over-
250 representation of secondary metabolism-associated gene expression and plant cell wall degrading
251 enzymes, for instance. The parallels between appressorium morphogenesis and transpressorium
252 function are also evident by the physiological functions over-represented in M7, including cell cycle
253 control– a key regulator of appressorium development(Saunders et al., 2010)–and associated DNA
254 replication functions. Further secondary metabolic functions are represented in M8 and M9 during the
255 onset of disease symptom development and conidiogenesis.
256 In a complementary analysis to WCGNA clustering, we defined expression profiles of all *M.*
257 *oryzae* genes at each stage during infection. Fungal read counts were normalized and compared to
258 expression in conidial mRNA using Sleuth (Pimentel et al., 2017), thereby identifying temporal changes
259 in gene expression (log2 fold change >1, and P-adj<0.05) that occur during pathogenesis compared to
260 the original inoculum. This analysis revealed that the largest change in *M. oryzae* gene expression
261 occurs at 48hpi compared to the conidial transcriptome, highlighting the substantial physiological
262 transition associated with invasive fungal growth, with 1920 genes up-regulated and 1012 down-
263 regulated at this time point. Metabolic pathway enrichment analysis revealed expression of many
264 growth-related functions, including cell division, translation, and regulated proteolysis, as well as the
265 switch to carbohydrate metabolism that accompanies fungal invasive growth (Supplemental Figure 3;
266 Supplemental Dataset 5). Differentially expressed genes that showed repression (or marked down-
267 regulation) during each stage of pathogenic development provided evidence of a general repression of
268 transport-associated functions, lipid and fatty acid metabolism occurs during invasive growth compared

269 to conidia (Supplemental Figure 3). This highlights how pathogenic development requires not only up-
270 regulation of specific gene functions, but also the orchestrated repression of many gene functions
271 compared to the relative pluripotency of the germinating spore.
272 Targeted analysis of secondary metabolic functions revealed specific expression of polyketide
273 synthase (PKS), fatty acid synthase (FAS), and cytochrome P450 mono-oxygenases during plant
274 infection (Supplemental Figures 4-6). Conidial-specific expression of 8 PKS genes occurs prior to
275 infection, followed by co-regulation of 4 PKS genes at 8h, 6 at 24 h and 7 at 48h, consistent with the
276 production of specific metabolites during each stage of development (Supplemental Figure 4). This is
277 mirrored by FAS gene expression occurring differentially during both biotrophic and necrotrophic
278 stages of development (Supplemental Figure 5) and, strikingly, by temporal expression of cytochrome
279 P450 genes at each timepoint with 21 genes expressed for example specifically at 24h (Supplemental
280 Figure 6). Consistent with these temporal changes in gene expression, a targeted analysis of the 495
281 predicted transcription factor-encoding genes from the *M. oryzae* genome (Park et al., 2013) showed a
282 pattern of co-expression, with large clusters of co-expressed TF genes in conidia, and at the 8h, 16h,
283 24h and 48h time points in particular (Supplemental Figure 7). A clear transition in transcriptional
284 regulation occurs after 48h, with most transcription factor-encoding genes from the earlier biotrophic
285 phase of growth being repressed after this time, accompanied by the expression of a completely separate
286 group of regulators between 72h and 144 h during disease symptom development. We conclude that
287 major regulatory changes in gene expression, associated with switches in both primary and secondary
288 metabolism occur during plant infection and the transition from biotrophic proliferation to necrotrophic
289 growth.
290
291 **A large family of *M. oryzae* effector genes is differentially expressed during rice infection.**
292 We next focused on defining the expression of *M. oryzae* genes predicted to encode secreted proteins,
293 including potential effector candidates. Secreted proteins were predicted using SignalP from data sets
294 of each inoculation method and strain-cultivar interaction. This revealed 68 candidate effector genes in
295 the spray inoculation of CO39, 467 effector candidates in the spray inoculation of Moukoto and 847
296 putative effectors in the leaf drop infection of CO39 (Figure 3 and Supplemental Datasets 3-5),
297 consistent with the increased resolution obtained by using a highly susceptible rice cultivar and leaf
298 drop infections. We then investigated the temporal expression profile of predicted effectors and
299 classified them into each WGCNA module (Figure 3A). This revealed distinct patterns of gene
300 expression, particularly during the initial stages of gene expression (M1-M5), with particular over-
301 representation of effector candidates in M4 and M5. The expression of well-characterized effector-
302 encoding genes corresponded to each module. M3, for example, includes *NIS1* which suppresses
303 Bak1/Bik1-dependent PAMP-triggered immunity (Mentlak et al., 2012; Irieda et al., 2019), the
304 apoplastic effector gene *SLP1* which suppresses chitin-triggered immunity (Mentlak et al., 2012) and
305 *MoSVP1*, encoding an effector required for appressorium-mediated penetration (Shimizu et al., 2019).

306 M4 includes the avirulence gene *ACE1*, *HEG13* which antagonizes cell death induced by Nep1 in
307 *Nicotiana benthaniana* (Mogga et al., 2016; Guo et al., 2019), and the *BAS1*, *BAS2* and *BAS4* effectors
308 (Bohnert et al., 2004; Mosquera et al., 2009). M5 includes *AVR-Pita1* and *BAS3* as well as the cell
309 death-inducing protein CDIP5 (Orbach et al., 2000; Mosquera et al., 2009), while M6 includes *SPD2*
310 which is a suppressor of cell death (Sharpee et al., 2017). Necrotrophy associated effectors are
311 meanwhile represented in later modules, such as the necrosis inducing protein *NLP1* in M10 (Mogga et
312 al., 2016).
313 We therefore defined a total of 863 putative *Magnaporthe* effector protein (*MEP*) genes
314 differentially expressed during plant infection and co-expressed with many previously reported
315 effectors (Supplemental Dataset 7). To test the hypothesis that these genes encode fungal effectors, we
316 used two algorithms designed to predict effector-like genes, the EffectorP algorithm and the
317 DeepRedEff algorithm (Kristianingsih and MacLean, 2021; Sperschneider and Dodds, 2022). A total
318 of 684 genes were predicted to be effector-encoding using EffectorP 3.0 and 849 genes using the
319 DeepRedEff algorithm, based on analysis of the entire *M. oryzae* predicted proteome (Figure 3C). In
320 total, 546 host-induced *MEP* genes are therefore predicted to encode effectors based on at least one of
321 the algorithms (Figure 3C). There are, however, 317 *MEP* genes predicted not to be effectors based on
322 either algorithm. We found that 442 predicted *MEP* effectors do not contain any PFAM domains. The
323 products of *MEP4, MEP12* and *MEP20*, however, contain a C2H2 zinc finger domain, and *MEP31*
324 encodes a predicted secreted homeodomain protein. *MEP12* and *MEP20* were independently identified
325 as *MoHTR1* and *MoHTR2* which encode nuclear effectors that modulate host immunity via
326 transcriptional reprogramming (Kim et al., 2020). *MEP161* has also been described as *MoSVP1*, an *in*
327 *planta*-expressed virulence effector (Shimizu et al., 2019), while *MEP11* is an ortholog of *AVR-Pik*
328 (Yoshida et al., 2009). We conclude that *M. oryzae* strain Guy11 has at least 546 effector genes and
329 potentially as many as 863, which we have classified as differentially expressed *MEP*s.
330
331 ***MEP* genes are unevenly distributed in chromosomes of *M. oryzae* strain Guy11**
332 To investigate the distribution of the differentially expressed *MEP* genes in the *M. oryzae* genome, we
333 investigated their chromosomal distribution (Supplemental Figure X). We observed the full potential
334 repertoire of 863 *MEP* genes at loci dispersed across all 7 chromosomes of *M. oryzae*. There appeared
335 to be enrichment in *MEP* loci in sub-telomeric regions of all chromosomes except chromosome 5, as
336 shown in Figure 3D. *BAS4*, *MEP4*, *MEP7*, *MEP11*, *MEP13* and *MEP24*, for example, are located near
337 telomeres and their enrichment is statistically significant (Figure 3D). There were also *MEP* genes
338 found adjacent to one another, for example, *MEP5* and *AVRPITA* are tightly linked in the sub-telomeric
339 region of one arm of chromosome 6 (Supplemental Figure 8).
340
341
342

343 **Structurally conserved *M. oryzae* effectors are temporally co-regulated during plant infection**
344 Fungal effectors seldom show sequence similarity, or homology to known proteins, but there is
345 increasing evidence that they may share structural conservation. Indeed, structural biology has
346 contributed significantly to our understanding of effector evolution and function (Franceschetti et al.,
347 2017). In *M. oryzae* the MAX effectors (Magnaporthe Avrs and ToxB like), for example, are not related
348 by sequence similarity but share a common β-sandwich fold shared by effectors from the wheat tan spot
349 pathogen *Pyrenophora tritici-repentis* (de Guillen et al., 2015). MAX effectors include *M. oryzae*
350 AVR1-CO39 and AVR-PikD which interact with heavy metal-associated (HMA) integrated domains
351 in the immune receptors by which they are perceived during incompatible interactions (De la
352 Concepcion et al., 2018; Guo et al., 2018).
353 Recently, a genome-wide computational structural analysis of the secreted proteome of *M.*
354 *oryzae* has been reported (Seong and Krasileva, 2021a), taking advantage of the development of *de*
355 *novo* folding algorithms, such as Alphafold (Jumper et al., 2021). A total of 1854 secreted proteins were
356 classified into 905 structure clusters, 740 of which are represented by single proteins (Seong and
357 Krasileva, 2021a). We decided to determine the relationship between the structurally conserved families
358 reported (Seong and Krasileva, 2021b) and the predicted *MEP* effector repertoire. We found that 863
359 *MEP* proteins fall into 366 predicted structure clusters (Supplemental Data Set 7). This includes 38
360 predicted MAX effectors including *MEP3*, *MEP11* (*AVRPikD*), *MEP19* and *MEP27*, which are
361 classified in structure cluster 8. We then selected the 10 largest structurally conserved clusters and
362 analysed their distribution in each WGCNA module, as shown in Figure 4. In most cases the structurally
363 conserved proteins were expressed throughout pathogenesis, but some striking patterns were observed.
364 First of all, the MAX effector group (cluster 8), were over-represented in M4 and M5, along with
365 structure cluster 7 proteins, which are predicted ADP-ribose transferases (ARTs), proposed to act as
366 effectors (Seong and Krasileva, 2021a). This was a very distinct pattern from all of the other structurally
367 conserved groups, which were much more evenly distributed. The other pattern observed was some
368 over-representation of proteins predicted to encode hydrolases (cluster 1), glucosidases (cluster 2), and
369 glycosyl hydrolases (clusters 4 and 6) in M8 and M9, associated with necrotrophy. We conclude that
370 structurally conserved effector candidates are temporally co-expressed during plant infection.
371
372 **Stage-specific expression of Mep effectors of *M. oryzae***
373 In order to focus on the most likely effector candidates for experimental analysis, we selected 63 *MEP*
374 genes identified in all experiments (Figure 3C and Supplemental Data Sets 3-5) and functionally
375 characterized 32 *MEPs* by live-cell imaging and targeted gene replacement. We first generated GFP
376 fusions of the 32 representative *MEP* genes, expressed these GFP fusions in Guy11, and visualized their
377 sub-cellular localisation patterns during fungal growth *in planta*. A sub-set of effectors could be
378 visualised very early during plant infection. *MEP1*, for example, is organized into a ring conformation
379 at the appressorium pore on the plant cell surface (Figure 5). The appressorium pore is organised by

380 septin GTPases and marks the point of penetration peg emergence and polarised exocytosis, mediated
381 by the exocyst complex (Gupta et al., 2015). Mep1 is therefore likely to be secreted at the point of
382 cuticle penetration from the penetration peg. After cuticle rupture, Mep1-GFP initially accumulates at
383 the tip of primary invasive hypha and then outlines invasive hyphae, suggesting that it localises to the
384 apoplast between the fungal cell wall and the plant plasma membrane, termed the Extra-Invasive
385 Hyphal Membrane (EIHM) (Kankanala et al., 2007), as shown in Figure 5B and Supplemental Movie
386 2. Consistent with this idea, Mep1-GFP co-localises with Bas4-RFP, an apoplastic effector (Giraldo et
387 al., 2013) around invasive hyphae 24h after infection, consistent with its classification in M4 (Figure
388 5B). By contrast, the M5 candidate effector gene, *MEP3*, localises exclusively to the BIC during
389 infection, peaking in expression at 48h (Figure 5C). Exclusive BIC localisation was observed for all
390 other Mep-GFP fusions examined within the initial cell penetrated (Supplemental Figure 5).
391 To investigate secretion of MEP effectors, we generated alleles in which the predicted signal
392 peptide region was removed and expressed these in *M. oryzae*. When Mep1$^{19-74}$-GFP was expressed
393 with Mep1-mCherry in Guy11, we observed cytoplasmic accumulation of Mep1$^{19-74}$-GFP, while Mep1-
394 mCherry was delivered to the apoplast around invasive hyphae (Figure 6A and Supplemental Figure
395 11). The signal peptide of cytoplasmic effectors was also necessary to enable delivery to the BIC, with
396 Mep3$^{25-145}$-GFP fluorescence observed intracellularly in invasive hyphae (Figure 6B). Because the
397 punctate localisation of BIC effectors might be interpreted as being a lower expression level than
398 predicted by RNA-seq analysis (Figure 6C), we also made gene fusions expressing free GFP driven by
399 each *MEP* promoter, as shown for *MEP1* and *MEP3* in Figure 6D and E. Fluorescence was observed
400 for *MEP1* in conidia and appressoria, as well as invasive hyphae, while *MEP3* was expressed at a very
401 high level exclusively in invasive hyphae (Figure 6D and E and Supplemental Figure 10). Cell
402 biological visualisation of MEP expression was therefore consistent with predictions from RNA-seq
403 analysis.
404
405 **The dynamics of the host-pathogen interface during plant infection**
406 To investigate the dynamics of the host-pathogen interface during plant infection, we infected a
407 transgenic rice line expressing the plasma membrane marker Lti6b-GFP (Kurup et al., 2005; Mentlak
408 et al., 2012), using a Guy11 strain expressing Mep1-mCherry. The Mep1-mCherry fluorescence
409 outlined invasive hyphae in initially colonised epidermal cell, bounded by the EIHM, which showed
410 Lti6b-GFP fluorescence, consistent with delivery of the effector to the apoplast between the fungal cell
411 wall and EIHM. The EIHM maintained integrity during the early stages of the plant infection (Figure
412 7A), but membrane integrity was lost once the fungus invaded neighbouring cells, resulting in loss of
413 host cell viability (Figure 7B). The Mep1-mCherry signal accumulated in the first invaded cell
414 suggesting rupture of the plant plasma membrane and closure of plasmodesmata. New BICs were,
415 meanwhile, formed immediately upon entry into neighbouring cells enriched with plant membrane.
416

417 **Mep effectors secreted to BICS are always delivered into host cells.**
418 Translocation of effectors into rice cells has previously been visualized by expressing fluorescent
419 effector fusion proteins in *M. oryzae* with an artificially added C-terminal nuclear localization signal
420 (NLS) (Khang et al., 2010). The NLS allows effector detection in plant cells by concentrating them in
421 the rice nucleus. The assay has previously been used, for example, to show that the *PWL2* effector,
422 which acts as a host specificity determinant in *M. oryzae,* is translocated into rice cells (Khang et al.,
423 2010). To confirm whether *MEP*-encoded effectors are translocated into host cells, we generated
424 translational fusions with the Mep effector fused in-frame to an NLS. As a control, we expressed GFP-
425 NLS driven by the constitutive TrpC promoter and found that the GFP signal accumulated
426 predominantly in fungal nuclei confirming that GFP-NLS is functional and can drive free GFP into
427 nuclei. However, unless specifically delivered, the signal will not move into a plant nucleus during plant
428 infection (Figure 8A).
429 To investigate whether the Mep1 effector, which we localised to the apoplast, can be
430 translocated into host cells, we expressed Mep1-GFP-NLS and infected rice seedlings. We found that
431 despite the effector possessing a signal peptide and normally localising to the appressorium pore (shown
432 previously in Figure 4a), fluorescence was observed predominantly in the fungal nucleus (Figure 8B).
433 No GFP signal was observed in the plant nucleus of the occupied rice cell, or surrounding plant nuclei
434 (Figure 8B). By contrast, when the BIC-localised effector Mep3 was fused to an NLS, the Mep3-GFP-
435 NLS signal was observed in the plant nucleus of the occupied cell and those of adjacent cells (Figure
436 8C). All BIC-localised effectors evaluated using this assay showed translocation to host cells, while
437 apoplastic effectors such as Mep1 were not translocated.
438 Apoplastic and cytoplasmic effectors of *M. oryzae* have been reported to be secreted by
439 different pathways during rice infection, but to date only a very limited sample has been analysed
440 (Giraldo et al., 2013). Cytoplasmic effectors, such as Pwl2, were shown to be secreted in a brefeldinA
441 (BFA)-insensitive manner, suggesting that they do not undergo conventional ER-to-Golgi secretion. By
442 contrast, apoplastic effectors such as Bas4 are secreted conventionally and are sensitive to BFA
443 treatment. We therefore applied brefeldin A to rice tissue infected with *M. oryzae* expressing Mep-GFP
444 fusions. We observed that secretion of Mep1-GFP was significantly inhibited in the presence of
445 brefeldin A, with fluorescence accumulating within invasive hyphae (Figure 8D). However, when we
446 assayed BIC-associated effectors such as Mep2 and Mep3, we found they were BFA-insensitive. We
447 observed that when a *M. oryzae* Guy11 isolate expressing Mep2-GFP and Bas4-mCherry was exposed
448 to BFA (Figure 8E), then the BAS4-mCherry signal was prevented from being delivered to the apoplast,
449 while the Mep2-GFP signal remained in the BIC. This was consistent for the whole set of analysed
450 putative effectors. We conclude that Mep effectors are secreted by two distinct secretory pathways
451 depending on their host destination (Giraldo et al., 2013).
452
453

454 **Mep effectors contribute to pathogen fitness**

455 Pathogenic fungi secrete a large battery of effector proteins during infection, but individual effector
456 genes have often been reported to display no discernable mutant phenotype with regard to virulence.
457 This has been interpreted as being a consequence of functional redundancy and overlapping effector
458 functions, such that the role of an individual effector is very hard to measure (Selin et al., 2016). In *M.*
459 *oryzae* most effectors characterized to date– such as Pwl2, Bas1, Bas2, Avr-Pik, and Avr-Pita –for
460 example, have been shown not to contribute substantially to the ability of the fungus to cause disease.
461 A much smaller number of effectors, such as the extracellular LysM effector Slp1, do contribute to
462 fungal virulence (Mentlak et al., 2012) but such reports are very rare. It is, however, obvious from an
463 increasing number of studies that effectors serve important functions in the suppression of plant
464 immunity. They interfere with the operation of pattern recognition receptors, impair host responses such
465 as reactive oxygen species generation, and suppress immunity signaling pathways and transcriptional
466 responses (Irieda et al., 2019; Kim et al., 2020). The contribution of an effector to fungal virulence is
467 normally evaluated by generating a targeted deletion mutant and infecting a susceptible host cultivar.
468 Disease symptoms are then measured compared to an isogenic wild type strain. We decided that this
469 assay was likely to be insufficiently sensitive to be able to accurately determine the contribution of a
470 Mep effector to rice blast disease. We therefore deployed a relative fitness assay (Ross-Gillespie et al.,
471 2007; Lindsay et al., 2016) to evaluate the contribution of an effector to fungal virulence. We generated
472 a Guy11 strain expressing cytoplasmic GFP under control of a high-level constitutive promoter, TrpC.
473 At the same time we generated a null mutant of the specific *MEP* effector gene (Supplemental Figure
474 12), in this instance *MEP1*, expressing cytoplasmic mCherry driven by the same TrpC promoter. We
475 then generated a spore inoculum in which we mixed wild type GFP spores and *Δmep1* mCherry spores
476 in a 1:1 ratio. This inoculum was used to inoculate CO39 seedlings. We allowed the disease to progress
477 and then recovered conidia from disease lesions (Figure 9A). We recorded the ratio of spores and then
478 used the same ratio to prepare inoculum to infect a second batch of rice seedlings. We repeated the
479 assay for each generation. We observed that in a mixed infection, the *Δmep1* mutant was driven close
480 to extinction after three rounds of infection (Figure 9B). Relative fitness was calculated using the
481 equation $x_2(1-x_1) / x_1 (1-x_2)$, where x_1 is the initial frequency of the Mep mutant in the population and
482 x_2 is the final frequency after three generations of infection (Figure 9C). In a control experiment, we
483 mixed the wild type and *Δmep1* mutant conidia in axenic plate culture and then recovered spores 12
484 days later. We observed that they maintained the same 1:1 ratio, showing that *Δmep1* mutants have
485 equivalent fitness when growing outside of a plant (Supplemental Figure 13). In this way, we were able
486 to calculate the fitness cost of losing an individual effector during plant infection and show that Mep1,
487 for example, contributes significantly to rice blast disease.
488
489

490 **Discussion**

491 The ability of the rice blast fungus to colonise plant tissue and cause disease is still relatively poorly
492 understood (Fernandez and Orth, 2018; Eseola et al., 2021). The most significant recent advances have
493 come from exploring the cellular changes that accompany fungal infection (Khang et al., 2010; Eseola
494 et al., 2021), the regulation of primary metabolism associated with biotrophic growth (Sun et al., 2018),
495 the secondary metabolic pathways associated with suppression of host immunity (Patkar et al., 2015;
496 Marroquin-Guzman et al., 2017), the definition of effector functions (Mentlak et al., 2012; Kim et al.,
497 2020), and the identification of signalling pathways associated with invasive growth (Sakulkoo et al.,
498 2018). These have provided insight into the substantial changes elicited by *M. oryzae* as it infects rice
499 plants, in order to cause disease (Fernandez et al., 2014; Cruz-Mireles et al., 2021). These advances
500 have been coupled with numerous studies to validate the roles of individual genes in pathogenesis,
501 although these have predominantly been associated with appressorium-mediated infection, with only a
502 small number of gene defined as being determinants of tissue colonisation (Fernandez and Orth, 2018).
503 Our understanding of the biology of rice tissue colonisation has therefore been limited because of a lack
504 of holistic studies of blast infection. The motivation for this study was to carry out transcriptional
505 profiling of the entire disease cycle of *M. oryzae* in order to reveal fundamental changes in pathogen
506 gene expression that occur during progression of the disease, and to use this information to identify the
507 full repertoire of fungal effector proteins deployed by the fungus.

508 Transcriptional profiling has been used in several plant-pathogen interactions to provide insight
509 into fungal development inside a host plant (Kawahara et al., 2012; Kleemann et al., 2012; Rudd et al.,
510 2015; Dobon et al., 2016; Wang et al., 2017; Lanver et al., 2018). These studies have suggested that
511 expression of effector proteins is an emerging characteristic of fungal invasion of plant hosts. In the
512 corn smut fungus *Ustilago maydis*, transcriptional profile analysis has provided significant insight into
513 the biology of biotrophic development. Distinct temporal expression profiles have, for instance, been
514 defined for a wide range of genes associated with fungal metabolism, nutrient acquisition, regulatory
515 networks and secrete effectors. In particular, *U.maydis* effectors were found to be expressed in three
516 distinct expression modules associated with growth on the leaf surface, biotrophic development in
517 maize cells, and during induction of tumour formation, when rapid plant cell division is stimulated
518 (Lanver et al., 2018). Until now, the studies carried out in *M. oryzae* have not reached such a level of
519 resolution.

520 The most comprehensive study to date in *M. oryzae* used laser capture microdissection to
521 enhance the proportion of rice cells containing fungal invasive hyphae and then employed microarray
522 analysis to define a total of 58 putative fungal effectors, of which 4 were localised during the infection
523 process (Mosquera et al., 2009). A more recent *M. oryzae* study using RNA-seq analysis, focused on a
524 single time point of infection, 24 hpi, when rice cells were initially occupied by the fungus. This led to
525 240 fungal transcripts being defined, which included some effector candidates (Kawahara et al., 2012).
526 These studies of *M. oryzae*, although influential, do have severe limitations in their coverage of the

527 development of rice blast and the level of resolution they were able to achieve. Laser capture
528 microdissection, for example, added a layer of perturbation to sample preparation (Mosquera et al.,
529 2009), while focusing on a single time point, (Kawahara et al., 2012) limited the identification of
530 effectors. We therefore decided to perform a comprehensive transcriptional profiling study in which 8
531 timepoints would be used, along with distinct inoculation methods and different fungal-rice cultivar
532 interactions, to identify the maximum number of fungal transcripts and provide the closest relationship
533 to natural blast infections.

534 The major findings of our study are (1), the definition of 10 distinct modules of differentially
535 regulated *M. oryzae* genes that encompass the entire process of pathogenic development from the time
536 of spore germination to the development of sporulating disease lesions; (2), the identification of distinct
537 physiological processes and genes involved in secondary metabolism expressed at specific stages of
538 pathogen development; (3), the identification of novel *MEP* effector genes that are temporally
539 expressed throughout pathogenesis in distinct temporal groups; (4), the discovery that structurally
540 conserved effectors are temporally co-regulated during invasive growth, providing a means of
541 identifying novel effector functions; (5), the classification of Mep effectors into cytoplasmic and
542 apoplastic proteins, delivered via two distinct secretory routes, validating this classification system for
543 the effector repertoire, and (6), the definition of Mep effector function based on contribution to pathogen
544 fitness using a mixed inoculation assay and fitness measure.

545 Temporal analysis of gene expression revealed the nature of changes in physiological function
546 during pathogenic development. This highlighted the rapid growth of *M. oryzae* during spore
547 germination and starvation stress associated with early development on the leaf surface. Consistent with
548 this, genes associated with autophagy, regulated proteolysis, and lipid metabolism were expressed.
549 During early biotrophic colonisation of leaf tissue significantly up-regulated genes associated with
550 carbon and nitrogen source acquisition from the plant host by 24h. The orchestration of secondary
551 metabolic pathways are also a feature of the biotrophic colonisation of initially occupied epidermal
552 cells, in addition to effector secretion. Another key feature recognised during infection is the pattern of
553 repression of gene expression that accompanies the developmental programme following appressorium
554 development. This is consistent with embryogenic specialisation in cell fate, constraining patterns of
555 gene expression and may be a largely unexplored feature of pathogenesis, as so many studies have
556 instead focused exclusively on genes induced during infection.

557 A pattern therefore emerges of how *M. oryzae* switches from a nutrient-free environment of the
558 leaf surface where its metabolism is dominated by lipid metabolism and re-cycling of the spore contents,
559 consistent with rapid generation of compatible solutes, such as glycerol, for appressorium turgor
560 generation. As the fungus encounters sugars and amino acids within the leaf, it switches to rapidly
561 acquiring nutrients, as it moves through rice cells. A transition to sucrose utilization and the pentose
562 phosphate pathway is apparent, consistent with experimental studies in which the *M. oryzae* glucose-6-
563 phosphate sensor, Tps1, has been shown to regulate carbon metabolism and link glucose availability to

564 glutathione-dependent antioxidation and the establishment of biotrophy (Wilson et al., 2010; Fernandez
565 et al., 2012). The biotrophy-associated gene *IMP1*, for example, which is linked to TOR-dependent
566 nutritional control of invasive growth (Sun et al., 2018) is in M6 and peaks in expression at 48h after
567 infection. Primary metabolism-associated gene expression is also consistent with previous metabolomic
568 analysis of plant infection by *M. oryzae* (Parker et al., 2009), which revealed fungal re-programming of
569 plant metabolism during infection, including suppression of the defence-associated ROS burst. The
570 nitronate mono-oxygenase gene, *NMO2*, for example, which is required to limit nitro-oxidative stress
571 during rice immune responses (Marroquin-Guzman et al., 2017) peaks in expression at 16h and 48h,
572 during the most active phases of biotrophic proliferation of the fungus. Our study also provides evidence
573 of a very large-scale change in gene expression during the later stages of infection after 48h associated
574 with the utilisation of completely distinct families of transcriptional regulators as the fungus transitions
575 to necrotrophy and disease symptom development.

576 Arguably, the most significant finding of this study is that the effector repertoire of *M. oryzae*
577 is likely to be much more substantial than previously thought, with at least 546 putative effectors
578 recognised, among a total of 863 differentially-regulated secreted proteins. Effector functions are
579 continually being described across phytopathogenic fungi, and in *M. oryzae* a range of effector targets
580 have been identified, including small heavy metal associated domain proteins, inhibitors of chitin-
581 triggered immunity and exocyst components (Franceschetti et al., 2017). In all cases so far described,
582 the effector exerts an effect to suppress pattern-triggered immunity (PTI). However, the sample size
583 evaluated so far is extremely small compared to the likely total repertoire revealed from this study (less
584 than 2%), suggesting that the fungus has the capacity to overwhelm plant defense, perhaps by
585 intervention at key points, with the same targets identified by many effectors, or conversely, suggesting
586 that there are many new effector functions to be discovered, including potentially some not associated
587 with PTI suppression, perhaps inducing morphological changes in rice cells essential for pathogen
588 development.

589 A limitation in fungal effector identification has been the lack of sequence similarity among
590 effectors and the absence of specific motifs, such as the RXLR motif found in many oomycete effectors
591 (Morgan and Kamoun, 2007). The use of genome-wide computational structural biology approaches
592 does, however, provide a powerful new means of identifying putative effectors, given the structural
593 similarity exhibited by the MAX effectors and ARTs (Seong and Krasileva, 2021a). We observed that
594 both of these structurally conserved effector families are temporally co-expressed within M4 and M5,
595 making them the most enriched for computationally predicted fungal effectors. This has provided a
596 wealth of noew potential effector candidates for functional analysis and also suggests that co-expression
597 in these tow WCGNA modules may provide a new means of mining for novel effector functions,
598 utilizing the combination of structural prediction and temporal expression profiling. It may also be
599 possible to combine these analyses with an evaluation of the chromosomal distribution of gene loci as
600 an additional diagnostic tool for predicting likely effector candidates.

601 The study of effectors has hitherto also been constrained by the fact that their contribution to
602 the biology of the pathogen has been very hard to assess. This is largely a consequence of the relatively
603 crude assays used to define their role in pathogenesis. Carrying out targeted deletion and simply
604 assaying their ability to generate disease symptoms has not, generally, led to discernible mutant
605 phenotypes. We therefore devised a mixed infection assay designed to allow the relative contribution
606 of an effector to pathogen fitness to be measured. We reasoned that, if an effector makes a small
607 contribution to the fitness of *M. oryzae* during disease development then a mutant lacking that effector
608 will be less likely to survive within a population. We therefore marked strains with different fluorescent
609 markers and produced inocula with equal numbers of spores to infect plants. This provided a simple
610 means of assessing fitness over several generations. In the case of the *MEP1* effector gene, targeted
611 deletion resulted in only a small change in disease lesion generation, but in mixed infection the *Δmep1*
612 mutant was driven to extinction in three generations. This simple assay has considerable utility for
613 evaluating effector function in future and could be further refined by bar-coding to enable mixed
614 populations to be defined in greater detail and with numerous effector mutants within a given
615 population.
616 In summary, this study has provided a resource for researchers to ask specific questions
617 regarding the major transcriptional changes associated with rice blast disease, including both repression
618 and activation of gene functions. The analyses reported here are a very small element of what could be
619 addressed with the data sets, which offer the deepest and most extensive transcriptome data available
620 for the rice-*M. oryzae* interaction. Furthermore, we have identified a very large battery of more than
621 546 *M. oryzae* effector candidates and classified these by temporal expression profile and structural
622 conservation, enabling new insights into the range of effector functions deployed by the fungus to cause
623 rice blast disease.
624
625 **Materials and Methods**
626 **Fungal and plant growth conditions**
627 Fungal strains and rice plant cultivars were maintained, as described previously (Talbot et al., 1993b).
628 Ten-day old plate cultures of *M. oryzae* were used to collect conidia for appressorium development
629 assays, leaf sheath infections and pathogenicity assays. Infected rice plants were incubated in a chamber
630 at 24 ºC, 12 h photoperiod and 90 % relative humidity.
631 **Preparation of healthy and infected rice samples for RNA-Seq analysis**
632 *M. oryzae* conidia were harvested from 10-day old complete medium (CM) plates (Oses-Ruiz et al.,
633 2021). To carry out plant infections by spray assay, 21-day-old, 3-leaf-stage rice plants were sprayed
634 with conidia of Guy11 at 1×10^5 spores mL^{-1} in 0.25% (w/v) gelatin. Infected rice leaves were harvested
635 at 8, 16, 24, 48, 72, 96 and 144 hours post inoculation. Rice leaves sprayed with 0.25% gelatin were
636 used as controls to compare differentially expressed plant genes. To carry out plant infections by leaf
637 drop infection, the third leaf of 3-leaf-stage rice plant was placed on a flat surface and inoculated with

638 a 20μL suspension of 1×10^6 spores mL^{-1} in 0.25% gelatin. A total of 20 lesions were harvested at each
639 time point (8, 16, 24, 48, 72, 96 and 144 hours post inoculation). Rice leaves inoculated with 0.25%
640 gelatin were used in control experiments to compare differentially expressed plant genes. All collected
641 samples were frozen in liquid nitrogen immediately for RNA extraction. Each experiment has 3
642 biological replicates.

643 **Total RNA purification and RNA sequencing**

644 Total RNA from each sample was extracted using RNeasy Plant Mini Kit (QIAGEN). RNase-Free
645 DNase Set (QIAGEN) was used to remove all genomic DNA. RNA quantity and integrity were
646 measured by Agilent 2100 Bioanalyzer, and purified RNA was used to make sequence libraries using
647 True-Seq RNA sample preparation kit from Illumina (Agilent). Sequencing was carried out using HiSeq
648 2500 standard mode. The raw data have been deposited to ENA with accession number PRJEB45007.

649 **Differential gene expression analysis**

650 Raw reads were separated by Taxonomy ID of *M. oryzae* and *O. sativa* (NCBI: txid 318829 and txid
651 4530) using Kraken 2 (Wood et al., 2019). The extracted fungal reads from Kraken 2 were used to
652 quantify the abundance of transcripts using Kallisto (Bray et al., 2016). TPM values were used to
653 perform fungal mass estimation, PCA analysis, and an overview of expression profiling analysis.
654 Differential gene expression analysis was performed using Sleuth (Pimentel et al., 2017). Genes defined
655 as up-regulated by having log2 fold change >1 and P-adjust < 0.05. Amino acid sequences of all coding
656 genes from *M. oryzae* 70-15 were used to predict effectors. Venn diagram was generated using jvenn
657 to compare different datasets (Bardou et al., 2014).
658

659 **Co-expression analysis and Pathway enrichment analysis**

660 WGCNA was used to analyse the gene co-expression network (Langfelder and Horvath, 2008). Only
661 genes with at least 5 fungal reads from all three replicates were considered. A total of 11990 genes were
662 therefore processed by WGCNA (version 1.69). The function Blockwisemodules was used to produce
663 a network of a Pearson correlation matrix to exam similarity between genes. A Soft power threshold of
664 12 was chosen because it was the lowest power to obtain the lowest correlation value (0.85) from
665 topology analysis. Module detection was generated by modified settings to minimize numbers of
666 clusters by using minModulesSize=100, mergeCutHeight=0.30. For each module, the expression level
667 of the module eigengene was calculated to visualize co-expression patterns. For KEGG enrichment
668 analysis, clusterProfiler (version 3.11) was used to perform Benjamini-Hochberg tests to gain P-values
669 and q-values(Yu et al., 2012). The enriched metabolic pathways were selected with a p-value < 0.05.
670

671 **Construction of vectors and transformation of *M. oryzae***

672 All 32 selected effector candidates were cloned with their native promoters and entire protein coding
673 sequences without stop codons, then tagged at the C-terminus with GFP using recombination *in vivo* in
674 yeast (Oldenburg et al., 1997). In brief, the linearized pNEB-Nat-Yeast1284 cloning vector was used

675 which contains the *URA3* gene, allowing complementation of uracil (-) auxotrophy. The positive in-
676 fusion plasmid was transformed into *E. coli* to obtain plasmid DNA for fungal transformation. To
677 construct Mep1-GFP-NLS, primers TrpC-F-SpeI and TrpCp-R-EcoRI were used to amplify the TrpC
678 promoter fragment from the hygromycin resistance gene cassette. Primers GFP-F-EcoRI and 3xNLS-
679 R were used to obtain GFP-3xNLS from Addgene plasmid pEGFP-C1 EGFP-3xNLS. Primers TtrpC-
680 nls-F and GFP-KpnI-R were used to amplify the TrpC terminator. All amplified fragments were inserted
681 into linearized pCB1532 digested with SpeI and KpnI to generate TrpC-GFP-3xNLS-TtrpC. To
682 generate Mep1-GFP-NLS, TrpC-GFP-3xNLS-TtrpC was digested with SpeI and EcoRI and the in-
683 fusion clone containing the Mep1 promoter and coding sequence, amplified with primers 353ProNLS-
684 F and 353NLS-R from Guy11 genomic DNA. Confirmed positive vectors were transformed into
685 protoplasts of corresponding *M. oryzae* strains, as described previously (Talbot et al., 1993a).
686
687 **Live-cell imaging of *M. oryzae* during vegetative and invasive growth**
688 For imaging conidia and mycelium of *M.oryzae*, samples were incubated on glass coverslips mounted
689 with water. For imaging appressorium development, conidia were placed on inductive hydrophobic
690 glass coverslips and samples checked during appressorium development. To visualize spatial
691 localisation of *M.oryzae* proteins of interest during plant infection, conidia were inoculated into 3-4
692 week old leaf sheath samples of rice cultivar CO-39.and infections allowed to proceed for 0h-48h.
693 Infected leaf sheaths were trimmed before microscopy (Kankanala et al., 2007). Confocal microscopy
694 was carried out using a Leica SP8 laser confocal microscope. Excitation/emission wavelengths were
695 488 nm/ 500-530 nm for eGFP, and 561 nm/ 590-640 nm for mCherry. Images were analysed using
696 Leica software and ImageJ. An illustration of key stages during rice blast disease development in Figure
697 2B was created with BioRender (https://biorender.com/).
698
699 **Statistical analyses**
700 Statistical analyses were performed using the software Prism8 GraphPad. Data sets were tested for
701 normal distribution before comparison. They were analysed using unpaired two-tailed Student's t-test
702 with Welch's correction when data sets were normally distributed. When data sets were non-normally
703 distributed, the non-parametric Mann-Whitney test was used for comparisons.
704
705 **Acknowledgements**
706 We acknowledge assistance from Dr D.M. Soanes and Dr M. J. Kershaw from the University of Exeter
707 at the beginning of this project. We are grateful for the discussion with F. Menke, Y. Gupta, R. K.
708 Shrestha, J. Win and S. Kamoun from The Sainsbury Laboratory. This work was supported by The
709 European Research Council under the European Union's Seventh Framework Programme (FP7/2007-
710 2013)/ERC grant agreement no. 294702 GENBLAST and by an award from The Gatsby Charitable
711 Foundation to NJT.

712
713 **Author contributions**
714 X.Y. and N.J.T. conceived and designed the project. X.Y., B.T., L.S.R., V.M.W., A.B.E., N.C., A.J.F
715 and M.O. performed experimental work. X.Y., B.T. and D.M performed bioinformatic analysis. X.Y.
716 and N.J.T. wrote the paper with help and input from co-authors.
717
718 Correspondence and requests for materials should be addressed to N.J.T.
719
720 **Competing interests**
721 The authors declare no competing interests.
722
723 **Figure Legends**
724
725 **Figure 1.** Transcriptional profile analysis of a time course of plant infection by the rice blast fungus
726 *M. oryzae.*
727 Rice infections were carried out using two distinct inoculation methods and two cultivars differing in
728 relative susceptibility to blast. **(A)** Micrographs of rice tissue of cultivar CO-39 inoculated with *M.*
729 *oryzae* Guy11 expressing free GFP driven by the constitutive promoter RP27 at 40 h post inoculation
730 (hpi) and 48 hpi to show progression of tissue invasion. Individual plant cells are outlined by the cyan
731 dotted line. Scale bars = 20 µm. **(B)** Comparison of rice blast disease symptoms 6 days post-inoculation
732 using either leaf drop infection or spray infection on rice cultivars with varying host susceptibility. I:
733 moderately susceptible rice cultivar CO-39 inoculated with water control; II: leaf drop infection of rice
734 CO-39 with Guy11; III: spray infection of rice CO-39 with Guy11; IV: spray infection of highly
735 susceptible rice cultivar Moukoto with Guy11. **(C)** Graph depicting proportion of fungal transcripts in
736 the plant and pathogen mixed transcriptome (CO-39 Leaf Spray, Moukoto Leaf Spray and CO-39 Leaf
737 Drop correspond to inoculation methods).
738
739 **Figure 2.** Temporal co-expression analysis reveals 10 modules of pathogen gene expression during
740 rice blast infection.
741 Analysis of co-expressed pathogen genes during rice blast disease development. **(A)** Weighted
742 correlation network analysis (WGCNA) identified 10 co-expressed modules during a time-course of
743 infection-related-development and plant infection (Modules 1-10). The representative eigengene is
744 shown for each module **(B)** Schematic representation of each stage of rice blast disease development
745 and corresponding WGCNA co-expression modules. Blast-infected rice tissue samples were collected
746 at 0 hpi, 8 hpi, 16 hpi, 24 hpi, 48 hpi, 72 hpi, 96 hpi and 144 hpi. **(C)** KEGG enrichment analysis of
747 genes in each WCGNA module using clusterProfiler reveals over-represented physiological functions
748 during blast disease development.

749

750 **Figure 3.** Stage-specific temporal expression of the *M. oryzae* secretome during rice infection.
751 **(A)** Heat map showing the hierarchical clustering of pathogen genes encoding putatively secreted
752 proteins from each WGCNA co-expression module. Distinct temporal patterns of secretome expression
753 occur during biotrophic and necrotrophic development. Expression levels are shown relative to the
754 mean expression TPM (transcript per kilobase million) value across all stages. **(B)** Venn diagram
755 showing comparison of differentially expressed secreted protein-encoding genes from three different
756 inoculation experiments (CO39 Leaf Spray, Moukoto Leaf Spray, and CO39 Leaf Drop Infections). In
757 total 68 effector candidates were identified from the CO39 leaf spray infections, 467 effector candidates
758 from Moukoto leaf spray inoculation, and 847 effector candidates from CO39 leaf drop infections.
759 Although leaf drop-CO39 infections revealed expression of many more differentially expressed effector
760 candidates, 20 effector candidates were revealed only in spray inoculation experiments. **(C)**
761 Comparison of effector predictions of host-induced secreted proteins using EffectorP 3.0 and
762 DeepRedEff algorithms with differentially expressed signal peptide containing genes (DEG Sec). **(D)**
763 Enrichment analysis of *MEP* gene loci on *M. oryzae* chromosomes 1-7, encoding predicted secreted
764 proteins. The number of *MEP* genes was compared to total gene number in 200kb windows across each
765 chromosome. Phyper was used to compute the hypergeometric distribution and obtain P-values.
766 (Johnson et al., 1992). The resulting graph in the bottom panel shows regions of each chromosome
767 where there is significant over-representation of *MEP* gene loci.
768

769 **Figure 4.** Structurally conserved *M. oryzae* effectors are temporally co-expressed during biotrophic
770 invasive growth.
771 AlphaFold and ChimeraX platforms were used to predict the three-dimensional structures of predicted
772 secreted proteins of *M.oryzae.* Structure clusters were then analysed against each WGCNA module.
773 Bar charts represent the number of predicted secreted proteins identified in each predicted structure
774 cluster (clusters 1-10), that are classified within each WGCNA co-expression module during
775 pathogenesis. Ribbon diagrams show a representative predicted protein structure for each *M. oryzae*
776 structure cluster. These are MGG_09840, which contains a cutinase domain for structure cluster 1;
777 MGG_04534 contains a chitin recognition protein domain for structure cluster 2; MGG_07497 contains
778 a cytochrome P450 domain for structure cluster 3; MGG_05785 (INV1/BAS113) contains a glycosyl
779 hydrolase family 32 domain for structure cluster 4; MGG_02347 (Nis1) for structure cluster 5;
780 MGG_08537 contains a glycosyl hydrolase family 12 domain for structure cluster 6; for structure
781 cluster; MGG_00230 is a predicted ADP-ribose transferase containing a heat-labile enterotoxin alpha
782 chain domain for structure cluster 7; MGG_12426 is a predicted MAX effector and homologue of
783 AvrPib for structure cluster 8; MGG_04305 contains a glycosyl hydrolase family 88 domain for
784 structure cluster 9; MGG_00276 contains berberine and berberine-like domains for structure cluster 10.
785 Protein structures were predicted by AlphaFold. and ChimeraX was used to visualise the protein
786 structure using PDB files generated by AlphaFold. The command "color bfactor palette alphafold" was
787 used to color-code the confidence for each prediction (scale from red = 0% confident - blue = 100%
788 confident). Genes encoding proteins in structure clusters 7 and 8 are over-represented in WGCNA M4
789 and M5.
790
791 **Figure 5.** Live-cell imaging of Mep candidates during plant infection reveals spatial localisation of
792 effectors during appressorium penetration and invasive growth.
793 **(A)** Micrographs showing the M4 effector Mep1-GFP localising in a ring confirmation at the
794 appressorium pore at the leaf surface in *M. oryzae* Guy11. Conidial suspensions at 5 x10^4 mL^{-1} were
795 inoculated onto rice leaf sheath and images captured at 24 hpi. The periphery of the appressorium is
796 indicated by a cyan dotted line. Line scans show Mep1-GFP fluorescence in a transverse section of the
797 appressorium. Scale bars = 10 µm. **(B)** Conidia were harvested from a *M. oryzae* transformant
798 expressing Mep1-GFP and Bas4-RFP gene fusions and inoculated onto rice leaf sheath preparations.
799 Images were captured at 28 hpi of invasive growth. Micrograph and linescan graphs show co-
800 localization of Mep1-GFP and Bas4-RFP in invasive hyphae of the *M. oryzae* wild- type strain Guy11.
801 Scale bars = 10 µm. **(C)** Micrographs showing localisation of representative M5 effector candidates
802 Mep2-GFP and Mep3-GFP from the 32 selected Mep proteins (Supplemental Figure 9) during plant
803 infection. Images were captured at 22 hpi- 24 hpi. Invasive hyphae are outlined by a white dotted line
804 and individual plant cells indicated with a cyan dotted line. Arrow indicates localisation of both Mep2-
805 GFP and Mep3-GFP at the biotrophic interfacial complex (BIC). Scale bars = 10 µm.

806

807 **Figure 6.** *MEP* genes are highly expressed in living plant tissue during plant infection.

808 **(A)** Conidia were harvested from a *M. oryzae* transformant expressing a Mep1$^{\Delta 19\text{-}74}$-GFP signal peptide
809 deletion and a Mep1-RFP full length gene fusion and inoculated onto CO39 rice leaf sheath. Images
810 were captured at 24 hpi of invasive growth. Micrograph and linescan graphs show that the Mep1 signal
811 peptide is required for correct protein secretion. Scale bars = 10 µm. **(B)** Micrographs showing the rice
812 plant infected by the *M.oryzae* wild-type strain Guy11 expressing a Mep3$^{\Delta 25\text{-}145}$-GFP signal peptide
813 deletion. Green fluorescence was retained inside the invasive hyphae, while red fluorescence (false
814 coloured to magenta) was exported to the apoplast. Images were captured at 24 hpi of invasive growth
815 **(C)** Micrographs showing rice plant tissue infected by the *M. oryzae* wild-type strain Guy11 expressing
816 full length *MEP3,* driven by its native promoter. Mep3-GFP could be observed as small puncta at the
817 BIC. Images were captured at 24 hpi of invasive growth **(D)** Micrographs showing rice CO-39 infected
818 with *M. oryzae* wild-type strain Guy11 expressing cytoplasmic GFP driven by the *MEP3* promoter. **(E)**
819 Conidia were harvested from *M. oryzae* transformants expressing GFP driven by the promotor of
820 Mep1p-GFP and Mep3p-GFP, respectively, and inoculated onto hydrophobic glass coverslips.
821 Micrographs of Mep1p-GFP showed fluorescent signal in both the conidium and the appressorium, in
822 contrast to Mep3p-GFP which displayed little signal. Appressorium formation was observed at 20 hpi.
823 Scale bars = 10 µm.

824

825 **Figure 7.** The rice plasma membrane is invaginated and accumulates at the Biotrophic Interfacial
826 Complex (BIC) during plant infection.

827 Laser confocal micrographs of *M. oryzae* expressing Mep1-mCherry colonising epidermal leaf cells of
828 a transgenic rice line expressing plasma membrane-localised LTi6B-GFP. Images were captured at 24
829 hpi **(A)** and 36 hpi **(B)**. The plant plasma membrane stays intact and invaginated at the early stages of
830 plant infection. LTi6B fluorescence accumulates at the bright biotrophic interfacial complex, indicating
831 the BIC is a plant membrane-rich structure. The fluorescence signal from secreted Mep1-mCherry is
832 surrounded by the fluorescence signal of the rice cell plant plasma membrane marker LTi6B-GFP as
833 the fungus invades new cells, but the initial epidermal cell occupied then loses viability and Mep1-
834 mCherry fluorescence fills the rice cell. Scale bars = 10 um.

835

836 **Figure 8.** Cytoplasmic Mep candidates, which accumulate at the BIC, are translocated into host cells.

837 **(A)** Cellular localisation of GFP with a nuclear localization signal (NLS) driven by the TrpC promoter
838 in *M. oryzae*. The fluorescence signal in the nuclei and nucleoli of conidia and the appressorium. The
839 outline of the fungus is depicted by a white dotted line. **(B)** Micrographs of Mep1-GFP^{NLS} inoculated
840 onto rice leaf sheath and captured at 28 hpi. Fluorescence could be observed in the nucleus and
841 nucleolus of the appressorium, but not in the fungus or plant cells. **(C)** Micrographs of AvrPia-GFP^{NLS}
842 and BIC-accumulating Mep effector candidates showing delivery into both the invaded host cell and

843 unoccupied neighbouring host cells. Arrows indicate plant nuclei. **(D)** Cellular localisation of Mep1-
844 GFP in *M. oryzae* during biotrophic growth on epidermal rice cells. Brefeldin A (BFA) was applied at
845 20 hpi and 0.1% DMSO was used for the control treatment. Images were captured at 3-4 h post
846 treatment. Mep1-GFP fluorescence showed accumulation within invasive hyphae and particularly in
847 the BIC-associated cell **(E)** Micrographs of *M. oryzae* expressing Mep2-GFP and Bas4-mCherry during
848 biotrophic growth on epidermal rice cells. BFA treatment was used to look at secretion of Mep2-GFP
849 and Bas4-mCherry. Mep2-GFP fluorescence accumulated in the BIC in the presence or absence of
850 BFA. By contrast, Bas4-mCherry fluorescence accumulated inside invasive hyphae. Scale bars = 10
851 µm.
852
853 **Figure 9.** Mep1 contributes to pathogen fitness during plant infection.
854 **(A)** Conidial suspensions of equal concentration ($5x10^4$ spores mL^{-1}) from *M. oryzae* Guy11 or Δ*mep1*
855 mutants were used to inoculate 21-day-old seedlings of the blast susceptible cultivar CO-39, and disease
856 symptoms recorded after 5 dpi. The box plot shows the mean lesion density of seedlings infected with
857 Guy11 and the Δ*mep1* mutant per unit area. (**B**) A relative fitness assay was carried out by mixing
858 conidia in equal amounts (1:1) from Guy11 expressing GFP and Δ*mep1* mutant expressing mCherry.
859 Spores were collected from disease lesions and used to inoculate new seedlings in the recovered
860 proportions. A dot plot showing the proportion of WT::GFP and the Δ*mep1*::mCherry conidia recovered
861 from each generation is shown. The Δ*mep1*::mCherry mutant was driven to near extinction in three
862 generations **(C)** Relative fitness was calculated using the calculation $x_2(1-x_1) / x_1 (1-x_2)$, where x1 is the
863 initial frequency of Δ*mep1*::mCherry conidia and x2 the final frequency.
864
865 **Supplemental Data**
866 **Supplemental Figure 1.** Assessment of the RNA-Seq Data Set of *M.oryzae* during rice infection.
867 **(A)** Graph showing comparison of total raw reads and *M. oryzae* extracted reads from each inoculation
868 method and cultivar-strain combination. **(B)** Principal Component Analysis (PCA) of fungal reads from
869 the three infection datasets; CO39 Leaf Drop Infection, CO39 Spray Infection and Moukoto Spray
870 Infection. Three independent biological replicates were generated for each time point 0h, 8h 16h, 24h,
871 48h, 72h, 96h, 144h.
872
873 **Supplemental Figure 2.** Sample clustering and the soft power analysis for WGCNA analysis.
874 **(A)** Sample cluster analysis of all infected rice RNA-seq data sets. Conidia RNA-seq data sets are
875 significantly different to those from the infection time course (shown in red). RNA-Seq Data Sets from
876 early time points of infection, 8h, 16h, 24h and 48h, all clustered into a single clade (shown in green)
877 while later time points from 72h, 96h and 144h grouped together into a third clade (shown in blue). **(B)**
878 Soft power analysis to obtain the optimised power number for WGCNA analysis. The cut-off threshold

879 indicated that the total RNA-Seq Data Set from infected rice samples could be divided into 10 co-
880 expression modules.
881
882 **Supplemental Figure 3.** Biological process enrichment analysis of *M. oryzae* genes differentially
883 expressed during plant infection.
884 *M. oryzae* differential gene expression during plant infection was evaluated by comparison to
885 expression in conidial mRNA using Sleuth (Pimentel et al., 2017), identifying genes showing a log2
886 fold change > 1, and P-adj < 0.05. Diagram shows up-regulated gene functions (top and marked 'up' in
887 legend) and down-regulated gene functions (bottom and marked 'd' in legend) during a time series of
888 *M. oryzae* infection based on leaf drop inoculation of rice cultivar CO-39 by strain Guy11. GO
889 enrichment analysis was carried out using the R package "mogo"
890 (https://github.com/TeamMacLean/mogo).
891
892 **Supplemental Figure 4.** Hierarchical clustering of the expression of *M. oryzae* genes predicted to
893 encode polyketide synthase during plant infection.
894 Heat map showing the temporal pattern of the relative transcript abundance of 29 genes predicted to
895 encode polyketide synthase during plant infection. Genome accession numbers are provided for each
896 gene. Each gene is scaled to the mean TPM (transcript per kilobase million) value across all stages of
897 infection-related-development and plant infection, with fold differences indicated according to the key.
898
899 **Supplemental Figure 5.** Hierarchical clustering of *M. oryzae* genes predicted to encode fatty acid
900 synthases during plant infection.
901 Heat map showing the temporal pattern of the relative transcript abundance of 14 genes predicted to
902 encode fatty acid synthases during rice infection. TPM (transcript per kilobase million) value across all
903 stages of infection-related-development and plant infection, with fold differences indicated according
904 to the key.
905
906 **Supplemental Figure 6.** Hierarchical clustering of *M. oryzae* genes predicted to encode cytochrome
907 P450 mono-oxygenases during plant infection.
908 Heat map showing the temporal pattern of the relative transcript abundance of 75 genes encoding
909 cytochrome P450 mono-oxygenases during rice infection. TPM (transcript per kilobase million) value
910 across all stages of infection-related-development and plant infection, with fold differences indicated
911 according to the key.
912
913 **Supplemental Figure 7.** Hierarchical clustering of *M. oryzae* genes predicted to encode transcription
914 factors during plant infection.

915 Heat map showing the temporal pattern of the relative transcript abundance of 495 genes predicted to
916 encode transcription factors during rice infection. All putative transcription factors were extracted from
917 the Fungal Transcription Factor Database (http://ftfd.snu.ac.kr/magnaporthe), a platform designed to
918 identify transcription factor-encoding genes in fungi. TPM (transcript per kilobase million) value across
919 all stages of infection-related-development and plant infection, with fold differences indicated
920 according to the key.
921
922 **Supplemental Figure 8.** Visualisation of the distribution of 863 *MEP* gene loci on the seven
923 chromosomes of *M. oryzae*.
924 Genetic map showing the order and relative distribution of *MEP* loci among the seven chromosomes
925 of *M. oryzae*. The positions were determined by analysis against the 70-15 reference genome (Dean et
926 al., 2005).
927
928 **Supplemental Figure 9.** Cytoplasmically targeted Meps consistently localise to the BIC during
929 biotrophic invasive growth of *M. oryzae*.
930 Micrographs showing the localisation of Mep4, Mep5, Mep6, Mep7, Mep8, Mep9, Mep10, Mep11 and
931 Mep12 which were all C-terminally tagged with GFP, transformed and expressed in Guy11 and used
932 to carry out infections of rice leaf sheath of cultivar CO39. Laser confocal images were captured at 22-
933 28 hpi. A single large fluorescent punctum, the BIC, was always observed in the initially invaded
934 epidermal cell. Scale bars = 10 µm.
935
936 **Supplemental Figure 10.** Assessment of the expression of Mep effector candidates during plant
937 infection.
938 Micrographs showing the expression of cytoplasmic GFP driven by the promoters of Mep effector
939 candidates during plant infection. Promoters of *MEP1, MEP2, MEP4, MEP5, MEP6* and *MEP7* were
940 fused to GFP, transformed into Guy11 and single copy transformants selected. A strong fluorescence
941 signal was specifically observed inside invasive hyphae during plant infection. Scale bars = 10 µm.
942
943 **Supplemental Figure 11.** Live-cell imaging of the secreted and non-secreted Mep1 protein variants
944 during plant infection.
945 Micrographs showing invasive hyphae at two infection sites of *M. oryzae* Guy11 expressing Mep1$^{19-74}$-
946 GFP and Mep1-mCherry. Two infection sites are present and can be observed by the GFP fluorescence
947 signal from Mep1$^{19-74}$-GFP and by observation in the bright field channel. At one infection site, the
948 green fluorescence from Mep1$^{19-74}$-GFP is uniformly enveloped by the magenta fluorescence from
949 Mep1-mCherry. This is consistent with delivery of Mep1-mCherry into the apoplast between the fungal
950 cell wall and extra-invasive hyphal membrane (EIHM). At the second infection site no Mep1-mCherry
951 fluorescence could be observed. This suggests breakdown of the EIHM in the second infected cell in

952 which Mep1-mCherry leaks into the whole cell, which loses viability. Laser confocal images were taken
953 at 24 hpi. Scale bars = 10 um.
954
955 **Supplemental Figure 12**. Targeted *MEP1* gene deletion in the rice blast fungus *Magnaporthe oryzae*.
956 **(A)** Schematic representation of the *MEP1* gene deletion strategy using the split-marker strategy, as
957 described in Methods. Two amplicons containing the left and right flanks of *MEP1* and each half of
958 the hygromycin resistance gene cassette are used to transform Guy11. This results in three crossover
959 events to generate a target gene replacement with re-synthesis of the whole hygromycin resistance
960 cassette. **(B)** Southern blot to confirm targeted gene replacement of the *MEP1* gene. The same
961 approach was used to generate gene replacement mutants for each *MEP* gene analysed in this study.
962
963 **Supplemental Figure 13.** Quantification of conidiogenesis from the *Δmep1* mutant.
964 In order to be able to use a mixed infection fitness assay, it was essential to ensure that each *M. oryzae*
965 strain sporulated with the same frequency **(A)** Conidia were collected from WT::TrpCp:GFP and
966 *Δmep1*::TrpCp:mCherry and counted using a haemocytometer. Conidiation was analysed by
967 quantifying conidia harvested from 10 day-old CM plate cultures of *M. oryzae*. Bar charts show the
968 mean and standard deviation. No significant difference ($P > 0.05$) in conidiation was observed in three
969 biological replicates of the experiment. **(B)** Laser confocal micrographs showing conidia of
970 WT::TrpCp:GFP and *Δmep1*::TrpCP:mCherry, respectively.
971
972 **Supplemental Movie 1.** Real-time observation of the rice blast fungus colonising plant cells.
973 Movie showing the colonisation of rice cells by the *M. oryzae* Guy11 expressing constitutively high
974 level expression vector RP27p:GFP. The starting point of imaging is 38 hpi and images were taken
975 every 30 min for 10 hours before assembling into a single time-lapse movie. Scale bars = 20 µm
976
977 **Supplemental Movie 2.** Three dimensional live-cell imaging to show co-localization of $Mep1^{19-74}$-
978 GFP and Mep1-mCherry fluorescence during plant infection.
979 Movie showing a three-dimensional projection of invasive hyphae of *M. oryzae* expressing $Mep1^{19-74}$-
980 GFP and Mep1-mCherry growing within a living rice cell. Green fluorescence from GFP is uniformly
981 enveloped by the magenta fluorescence from the secreted Mep1-mCherry. Laser confocal mages were
982 taken at 24 hpi. Scale bars = 10 um
983
984 **Supplemental Dataset 1.** Summary of read counts in this study.
985 **Supplemental Dataset 2.** Gene list of members of each WGCNA co-expression module during rice
986 blast disease development.

987 **Supplemental Dataset 3.** Expression profile of predicted secreted protein-encoding genes
988 differentially expressed during spray-infection of rice cultivar CO39 by *M. oryzae*.
989 **Supplemental Dataset 4.** Expression profile of predicted secreted protein-encoding genes
990 differentially expressed during spray-infection of rice cultivar Moukoto by *M. oryzae*
991 **Supplemental Dataset 5.** Expression profile of differentially expressed signal peptide containing
992 genes of *M. oryzae* during leaf drop-infection of rice cultivar CO39.
993 **Supplemental Dataset 6.** List of differentially expressed *MEP* genes that are dependent on the Pmk1
994 MAP kinase for the differential expression during plant infection.
995 **Supplemental Dataset 7.** Expression modules and computationally predicted structural clusters of *M.*
996 *oryzae* secreted proteins.
997 **Supplemental Dataset 8.** List of *M. oryzae* effector candidates studied by live-cell imaging in this
998 study.
999 **Supplemental Dataset 9.** Oligonucleotide primers used in this study.
1000 **Supplemental Dataset 10.** Plasmids used in this study.
1001 **Supplemental Dataset 11.** *M. oryzae* strains generated in this study.
1002
1003 **References**

1004 **Bardou, P., Mariette, J., Escudié, F., Djemiel, C., and Klopp, C.** (2014). jvenn: an interactive
1005 Venn diagram viewer. BMC Bioinformatics **15:** 293.
1006 **Bjornson, M., Pimprikar, P., Nürnberger, T., and Zipfel, C.** (2021). The transcriptional
1007 landscape of Arabidopsis thaliana pattern-triggered immunity. Nature Plants **7:** 579-
1008 586.
1009 **Bohnert, H.U., Fudal, I., Dioh, W., Tharreau, D., Notteghem, J.L., and Lebrun, M.H.** (2004).
1010 A putative polyketide synthase/peptide synthetase from Magnaporthe grisea signals
1011 pathogen attack to resistant rice. Plant Cell **16:** 2499-2513.
1012 **Bray, N.L., Pimentel, H., Melsted, P., and Pachter, L.** (2016). Near-optimal probabilistic
1013 RNA-seq quantification. Nat Biotechnol **34:** 525-527.
1014 **Cao, H., Huang, P., Zhang, L., Shi, Y., Sun, D., Yan, Y., Liu, X., Dong, B., Chen, G., Snyder,**
1015 **J.H., Lin, F., and Lu, J.** (2016). Characterization of 47 Cys2 -His2 zinc finger proteins
1016 required for the development and pathogenicity of the rice blast fungus
1017 Magnaporthe oryzae. New Phytol **211:** 1035-1051.
1018 **Cesari, S., Thilliez, G., Ribot, C., Chalvon, V., Michel, C., Jauneau, A., Rivas, S., Alaux, L.,**
1019 **Kanzaki, H., Okuyama, Y., Morel, J.B., Fournier, E., Tharreau, D., Terauchi, R., and**
1020 **Kroj, T.** (2013). The rice resistance protein pair RGA4/RGA5 recognizes the
1021 Magnaporthe oryzae effectors AVR-Pia and AVR1-CO39 by direct binding. Plant Cell
1022 **25:** 1463-1481.
1023 **Chauhan, R.S., Farman, M.L., Zhang, H.B., and Leong, S.A.** (2002). Genetic and physical
1024 mapping of a rice blast resistance locus, Pi-CO39(t), that corresponds to the
1025 avirulence gene AVR1-CO39 of Magnaporthe grisea. Mol Genet Genomics **267:** 603-
1026 612.

1027 **Chen, S., Songkumarn, P., Venu, R.C., Gowda, M., Bellizzi, M., Hu, J., Liu, W., Ebbole, D.,**
1028 **Meyers, B., Mitchell, T., and Wang, G.-L.** (2012). Identification and Characterization
1029 of In planta–Expressed Secreted Effector Proteins from Magnaporthe oryzae That
1030 Induce Cell Death in Rice. Mol Plant Microbe Interact **26:** 191-202.
1031 **Copley, T.R., Duggavathi, R., and Jabaji, S.** (2017). The transcriptional landscape of
1032 Rhizoctonia solani AG1-IA during infection of soybean as defined by RNA-seq. PLoS
1033 One **12:** e0184095.
1034 **Cruz-Mireles, N., Eseola, A.B., Oses-Ruiz, M., Ryder, L.S., and Talbot, N.J.** (2021). From
1035 appressorium to transpressorium-Defining the morphogenetic basis of host cell
1036 invasion by the rice blast fungus. PLoS Pathog **17:** e1009779.
1037 **Dagdas, Y.F., Yoshino, K., Dagdas, G., Ryder, L.S., Bielska, E., Steinberg, G., and Talbot, N.J.**
1038 (2012). Septin-Mediated Plant Cell Invasion by the Rice Blast Fungus,
1039 <em>Magnaporthe oryzae</em&gt. Science **336:** 1590.
1040 **de Guillen, K., Ortiz-Vallejo, D., Gracy, J., Fournier, E., Kroj, T., and Padilla, A.** (2015).
1041 Structure Analysis Uncovers a Highly Diverse but Structurally Conserved Effector
1042 Family in Phytopathogenic Fungi. PLoS Pathog **11:** e1005228.
1043 **De la Concepcion, J.C., Franceschetti, M., Maqbool, A., Saitoh, H., Terauchi, R., Kamoun,**
1044 **S., and Banfield, M.J.** (2018). Polymorphic residues in rice NLRs expand binding and
1045 response to effectors of the blast pathogen. Nat Plants **4:** 576-585.
1046 **Dean, R.A., Talbot, N.J., Ebbole, D.J., Farman, M.L., Mitchell, T.K., Orbach, M.J., Thon, M.,**
1047 **Kulkarni, R., Xu, J.-R., Pan, H., Read, N.D., Lee, Y.-H., Carbone, I., Brown, D., Oh,**
1048 **Y.Y., Donofrio, N., Jeong, J.S., Soanes, D.M., Djonovic, S., Kolomiets, E., Rehmeyer,**
1049 **C., Li, W., Harding, M., Kim, S., Lebrun, M.-H., Bohnert, H., Coughlan, S., Butler, J.,**
1050 **Calvo, S., Ma, L.-J., Nicol, R., Purcell, S., Nusbaum, C., Galagan, J.E., and Birren,**
1051 **B.W.** (2005). The genome sequence of the rice blast fungus Magnaporthe grisea.
1052 Nature **434:** 980-986.
1053 **Deng, S., Gu, Z., Yang, N., Li, L., Yue, X., Que, Y., Sun, G., Wang, Z., and Wang, J.** (2016).
1054 Identification and characterization of the peroxin 1 gene MoPEX1 required for
1055 infection-related morphogenesis and pathogenicity in Magnaporthe oryzae. Sci Rep
1056 **6:** 36292.
1057 **Dobon, A., Bunting, D.C., Cabrera-Quio, L.E., Uauy, C., and Saunders, D.G.** (2016). The host-
1058 pathogen interaction between wheat and yellow rust induces temporally
1059 coordinated waves of gene expression. BMC Genomics **17:** 380.
1060 **Dong, Y., Li, Y., Zhao, M., Jing, M., Liu, X., Liu, M., Guo, X., Zhang, X., Chen, Y., Liu, Y., Liu,**
1061 **Y., Ye, W., Zhang, H., Wang, Y., Zheng, X., Wang, P., and Zhang, Z.** (2015). Global
1062 genome and transcriptome analyses of Magnaporthe oryzae epidemic isolate 98-06
1063 uncover novel effectors and pathogenicity-related genes, revealing gene gain and
1064 lose dynamics in genome evolution. PLoS Pathog **11:** e1004801.
1065 **Eseola, A.B., Ryder, L.S., Oses-Ruiz, M., Findlay, K., Yan, X., Cruz-Mireles, N., Molinari, C.,**
1066 **Garduno-Rosales, M., and Talbot, N.J.** (2021). Investigating the cell and
1067 developmental biology of plant infection by the rice blast fungus Magnaporthe
1068 oryzae. Fungal Genet Biol**:** 103562.
1069 **Fang, Y.L., Peng, Y.L., and Fan, J.** (2017). The Nep1-like protein family of Magnaporthe
1070 oryzae is dispensable for the infection of rice plants. Sci Rep **7:** 4372.
1071 **Fernandez, J., and Orth, K.** (2018). Rise of a Cereal Killer: The Biology of Magnaporthe
1072 oryzae Biotrophic Growth. Trends Microbiol **26:** 582-597.

1073 **Fernandez, J., Marroquin-Guzman, M., and Wilson, R.A.** (2014). Mechanisms of nutrient
1074 acquisition and utilization during fungal infections of leaves. Annu Rev Phytopathol
1075 **52:** 155-174.
1076 **Fernandez, J., Wright, J.D., Hartline, D., Quispe, C.F., Madayiputhiya, N., and Wilson, R.A.**
1077 (2012). Principles of carbon catabolite repression in the rice blast fungus: Tps1,
1078 Nmr1-3, and a MATE-family pump regulate glucose metabolism during infection.
1079 PLoS Genet **8:** e1002673.
1080 **Foster, A.J., Were, V.M., Yan, X., Win, J., Harant, A., Langner, T., Kamoun, S., Ryder, L.S.,**
1081 **and Talbot, N.J.** (2021). MagnaGenes (v.1.0): an open science database of gene
1082 function studies in the blast fungus Magnaporthe oryzae. zenodo.
1083 **Franceschetti, M., Maqbool, A., Jimenez-Dalmaroni, M.J., Pennington, H.G., Kamoun, S.,**
1084 **and Banfield, M.J.** (2017). Effectors of Filamentous Plant Pathogens: Commonalities
1085 amid Diversity. Microbiol Mol Biol Rev **81**.
1086 **Galhano, R., Illana, A., Ryder, L.S., Rodriguez-Romero, J., Demuez, M., Badaruddin, M.,**
1087 **Martinez-Rocha, A.L., Soanes, D.M., Studholme, D.J., Talbot, N.J., and Sesma, A.**
1088 (2017). Tpc1 is an important Zn(II)2Cys6 transcriptional regulator required for
1089 polarized growth and virulence in the rice blast fungus. PLoS Pathog **13:** e1006516.
1090 **Giraldo, M.C., Dagdas, Y.F., Gupta, Y.K., Mentlak, T.A., Yi, M., Martinez-Rocha, A.L., Saitoh,**
1091 **H., Terauchi, R., Talbot, N.J., and Valent, B.** (2013). Two distinct secretion systems
1092 facilitate tissue invasion by the rice blast fungus Magnaporthe oryzae. Nat Commun
1093 **4:** 1996.
1094 **Guo, L., Cesari, S., de Guillen, K., Chalvon, V., Mammri, L., Ma, M., Meusnier, I., Bonnot, F.,**
1095 **Padilla, A., Peng, Y.L., Liu, J., and Kroj, T.** (2018). Specific recognition of two MAX
1096 effectors by integrated HMA domains in plant immune receptors involves distinct
1097 binding surfaces. Proc Natl Acad Sci U S A **115:** 11637-11642.
1098 **Guo, X., Zhong, D., Xie, W., He, Y., Zheng, Y., Lin, Y., Chen, Z., Han, Y., Tian, D., Liu, W.,**
1099 **Wang, F., Wang, Z., and Chen, S.** (2019). Functional Identification of Novel Cell
1100 Death-inducing Effector Proteins from Magnaporthe oryzae. Rice (N Y) **12:** 59.
1101 **Gupta, Y.K., Dagdas, Y.F., Martinez-Rocha, A.L., Kershaw, M.J., Littlejohn, G.R., Ryder, L.S.,**
1102 **Sklenar, J., Menke, F., and Talbot, N.J.** (2015). Septin-Dependent Assembly of the
1103 Exocyst Is Essential for Plant Infection by Magnaporthe oryzae. Plant Cell **27:** 3277-
1104 3289.
1105 **He, P., Williams, B.A., Trout, D., Marinov, G.K., Amrhein, H., Berghella, L., Goh, S.-T.,**
1106 **Plajzer-Frick, I., Afzal, V., Pennacchio, L.A., Dickel, D.E., Visel, A., Ren, B., Hardison,**
1107 **R.C., Zhang, Y., and Wold, B.J.** (2020). The changing mouse embryo transcriptome at
1108 whole tissue and single-cell resolution. Nature **583:** 760-767.
1109 **Inoue, Y., Vy, T.T.P., Yoshida, K., Asano, H., Mitsuoka, C., Asuke, S., Anh, V.L., Cumagun,**
1110 **C.J.R., Chuma, I., Terauchi, R., Kato, K., Mitchell, T., Valent, B., Farman, M., and**
1111 **Tosa, Y.** (2017). Evolution of the wheat blast fungus through functional losses in a
1112 host specificity determinant. Science **357:** 80-83.
1113 **Irieda, H., Inoue, Y., Mori, M., Yamada, K., Oshikawa, Y., Saitoh, H., Uemura, A., Terauchi,**
1114 **R., Kitakura, S., Kosaka, A., Singkaravanit-Ogawa, S., and Takano, Y.** (2019).
1115 Conserved fungal effector suppresses PAMP-triggered immunity by targeting plant
1116 immune kinases. Proc Natl Acad Sci U S A **116:** 496-505.
1117 **Islam, M.T., Croll, D., Gladieux, P., Soanes, D.M., Persoons, A., Bhattacharjee, P., Hossain,**
1118 **M.S., Gupta, D.R., Rahman, M.M., Mahboob, M.G., Cook, N., Salam, M.U., Surovy,**
1119 **M.Z., Sancho, V.B., Maciel, J.L.N., NhaniJúnior, A., Castroagudín, V.L., Reges,**

1120 **J.T.d.A., Ceresini, P.C., Ravel, S., Kellner, R., Fournier, E., Tharreau, D., Lebrun, M.-**
1121 **H., McDonald, B.A., Stitt, T., Swan, D., Talbot, N.J., Saunders, D.G.O., Win, J., and**
1122 **Kamoun, S.** (2016). Emergence of wheat blast in Bangladesh was caused by a South
1123 American lineage of Magnaporthe oryzae. BMC Biology **14:** 84.
1124 **Johnson, N.L., Kotz, S., and Kemp, A.W.** (1992). Univariate Discrete Distributions. New
1125 York : Wiley **Second Edition**.
1126 **Jones, J.D., and Dangl, J.L.** (2006). The plant immune system. Nature **444:** 323-329.
1127 **Jumper, J., Evans, R., Pritzel, A., Green, T., Figurnov, M., Ronneberger, O.,**
1128 **Tunyasuvunakool, K., Bates, R., Zidek, A., Potapenko, A., Bridgland, A., Meyer, C.,**
1129 **Kohl, S.A.A., Ballard, A.J., Cowie, A., Romera-Paredes, B., Nikolov, S., Jain, R., Adler,**
1130 **J., Back, T., Petersen, S., Reiman, D., Clancy, E., Zielinski, M., Steinegger, M.,**
1131 **Pacholska, M., Berghammer, T., Bodenstein, S., Silver, D., Vinyals, O., Senior, A.W.,**
1132 **Kavukcuoglu, K., Kohli, P., and Hassabis, D.** (2021). Highly accurate protein structure
1133 prediction with AlphaFold. Nature **596:** 583-589.
1134 **Kamoun, S.** (2006). A Catalogue of the Effector Secretome of Plant Pathogenic Oomycetes.
1135 Annual Review of Phytopathology **44:** 41-60.
1136 **Kankanala, P., Czymmek, K., and Valent, B.** (2007). Roles for rice membrane dynamics and
1137 plasmodesmata during biotrophic invasion by the blast fungus. Plant Cell **19:** 706-
1138 724.
1139 **Kawahara, Y., Oono, Y., Kanamori, H., Matsumoto, T., Itoh, T., and Minami, E.** (2012).
1140 Simultaneous RNA-seq analysis of a mixed transcriptome of rice and blast fungus
1141 interaction. PLoS One **7:** e49423.
1142 **Kershaw, M.J., Basiewicz, M., Soanes, D.M., Yan, X., Ryder, L.S., Csukai, M., Oses-Ruiz, M.,**
1143 **Valent, B., and Talbot, N.J.** (2019). Conidial Morphogenesis and Septin-Mediated
1144 Plant Infection Require Smo1, a Ras GTPase-Activating Protein in Magnaporthe
1145 oryzae. Genetics **211:** 151-167.
1146 **Khang, C.H., Berruyer, R., Giraldo, M.C., Kankanala, P., Park, S.Y., Czymmek, K., Kang, S.,**
1147 **and Valent, B.** (2010). Translocation of Magnaporthe oryzae effectors into rice cells
1148 and their subsequent cell-to-cell movement. Plant Cell **22:** 1388-1403.
1149 **Kim, S., Park, S.Y., Kim, K.S., Rho, H.S., Chi, M.H., Choi, J., Park, J., Kong, S., Park, J., Goh, J.,**
1150 **and Lee, Y.H.** (2009). Homeobox transcription factors are required for conidiation
1151 and appressorium development in the rice blast fungus Magnaporthe oryzae. PLoS
1152 Genet **5:** e1000757.
1153 **Kim, S., Kim, C.Y., Park, S.Y., Kim, K.T., Jeon, J., Chung, H., Choi, G., Kwon, S., Choi, J., Jeon,**
1154 **J., Jeon, J.S., Khang, C.H., Kang, S., and Lee, Y.H.** (2020). Two nuclear effectors of the
1155 rice blast fungus modulate host immunity via transcriptional reprogramming. Nat
1156 Commun **11:** 5845.
1157 **Kleemann, J., Rincon-Rivera, L.J., Takahara, H., Neumann, U., Ver Loren van Themaat, E.,**
1158 **van der Does, H.C., Hacquard, S., Stuber, K., Will, I., Schmalenbach, W., Schmelzer,**
1159 **E., and O'Connell, R.J.** (2012). Sequential delivery of host-induced virulence effectors
1160 by appressoria and intracellular hyphae of the phytopathogen Colletotrichum
1161 higginsianum. PLoS Pathog **8:** e1002643.
1162 **Kristianingsih, R., and MacLean, D.** (2021). Accurate plant pathogen effector protein
1163 classification ab initio with deepredeff: an ensemble of convolutional neural
1164 networks. BMC Bioinformatics **22:** 372.
1165 **Kurup, S., Runions, J., Kohler, U., Laplaze, L., Hodge, S., and Haseloff, J.** (2005). Marking cell
1166 lineages in living tissues. Plant J **42:** 444-453.

1167 **Langfelder, P., and Horvath, S.** (2008). WGCNA: an R package for weighted correlation
1168 network analysis. BMC Bioinformatics **9:** 559.
1169 **Lanver, D., Muller, A.N., Happel, P., Schweizer, G., Haas, F.B., Franitza, M., Pellegrin, C.,**
1170 **Reissmann, S., Altmuller, J., Rensing, S.A., and Kahmann, R.** (2018). The Biotrophic
1171 Development of Ustilago maydis Studied by RNA-Seq Analysis. Plant Cell **30:** 300-
1172 323.
1173 **Latorre, S.M., Were, V.M., Foster, A.J., Langner, T., Malmgren, A., Harant, A., Asuke, S.,**
1174 **Reyes-Avila, S., Gupta, D.R., Jensen, C., Ma, W., Mahmud, N.U., Mehebub, M.S.,**
1175 **Mulenga, R.M., Muzahid, A.N.M., Paul, S.K., Rabby, S.M.F., Raha, A.A.M., Ryder, L.,**
1176 **Shrestha, R.-K., Sichilima, S., Soanes, D.M., Singh, P.K., Bentley, A.R., Saunders,**
1177 **D.G.O., Tosa, Y., Croll, D., Lamour, K.H., Islam, T., Tembo, B., Win, J., Talbot, N.J.,**
1178 **Burbano, H.A., and Kamoun, S.** (2022). A pandemic clonal lineage of the wheat blast
1179 fungus. bioRxiv. DOI 10.1101/2022.06.06.494979.
1180 **Lindsay, R.J., Kershaw, M.J., Pawlowska, B.J., Talbot, N.J., and Gudelj, I.** (2016). Harbouring
1181 public good mutants within a pathogen population can increase both fitness and
1182 virulence. eLife **5:** e18678.
1183 **Liu, S., and Dean, R.A.** (1997). G protein alpha subunit genes control growth, development,
1184 and pathogenicity of Magnaporthe grisea. Mol Plant Microbe Interact **10:** 1075-
1185 1086.
1186 **Liu, W., Zhou, X., Li, G., Li, L., Kong, L., Wang, C., Zhang, H., and Xu, J.R.** (2011). Multiple
1187 plant surface signals are sensed by different mechanisms in the rice blast fungus for
1188 appressorium formation. PLoS Pathog **7:** e1001261.
1189 **Liu, X., and Zhang, Z.** (2021). A double-edged sword: reactive oxygen species (ROS) during
1190 the rice blast fungus and host interaction. FEBS J.
1191 **Liu, X.-H., Chen, S.-M., Gao, H.-M., Ning, G.-A., Shi, H.-B., Wang, Y., Dong, B., Qi, Y.-Y.,**
1192 **Zhang, D.-M., Lu, G.-D., Wang, Z.-H., Zhou, J., and Lin, F.-C.** (2015). The small
1193 GTPase MoYpt7 is required for membrane fusion in autophagy and pathogenicity of
1194 Magnaporthe oryzae. Environmental Microbiology **17:** 4495-4510.
1195 **Lo Presti, L., Lanver, D., Schweizer, G., Tanaka, S., Liang, L., Tollot, M., Zuccaro, A.,**
1196 **Reissmann, S., and Kahmann, R.** (2015). Fungal Effectors and Plant Susceptibility.
1197 Annual Review of Plant Biology **66:** 513-545.
1198 **Maqbool, A., Saitoh, H., Franceschetti, M., Stevenson, C.E., Uemura, A., Kanzaki, H.,**
1199 **Kamoun, S., Terauchi, R., and Banfield, M.J.** (2015). Structural basis of pathogen
1200 recognition by an integrated HMA domain in a plant NLR immune receptor. Elife **4**.
1201 **Marroquin-Guzman, M., Hartline, D., Wright, J.D., Elowsky, C., Bourret, T.J., and Wilson,**
1202 **R.A.** (2017). The Magnaporthe oryzae nitrooxidative stress response suppresses rice
1203 innate immunity during blast disease. Nat Microbiol **2:** 17054.
1204 **Mentlak, T.A., Kombrink, A., Shinya, T., Ryder, L.S., Otomo, I., Saitoh, H., Terauchi, R.,**
1205 **Nishizawa, Y., Shibuya, N., Thomma, B.P., and Talbot, N.J.** (2012). Effector-
1206 mediated suppression of chitin-triggered immunity by magnaporthe oryzae is
1207 necessary for rice blast disease. Plant Cell **24:** 322-335.
1208 **Mitchell, T.K., and Dean, R.A.** (1995). The cAMP-dependent protein kinase catalytic subunit
1209 is required for appressorium formation and pathogenesis by the rice blast pathogen
1210 Magnaporthe grisea. Plant Cell **7:** 1869-1878.
1211 **Mogga, V., Delventhal, R., Weidenbach, D., Langer, S., Bertram, P.M., Andresen, K.,**
1212 **Thines, E., Kroj, T., and Schaffrath, U.** (2016). Magnaporthe oryzae effectors

1213 MoHEG13 and MoHEG16 interfere with host infection and MoHEG13 counteracts
1214 cell death caused by Magnaporthe-NLPs in tobacco. Plant Cell Rep **35:** 1169-1185.
1215 **Morgan, W., and Kamoun, S.** (2007). RXLR effectors of plant pathogenic oomycetes. Curr
1216 Opin Microbiol **10:** 332-338.
1217 **Mosquera, G., Giraldo, M.C., Khang, C.H., Coughlan, S., and Valent, B.** (2009). Interaction
1218 transcriptome analysis identifies Magnaporthe oryzae BAS1-4 as Biotrophy-
1219 associated secreted proteins in rice blast disease. Plant Cell **21:** 1273-1290.
1220 **Nishimura, T., Mochizuki, S., Ishii-Minami, N., Fujisawa, Y., Kawahara, Y., Yoshida, Y.,**
1221 **Okada, K., Ando, S., Matsumura, H., Terauchi, R., Minami, E., and Nishizawa, Y.**
1222 (2016). Magnaporthe oryzae Glycine-Rich Secretion Protein, Rbf1 Critically
1223 Participates in Pathogenicity through the Focal Formation of the Biotrophic
1224 Interfacial Complex. PLoS Pathog **12:** e1005921.
1225 **Oldenburg, K.R., Vo, K.T., Michaelis, S., and Paddon, C.** (1997). Recombination-mediated
1226 PCR-directed plasmid construction in vivo in yeast. Nucleic Acids Res **25:** 451-452.
1227 **Oses-Ruiz, M., Cruz-Mireles, N., Martin-Urdiroz, M., Soanes, D.M., Eseola, A.B., Tang, B.,**
1228 **Derbyshire, P., Nielsen, M., Cheema, J., Were, V., Eisermann, I., Kershaw, M.J., Yan,**
1229 **X., Valdovinos-Ponce, G., Molinari, C., Littlejohn, G.R., Valent, B., Menke, F.L.H.,**
1230 **and Talbot, N.J.** (2021). Appressorium-mediated plant infection by Magnaporthe
1231 oryzae is regulated by a Pmk1-dependent hierarchical transcriptional network. Nat
1232 Microbiol **6:** 1383-1397.
1233 **Park, C.H., Chen, S., Shirsekar, G., Zhou, B., Khang, C.H., Songkumarn, P., Afzal, A.J., Ning,**
1234 **Y., Wang, R., Bellizzi, M., Valent, B., and Wang, G.L.** (2012). The Magnaporthe
1235 oryzae effector AvrPiz-t targets the RING E3 ubiquitin ligase APIP6 to suppress
1236 pathogen-associated molecular pattern-triggered immunity in rice. Plant Cell **24:**
1237 4748-4762.
1238 **Park, G., Xue, C., Zheng, L., Lam, S., and Xu, J.-R.** (2002). MST12 Regulates Infectious
1239 Growth But Not Appressorium Formation in the Rice Blast Fungus Magnaporthe
1240 grisea. Mol Plant Microbe Interact **15:** 183-192.
1241 **Park, G., Xue, C., Zhao, X., Kim, Y., Orbach, M., and Xu, J.R.** (2006). Multiple upstream
1242 signals converge on the adaptor protein Mst50 in Magnaporthe grisea. Plant Cell **18:**
1243 2822-2835.
1244 **Park, S.Y., Choi, J., Lim, S.E., Lee, G.W., Park, J., Kim, Y., Kong, S., Kim, S.R., Rho, H.S., Jeon,**
1245 **J., Chi, M.H., Kim, S., Khang, C.H., Kang, S., and Lee, Y.H.** (2013). Global expression
1246 profiling of transcription factor genes provides new insights into pathogenicity and
1247 stress responses in the rice blast fungus. PLoS Pathog **9:** e1003350.
1248 **Parker, D., Beckmann, M., Zubair, H., Enot, D.P., Caracuel-Rios, Z., Overy, D.P., Snowdon,**
1249 **S., Talbot, N.J., and Draper, J.** (2009). Metabolomic analysis reveals a common
1250 pattern of metabolic re-programming during invasion of three host plant species by
1251 Magnaporthe grisea. Plant J **59:** 723-737.
1252 **Patkar, R.N., Benke, P.I., Qu, Z., Chen, Y.Y., Yang, F., Swarup, S., and Naqvi, N.I.** (2015). A
1253 fungal monooxygenase-derived jasmonate attenuates host innate immunity. Nat
1254 Chem Biol **11:** 733-740.
1255 **Pimentel, H., Bray, N.L., Puente, S., Melsted, P., and Pachter, L.** (2017). Differential analysis
1256 of RNA-seq incorporating quantification uncertainty. Nat Methods **14:** 687-690.
1257 **Poloni, N.M., Carvalho, G., Vicentini, S., Dorigan, A., Maciel, J.L., McDonald, B.A., Moreira,**
1258 **S., Hawkins, N., Fraaije, B.A., Kelly, D.E., Kelly, S.L., and Ceresini, P.C.** (2020).

1259 Widespread distribution of resistance to triazole fungicides in Brazilian populations
1260 of the wheat blast pathogen. Plant Pathology **70:** 436-448.
1261 **Que, Y., Yue, X., Yang, N., Xu, Z., Tang, S., Wang, C., Lv, W., Xu, L., Talbot, N.J., and Wang,**
1262 **Z.** (2020). Leucine biosynthesis is required for infection-related morphogenesis and
1263 pathogenicity in the rice blast fungus Magnaporthe oryzae. Curr Genet **66:** 155-171.
1264 **Ross-Gillespie, A., Gardner, A., West, S.A., and Griffin, A.S.** (2007). Frequency dependence
1265 and cooperation: theory and a test with bacteria. Am Nat **170:** 331-342.
1266 **Rudd, J.J., Kanyuka, K., Hassani-Pak, K., Derbyshire, M., Andongabo, A., Devonshire, J.,**
1267 **Lysenko, A., Saqi, M., Desai, N.M., Powers, S.J., Hooper, J., Ambroso, L., Bharti, A.,**
1268 **Farmer, A., Hammond-Kosack, K.E., Dietrich, R.A., and Courbot, M.** (2015).
1269 Transcriptome and metabolite profiling of the infection cycle of Zymoseptoria tritici
1270 on wheat reveals a biphasic interaction with plant immunity involving differential
1271 pathogen chromosomal contributions and a variation on the hemibiotrophic lifestyle
1272 definition. Plant Physiol **167:** 1158-1185.
1273 **Ryder, L.S., Dagdas, Y.F., Kershaw, M.J., Venkataraman, C., Madzvamuse, A., Yan, X., Cruz-**
1274 **Mireles, N., Soanes, D.M., Oses-Ruiz, M., Styles, V., Sklenar, J., Menke, F.L.H., and**
1275 **Talbot, N.J.** (2019). A sensor kinase controls turgor-driven plant infection by the rice
1276 blast fungus. Nature **574:** 423-427.
1277 **Sakulkoo, W., Osés-Ruiz, M., Oliveira Garcia, E., Soanes, D.M., Littlejohn, G.R., Hacker, C.,**
1278 **Correia, A., Valent, B., and Talbot, N.J.** (2018). A single fungal MAP kinase controls
1279 plant cell-to-cell invasion by the rice blast fungus. Science **359:** 1399.
1280 **Sangappillai, V., and Nadarajah, K.** (2020). Fatty Acid Synthase Beta Dehydratase in the
1281 Lipid Biosynthesis Pathway Is Required for Conidiogenesis, Pigmentation and
1282 Appressorium Formation in Magnaporthe oryzae S6. Int J Mol Sci **21**.
1283 **Saunders, D.G., Aves, S.J., and Talbot, N.J.** (2010). Cell cycle-mediated regulation of plant
1284 infection by the rice blast fungus. Plant Cell **22:** 497-507.
1285 **Selin, C., de Kievit, T.R., Belmonte, M.F., and Fernando, W.G.** (2016). Elucidating the Role
1286 of Effectors in Plant-Fungal Interactions: Progress and Challenges. Front Microbiol **7:**
1287 600.
1288 **Seong, K., and Krasileva, K.V.** (2021a). Computational Structural Genomics Unravels
1289 Common Folds and Novel Families in the Secretome of Fungal Phytopathogen
1290 Magnaporthe oryzae. Mol Plant Microbe Interact **34:** 1267-1280.
1291 **Seong, K., and Krasileva, K.** (2021b). Computational structural genomics unravels common
1292 folds and predicted functions in the secretome of fungal phytopathogen
1293 Magnaporthe oryzae. zenodo. doi:10.5281/zenodo.5525101.
1294 **Sharpee, W., Oh, Y., Yi, M., Franck, W., Eyre, A., Okagaki, L.H., Valent, B., and Dean, R.A.**
1295 (2017). Identification and characterization of suppressors of plant cell death (SPD)
1296 effectors from Magnaporthe oryzae. Mol Plant Pathol **18:** 850-863.
1297 **Shimizu, M., Nakano, Y., Hirabuchi, A., Yoshino, K., Kobayashi, M., Yamamoto, K.,**
1298 **Terauchi, R., and Saitoh, H.** (2019). RNA-Seq of in planta-expressed Magnaporthe
1299 oryzae genes identifies MoSVP as a highly expressed gene required for pathogenicity
1300 at the initial stage of infection. Mol Plant Pathol **20:** 1682-1695.
1301 **Soanes, D.M., Chakrabarti, A., Paszkiewicz, K.H., Dawe, A.L., and Talbot, N.J.** (2012).
1302 Genome-wide transcriptional profiling of appressorium development by the rice
1303 blast fungus Magnaporthe oryzae. PLoS Pathog **8:** e1002514.

1304 **Sperschneider, J., and Dodds, P.N.** (2022). EffectorP 3.0: Prediction of Apoplastic and
1305 Cytoplasmic Effectors in Fungi and Oomycetes. Mol Plant Microbe Interact **35:** 146-
1306 156.
1307 **Stam, R., and McDonald, B.A.** (2018). When resistance gene pyramids are not durable-the
1308 role of pathogen diversity. Mol Plant Pathol **19:** 521-524.
1309 **Sun, G., Elowsky, C., Li, G., and Wilson, R.A.** (2018). TOR-autophagy branch signaling via
1310 Imp1 dictates plant-microbe biotrophic interface longevity. PLoS Genet **14:**
1311 e1007814.
1312 **Sweigard, J.A., Carroll, A.M., Farrall, L., Chumley, F.G., and Valent, B.** (1998). Magnaporthe
1313 grisea pathogenicity genes obtained through insertional mutagenesis. Mol Plant
1314 Microbe Interact **11:** 404-412.
1315 **Talbot, N.J., Ebbole, D.J., and Hamer, J.E.** (1993a). Identification and characterization of
1316 MPG1, a gene involved in pathogenicity from the rice blast fungus Magnaporthe
1317 grisea. The Plant cell **5:** 1575-1590.
1318 **Talbot, N.J., Salch, Y.P., Ma, M., and Hamer, J.E.** (1993b). Karyotypic Variation within Clonal
1319 Lineages of the Rice Blast Fungus, Magnaporthe grisea. Appl Environ Microbiol **59:**
1320 585-593.
1321 **Tang, W., Jiang, H., Zheng, Q., Chen, X., Wang, R., Yang, S., Zhao, G., Liu, J., Norvienyeku,**
1322 **J., and Wang, Z.** (2019). Isopropylmalate isomerase MoLeu1 orchestrates leucine
1323 biosynthesis, fungal development, and pathogenicity in Magnaporthe oryzae. Appl
1324 Microbiol Biotechnol **103:** 327-337.
1325 **Urashima., A.S., Igarashi., S., and Kato., H.** (1993). Host Range, Mating Type, and Fertility of
1326 Pyricularia grisea from Wheat in Brazil. Plant Disease **77:** 1211-1216.
1327 **Valent, B., Farrall, L., and Chumley, F.G.** (1991). Magnaporthe grisea genes for
1328 pathogenicity and virulence identified through a series of backcrosses. Genetics **127:**
1329 87-101.
1330 **Wang, G.-L., and Valent, B.** (2017). Durable resistance to rice blast. Science **355:** 906.
1331 **Wang, Z.D., Yan, N., Wang, Z.H., Zhang, X.H., Zhang, J.Z., Xue, H.M., Wang, L.X., Zhan, Q.,**
1332 **Xu, Y.P., and Guo, D.P.** (2017). RNA-seq analysis provides insight into
1333 reprogramming of culm development in Zizania latifolia induced by Ustilago
1334 esculenta. Plant Mol Biol **95:** 533-547.
1335 **Wilson, R.A., Gibson, R.P., Quispe, C.F., Littlechild, J.A., and Talbot, N.J.** (2010). An NADPH-
1336 dependent genetic switch regulates plant infection by the rice blast fungus. Proc Natl
1337 Acad Sci U S A **107:** 21902-21907.
1338 **Wingrove, E., Liu, Z.Z., Patel, K.D., Arnal-Estape, A., Cai, W.L., Melnick, M.A., Politi, K.,**
1339 **Monteiro, C., Zhu, L., Valiente, M., Kluger, H.M., Chiang, V.L., and Nguyen, D.X.**
1340 (2019). Transcriptomic Hallmarks of Tumor Plasticity and Stromal Interactions in
1341 Brain Metastasis. Cell Rep **27:** 1277-1292 e1277.
1342 **Wood, D.E., Lu, J., and Langmead, B.** (2019). Improved metagenomic analysis with Kraken
1343 2. Genome Biol **20:** 257.
1344 **Xu, J.-R., Staiger Christopher, J., and Hamer John, E.** (1998). Inactivation of the mitogen-
1345 activated protein kinase Mps1 from the rice blast fungus prevents penetration of
1346 host cells but allows activation of plant defense responses. Proceedings of the
1347 National Academy of Sciences **95:** 12713-12718.
1348 **Yamaguchi, I.** (2004). Overview on the Chemical Control of Rice Blast Disease. In Rice Blast:
1349 Interaction with Rice and Control, S. Kawasaki, ed (Dordrecht: Springer Netherlands),
1350 pp. 1-13.

1351 **Yan, X., Li, Y., Yue, X., Wang, C., Que, Y., Kong, D., Ma, Z., Talbot, N.J., and Wang, Z.** (2011).
1352 Two novel transcriptional regulators are essential for infection-related
1353 morphogenesis and pathogenicity of the rice blast fungus Magnaporthe oryzae. PLoS
1354 Pathog **7:** e1002385.
1355 **Yan, X., Que, Y., Wang, H., Wang, C., Li, Y., Yue, X., Ma, Z., Talbot, N.J., and Wang, Z.**
1356 (2013). The MET13 methylenetetrahydrofolate reductase gene is essential for
1357 infection-related morphogenesis in the rice blast fungus Magnaporthe oryzae. PLoS
1358 One **8:** e76914.
1359 **Yang, J., Liu, M., Liu, X., Yin, Z., Sun, Y., Zhang, H., Zheng, X., Wang, P., and Zhang, Z.**
1360 (2018). Heat-Shock Proteins MoSsb1, MoSsz1, and MoZuo1 Attenuate MoMkk1-
1361 Mediated Cell-Wall Integrity Signaling and Are Important for Growth and
1362 Pathogenicity of Magnaporthe oryzae. Mol Plant Microbe Interact **31:** 1211-1221.
1363 **Yoshida, K., Saitoh, H., Fujisawa, S., Kanzaki, H., Matsumura, H., Yoshida, K., Tosa, Y.,**
1364 **Chuma, I., Takano, Y., Win, J., Kamoun, S., and Terauchi, R.** (2009). Association
1365 genetics reveals three novel avirulence genes from the rice blast fungal pathogen
1366 Magnaporthe oryzae. Plant Cell **21:** 1573-1591.
1367 **Yu, G., Wang, L.G., Han, Y., and He, Q.Y.** (2012). clusterProfiler: an R package for comparing
1368 biological themes among gene clusters. OMICS **16:** 284-287.
1369 **Yue, X., Que, Y., Xu, L., Deng, S., Peng, Y., Talbot, N.J., and Wang, Z.** (2016). ZNF1 Encodes a
1370 Putative C2H2 Zinc-Finger Protein Essential for Appressorium Differentiation by the
1371 Rice Blast Fungus Magnaporthe oryzae. Mol Plant Microbe Interact **29:** 22-35.
1372 **Zeng, F.S., Menardo, F., Xue, M.F., Zhang, X.J., Gong, S.J., Yang, L.J., Shi, W.Q., and Yu, D.Z.**
1373 (2017). Transcriptome Analyses Shed New Insights into Primary Metabolism and
1374 Regulation of Blumeria graminis f. sp. tritici during Conidiation. Front Plant Sci **8:**
1375 1146.
1376 **Zhai, K., Liang, D., Li, H., Jiao, F., Yan, B., Liu, J., Lei, Z., Huang, L., Gong, X., Wang, X., Miao,**
1377 **J., Wang, Y., Liu, J.Y., Zhang, L., Wang, E., Deng, Y., Wen, C.K., Guo, H., Han, B., and**
1378 **He, Z.** (2022). NLRs guard metabolism to coordinate pattern- and effector-triggered
1379 immunity. Nature **601:** 245-251.
1380 **Zhang, B., and Horvath, S.** (2005). A general framework for weighted gene co-expression
1381 network analysis. Stat Appl Genet Mol Biol **4:** Article17.
1382 **Zhang, H., Liu, K., Zhang, X., Song, W., Zhao, Q., Dong, Y., Guo, M., Zheng, X., and Zhang, Z.**
1383 (2010). A two-component histidine kinase, MoSLN1, is required for cell wall integrity
1384 and pathogenicity of the rice blast fungus, Magnaporthe oryzae. Curr Genet **56:** 517-
1385 528.
1386 **Zhang, H., Tang, W., Liu, K., Huang, Q., Zhang, X., Yan, X., Chen, Y., Wang, J., Qi, Z., Wang,**
1387 **Z., Zheng, X., Wang, P., and Zhang, Z.** (2011). Eight RGS and RGS-like proteins
1388 orchestrate growth, differentiation, and pathogenicity of Magnaporthe oryzae. PLoS
1389 Pathog **7:** e1002450.
1390 **Zhang, N., Luo, J., Rossman, A.Y., Aoki, T., Chuma, I., Crous, P.W., Dean, R., de Vries, R.P.,**
1391 **Donofrio, N., Hyde, K.D., Lebrun, M.H., Talbot, N.J., Tharreau, D., Tosa, Y., Valent,**
1392 **B., Wang, Z., and Xu, J.R.** (2016). Generic names in Magnaporthales. IMA Fungus **7:**
1393 155-159.
1394 **Zhu, Xu-dong, Shen, Ying, Henri, Adreit, Julien, Frouin, R., Didier, and Harreau.** (2004).
1395 Resistance Evaluation of Some Chinese Leading Rice Maintainer, Restorer lines and
1396 Their Hybrids to Magnaporthe grisea. Rice Science**:** 101-105.

1397

The transcriptional landscape of plant infection by the rice blast fungus *Magnaporthe oryzae* reveals distinct families of temporally co-regulated and structurally conserved effectors

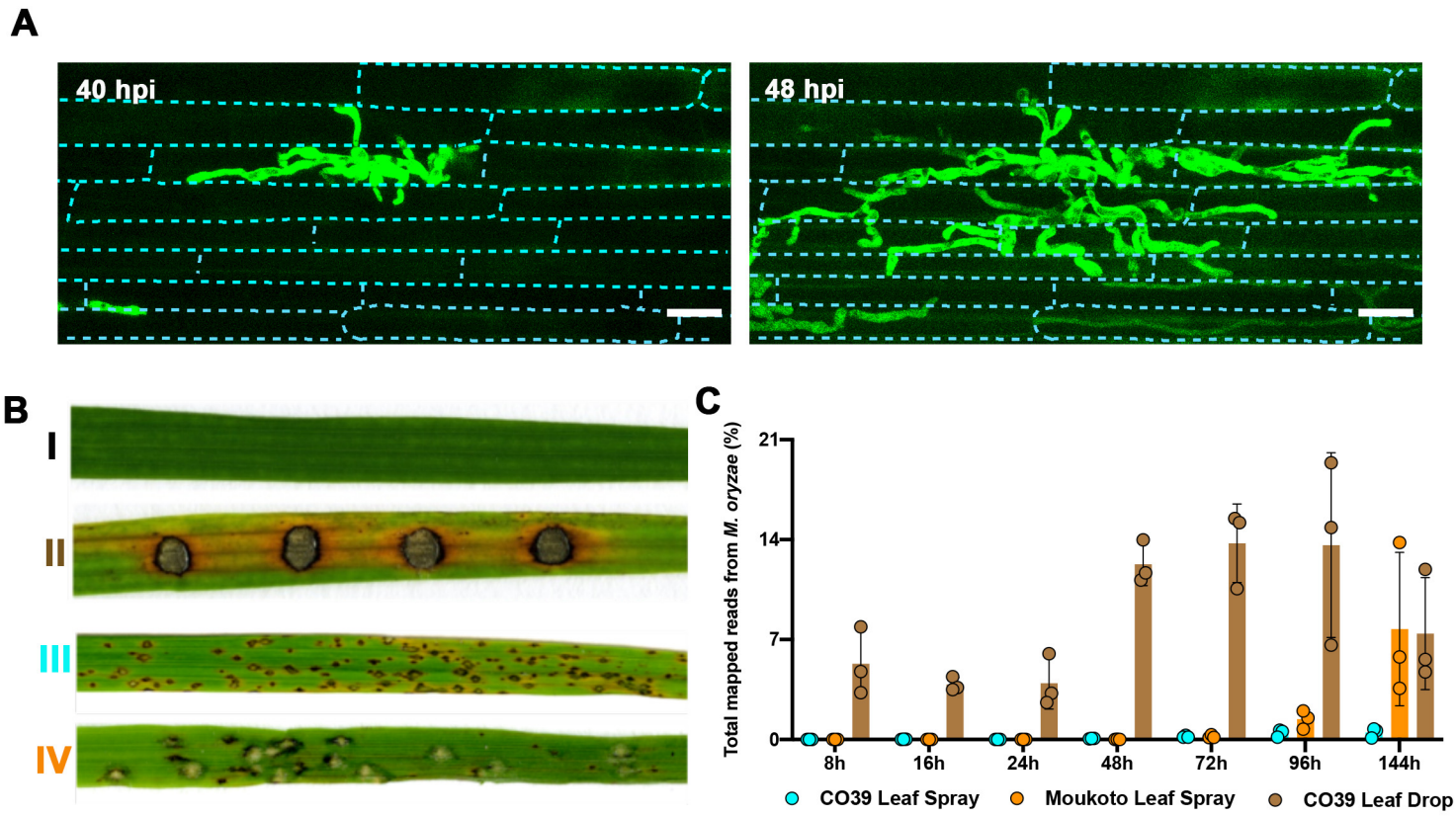

Figure 1. Transcriptional profile analysis of a time course of plant infection by the rice blast fungus *M. oryzae.*

Rice infections were carried out using two distinct inoculation methods and two cultivars differing in relative susceptibility to blast. **(A)** Micrographs of rice tissue of cultivar CO-39 inoculated with *M. oryzae* Guy11 expressing free GFP driven by the constitutive promoter RP27 at 40 h post inoculation (hpi) and 48 hpi to show progression of tissue invasion. Individual plant cells are outlined by the cyan dotted line. Scale bars = 20 µm. **(B)** Comparison of rice blast disease symptoms 6 days post-inoculation using either leaf drop infection or spray infection on rice cultivars with varying host susceptibility. I: moderately susceptible rice cultivar CO-39 inoculated with water control; II: leaf drop infection of rice CO-39 with Guy11; III: spray infection of rice CO-39 with Guy11; IV: spray infection of highly susceptible rice cultivar Moukoto with Guy11. **(C)** Graph depicting proportion of fungal transcripts in the plant and pathogen mixed transcriptome (CO-39 Leaf Spray, Moukoto Leaf Spray and CO-39 Leaf Drop correspond to inoculation methods).

Figure 1

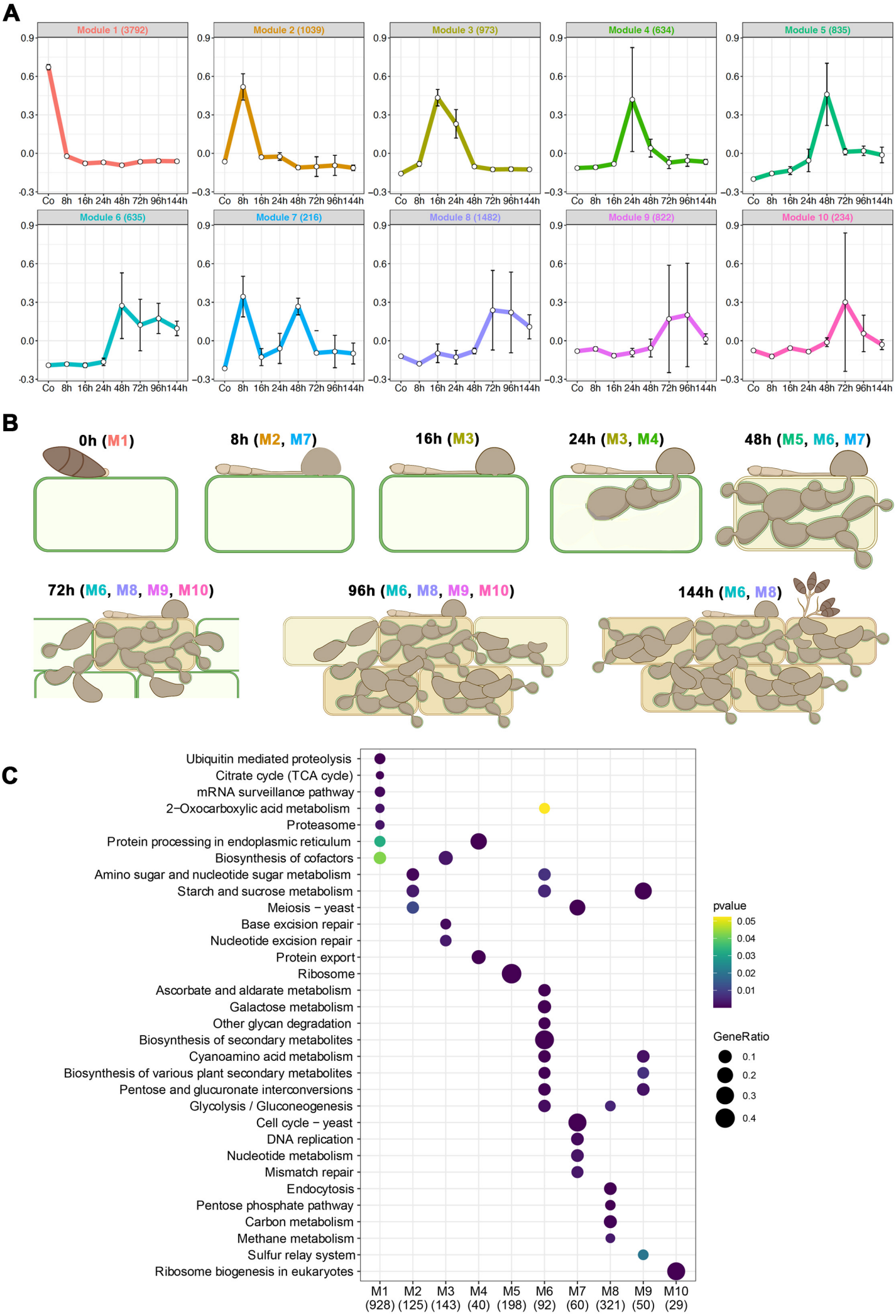
A
Module 1 (3792)
Module 2 (1039)
Module 3 (973)
Module 4 (634)
Module 5 (835)
Module 6 (635)
Module 7 (216)
Module 8 (1482)
Module 9 (822)
Module 10 (234)
0.9
0.6
0.3
0.0
-0.3
Co 8h 16h 24h 48h 72h 96h 144h
B
0h (M1)
8h (M2, M7)
16h (M3)
24h (M3, M4)
48h (M5, M6, M7)
72h (M6, M8, M9, M10)
96h (M6, M8, M9, M10)
144h (M6, M8)
C
Ubiquitin mediated proteolysis
Citrate cycle (TCA cycle)
mRNA surveillance pathway
2−Oxocarboxylic acid metabolism
Proteasome
Protein processing in endoplasmic reticulum
Biosynthesis of cofactors
Amino sugar and nucleotide sugar metabolism
Starch and sucrose metabolism
Meiosis − yeast
Base excision repair
Nucleotide excision repair
Protein export
Ribosome
Ascorbate and aldarate metabolism
Galactose metabolism
Other glycan degradation
Biosynthesis of secondary metabolites
Cyanoamino acid metabolism
Biosynthesis of various plant secondary metabolites
Pentose and glucuronate interconversions
Glycolysis / Gluconeogenesis
Cell cycle − yeast
DNA replication
Nucleotide metabolism
Mismatch repair
Endocytosis
Pentose phosphate pathway
Carbon metabolism
Methane metabolism
Sulfur relay system
Ribosome biogenesis in eukaryotes
M1 (928)
M2 (125)
M3 (143)
M4 (40)
M5 (198)
M6 (92)
M7 (60)
M8 (321)
M9 (50)
M10 (29)
pvalue
0.05
0.04
0.03
0.02
0.01
GeneRatio
0.1
0.2
0.3
0.4

Figure 2

Figure 2. Temporal co-expression analysis reveals 10 modules of pathogen gene expression during rice blast infection.

Analysis of co-expressed pathogen genes during rice blast disease development. **(A)** Weighted correlation network analysis (WGCNA) identified 10 co-expressed modules during a time-course of infection-related-development and plant infection (Modules 1-10). The representative eigengene is shown for each module **(B)** Schematic representation of each stage of rice blast disease development and corresponding WGCNA co-expression modules. Blast-infected rice tissue samples were collected at 0 hpi, 8 hpi, 16 hpi, 24 hpi, 48 hpi, 72 hpi, 96 hpi and 144 hpi. **(C)** KEGG enrichment analysis of genes in each WCGNA module using clusterProfiler reveals over-represented physiological functions during blast disease development.

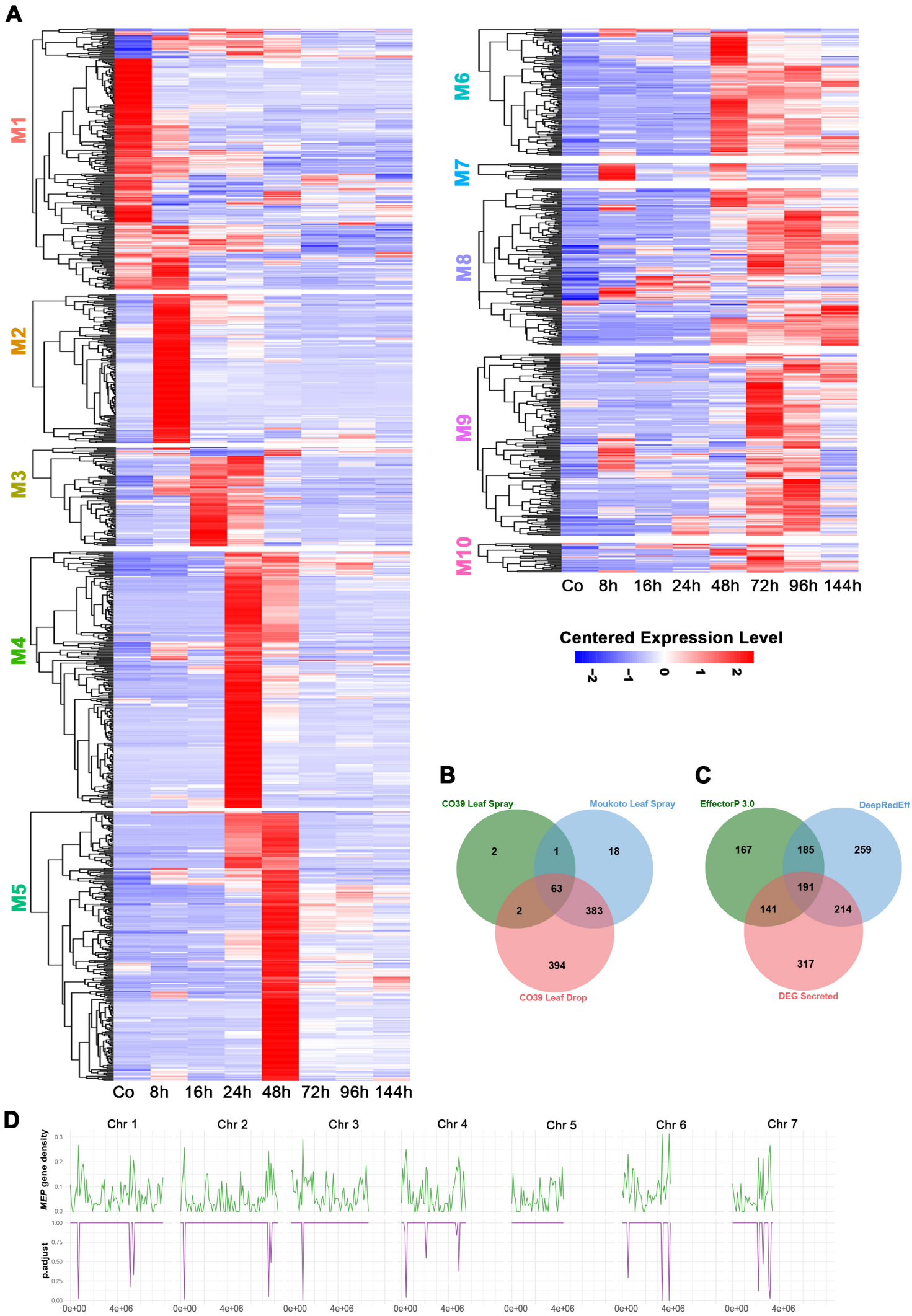
A
M1
M2
M3
M4
M5
M6
M7
M8
M9
M10
Co 8h 16h 24h 48h 72h 96h 144h
Centered Expression Level
-2 -1 0 1 2
B
CO39 Leaf Spray
Moukoto Leaf Spray
CO39 Leaf Drop
2
1
18
63
2
383
394
C
EffectorP 3.0
DeepRedEff
DEG Secreted
167
185
259
191
141
214
317
D
Chr 1
Chr 2
Chr 3
Chr 4
Chr 5
Chr 6
Chr 7
MEP gene density
p.adjust
0e+00
4e+06

Figure 3

Figure 3. Stage-specific temporal expression of the *M. oryzae* secretome during rice infection.

(A) Heat map showing the hierarchical clustering of pathogen genes encoding putatively secreted proteins from each WGCNA co-expression module. Distinct temporal patterns of secretome expression occur during biotrophic and necrotrophic development. Expression levels are shown relative to the mean expression TPM (transcript per kilobase million) value across all stages. **(B)** Venn diagram showing comparison of differentially expressed secreted protein-encoding genes from three different inoculation experiments (CO39 Leaf Spray, Moukoto Leaf Spray, and CO39 Leaf Drop Infections). In total 68 effector candidates were identified from the CO39 leaf spray infections, 467 effector candidates from Moukoto leaf spray inoculation, and 847 effector candidates from CO39 leaf drop infections. Although leaf drop-CO39 infections revealed expression of many more differentially expressed effector candidates, 20 effector candidates were revealed only in spray inoculation experiments. **(C)** Comparison of effector predictions of host-induced secreted proteins using EffectorP 3.0 and DeepRedEff algorithms with differentially expressed signal peptide containing genes (DEG Sec). **(D)** Enrichment analysis of *MEP* gene loci on *M. oryzae* chromosomes 1-7, encoding predicted secreted proteins. The number of *MEP* genes was compared to total gene number in 200kb windows across each chromosome. Phyper was used to compute the hypergeometric distribution and obtain P-values. (Johnson et al., 1992). The resulting graph in the bottom panel shows regions of each chromosome where there is significant over-representation of *MEP* gene loci.

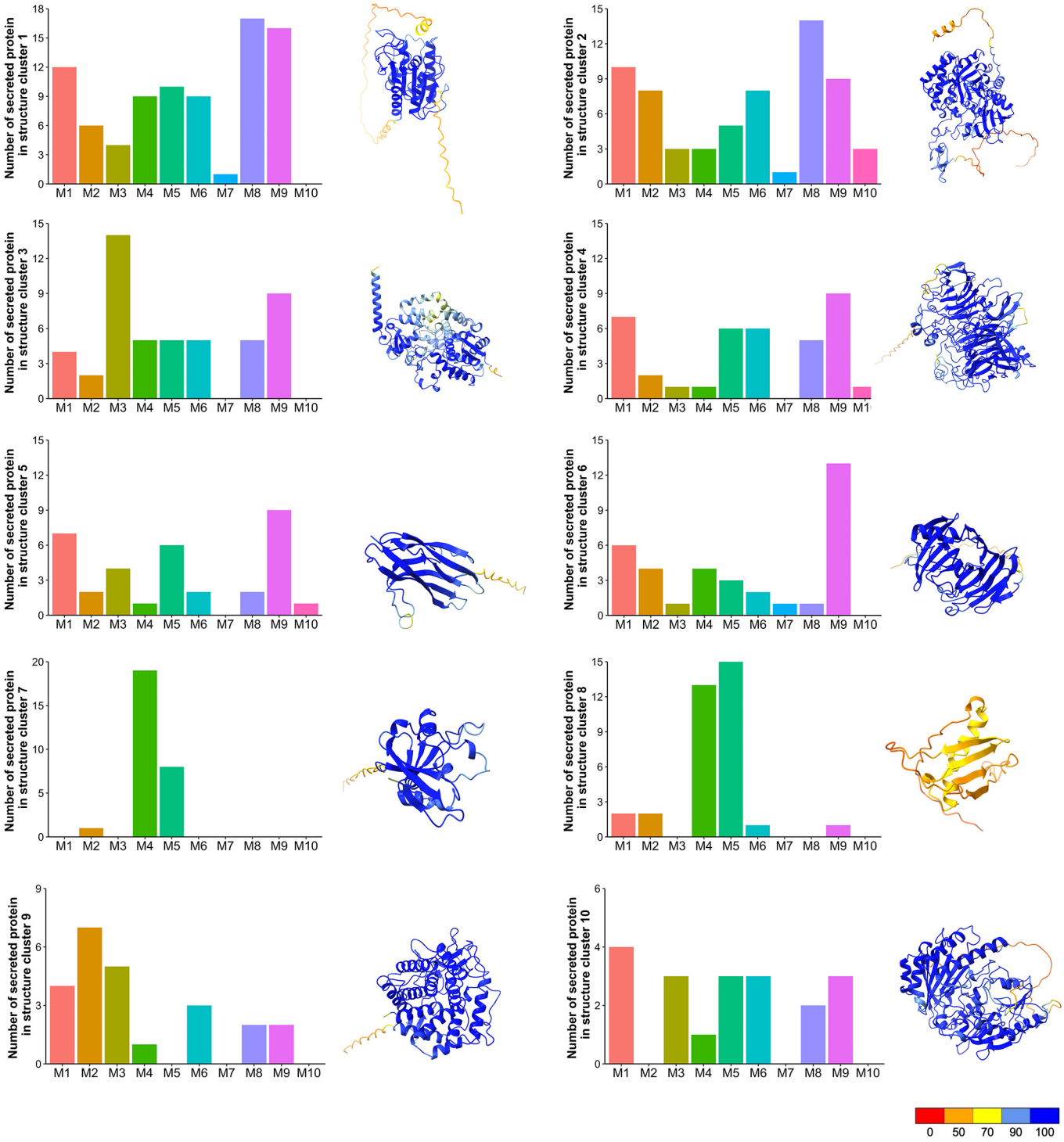
Number of secreted protein in structure cluster 1
Number of secreted protein in structure cluster 2
Number of secreted protein in structure cluster 3
Number of secreted protein in structure cluster 4
Number of secreted protein in structure cluster 5
Number of secreted protein in structure cluster 6
Number of secreted protein in structure cluster 7
Number of secreted protein in structure cluster 8
Number of secreted protein in structure cluster 9
Number of secreted protein in structure cluster 10
M1 M2 M3 M4 M5 M6 M7 M8 M9 M10
0 50 70 90 100

Figure 4

Figure 4. Structurally conserved *M. oryzae* effectors are temporally co-expressed during biotrophic invasive growth.

AlphaFold and ChimeraX platforms were used to predict the three-dimensional structures of predicted secreted proteins of *M.oryzae.* Structure clusters were then analysed against each WGCNA module. Bar charts represent the number of predicted secreted proteins identified in each predicted structure cluster (clusters 1-10), that are classified within each WGCNA co-expression module during pathogenesis. Ribbon diagrams show a representative predicted protein structure for each *M. oryzae* structure cluster. These are MGG_09840, which contains a cutinase domain for structure cluster 1; MGG_04534 contains a chitin recognition protein domain for structure cluster 2; MGG_07497 contains a cytochrome P450 domain for structure cluster 3; MGG_05785 (INV1/BAS113) contains a glycosyl hydrolase family 32 domain for structure cluster 4; MGG_02347 (Nis1) for structure cluster 5; MGG_08537 contains a glycosyl hydrolase family 12 domain for structure cluster 6; for structure cluster; MGG_00230 is a predicted ADP-ribose transferase containing a heat-labile enterotoxin alpha chain domain for structure cluster 7; MGG_12426 is a predicted MAX effector and homologue of AvrPib for structure cluster 8; MGG_04305 contains a glycosyl hydrolase family 88 domain for structure cluster 9; MGG_00276 contains berberine and berberine-like domains for structure cluster 10. Protein structures were predicted by AlphaFold. and ChimeraX was used to visualise the protein structure using PDB files generated by AlphaFold. The command “color bfactor palette alphafold” was used to color-code the confidence for each prediction (scale from red = 0% confident - blue = 100% confident). Genes encoding proteins in structure clusters 7 and 8 are over-represented in WGCNA M4 and M5.

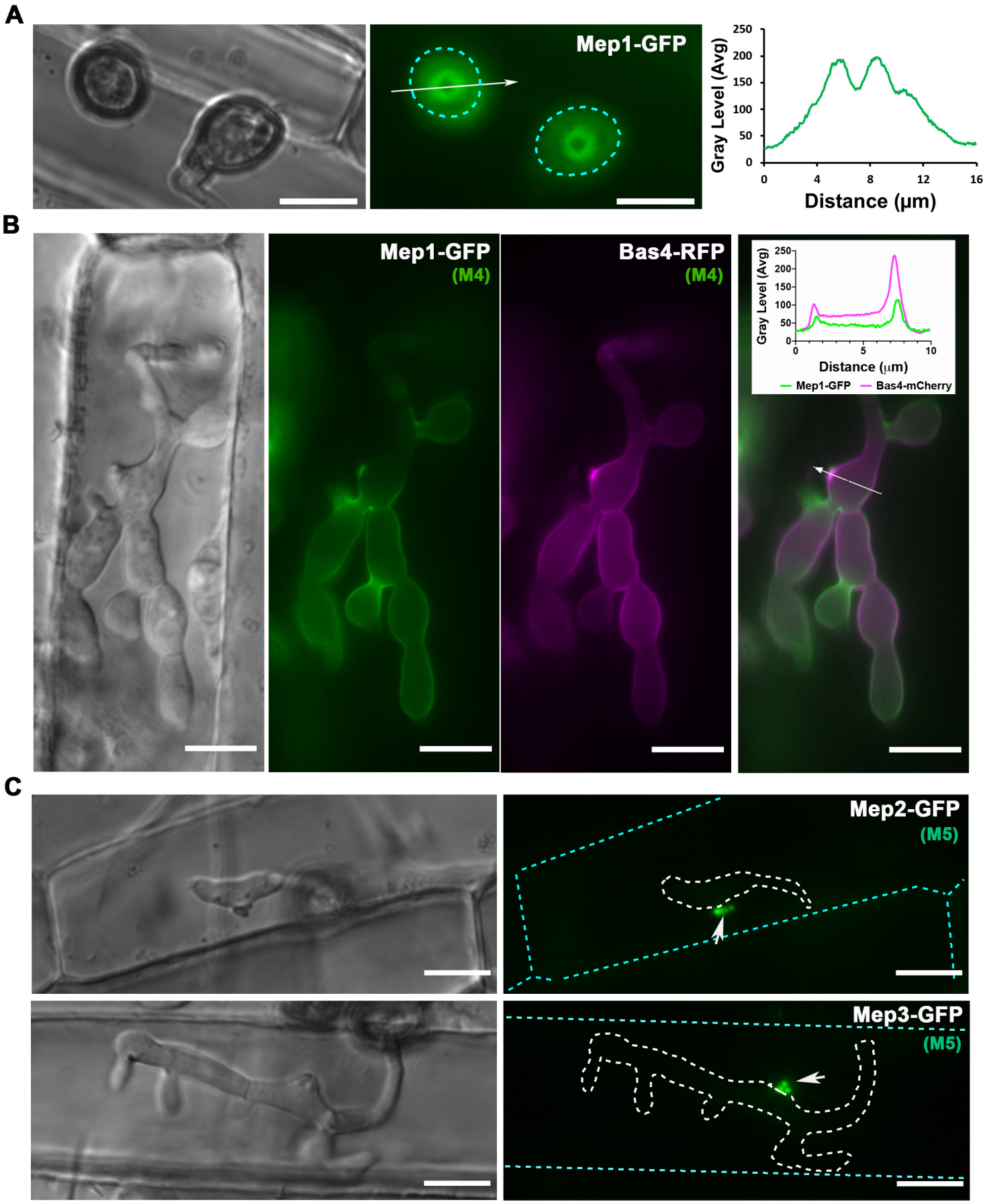
A
Mep1-GFP
Gray Level (Avg)
250
200
150
100
50
0
0
4
8
12
16
Distance (µm)
B
Mep1-GFP
(M4)
Bas4-RFP
(M4)
Gray Level (Avg)
250
200
150
100
50
0
0
5
10
Distance (µm)
Mep1-GFP
Bas4-mCherry
C
Mep2-GFP
(M5)
Mep3-GFP
(M5)

Figure 5

Figure 5. Live-cell imaging of Mep candidates during plant infection reveals spatial localisation of effectors during appressorium penetration and invasive growth.

(A) Micrographs showing the M4 effector Mep1-GFP localising in a ring confirmation at the appressorium pore at the leaf surface in *M. oryzae* Guy11. Conidial suspensions at 5 x10^4 mL^{-1} were inoculated onto rice leaf sheath and images captured at 24 hpi. The periphery of the appressorium is indicated by a cyan dotted line. Line scans show Mep1-GFP fluorescence in a transverse section of the appressorium. Scale bars = 10 µm. **(B)** Conidia were harvested from a *M. oryzae* transformant expressing Mep1-GFP and Bas4-RFP gene fusions and inoculated onto rice leaf sheath preparations. Images were captured at 28 hpi of invasive growth. Micrograph and linescan graphs show co-localization of Mep1-GFP and Bas4-RFP in invasive hyphae of the *M. oryzae* wild- type strain Guy11. Scale bars = 10 µm. **(C)** Micrographs showing localisation of representative M5 effector candidates Mep2-GFP and Mep3-GFP from the 32 selected Mep proteins (Supplemental Figure 9) during plant infection. Images were captured at 22 hpi- 24 hpi. Invasive hyphae are outlined by a white dotted line and individual plant cells indicated with a cyan dotted line. Arrow indicates localisation of both Mep2-GFP and Mep3-GFP at the biotrophic interfacial complex (BIC). Scale bars = 10 µm.

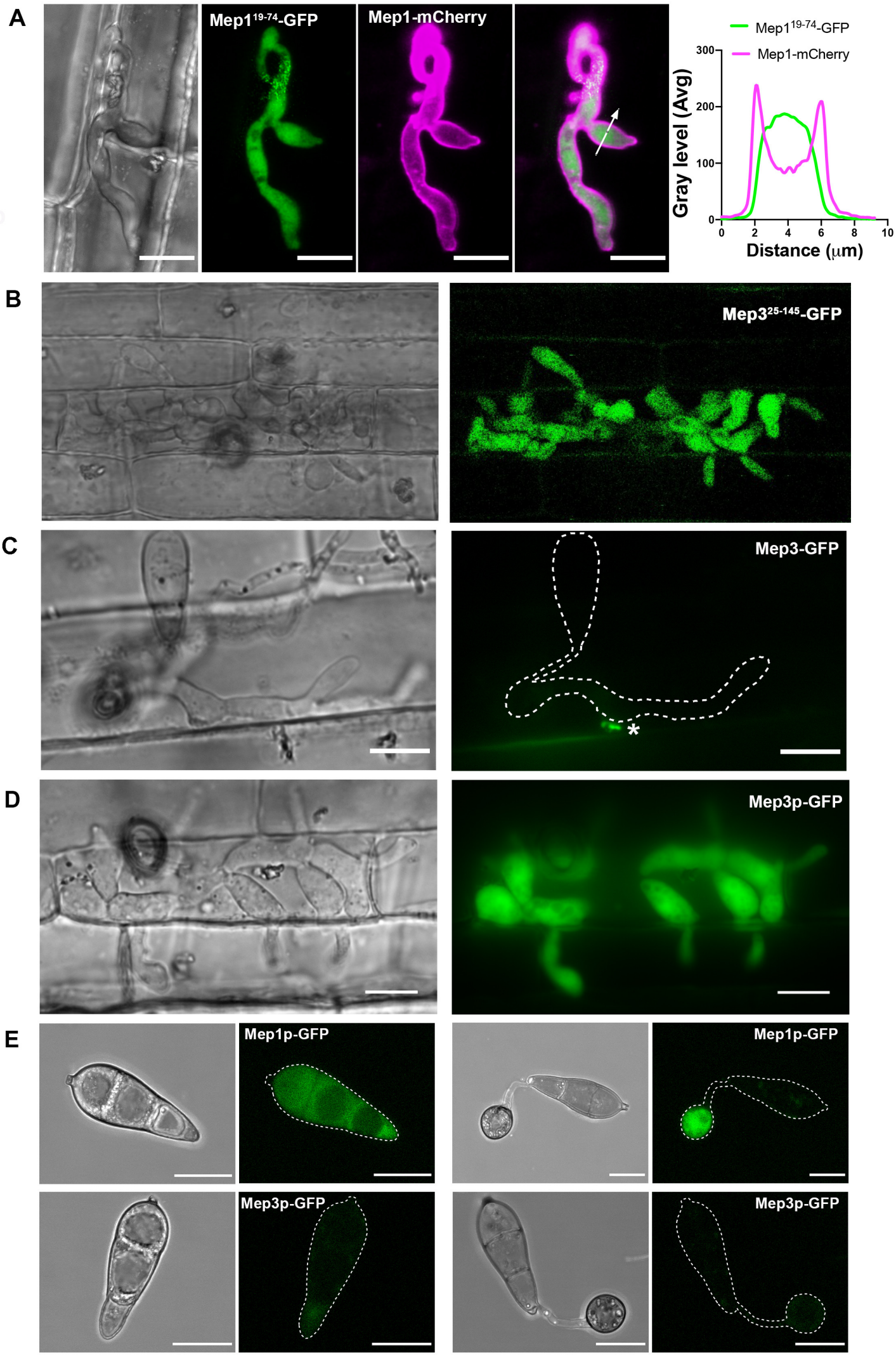
A
Mep1$^{19-74}$-GFP
Mep1-mCherry
Mep1$^{19-74}$-GFP
Mep1-mCherry
Gray level (Avg)
300
200
100
0
0
2
4
6
8
10
Distance (μm)
B
Mep3$^{25-145}$-GFP
C
Mep3-GFP
*
D
Mep3p-GFP
E
Mep1p-GFP
Mep1p-GFP
Mep3p-GFP
Mep3p-GFP

Figure 6

Figure 6. *MEP* genes are highly expressed in living plant tissue during plant infection.

(A) Conidia were harvested from a *M. oryzae* transformant expressing a Mep1$^{\Delta 19\text{-}74}$-GFP signal peptide deletion and a Mep1-RFP full length gene fusion and inoculated onto CO39 rice leaf sheath. Images were captured at 24 hpi of invasive growth. Micrograph and linescan graphs show that the Mep1 signal peptide is required for correct protein secretion. Scale bars = 10 µm. **(B)** Micrographs showing the rice plant infected by the *M.oryzae* wild-type strain Guy11 expressing a Mep3$^{\Delta 25\text{-}145}$-GFP signal peptide deletion. Green fluorescence was retained inside the invasive hyphae, while red fluorescence (false coloured to magenta) was exported to the apoplast. Images were captured at 24 hpi of invasive growth **(C)** Micrographs showing rice plant tissue infected by the *M. oryzae* wild-type strain Guy11 expressing full length *MEP3,* driven by its native promoter. Mep3-GFP could be observed as small puncta at the BIC. Images were captured at 24 hpi of invasive growth **(D)** Micrographs showing rice CO-39 infected with *M. oryzae* wild-type strain Guy11 expressing cytoplasmic GFP driven by the *MEP3* promoter. **(E)** Conidia were harvested from *M. oryzae* transformants expressing GFP driven by the promotor of Mep1p-GFP and Mep3p-GFP, respectively, and inoculated onto hydrophobic glass coverslips. Micrographs of Mep1p-GFP showed fluorescent signal in both the conidium and the appressorium, in contrast to Mep3p-GFP which displayed little signal. Appressorium formation was observed at 20 hpi. Scale bars = 10 µm.

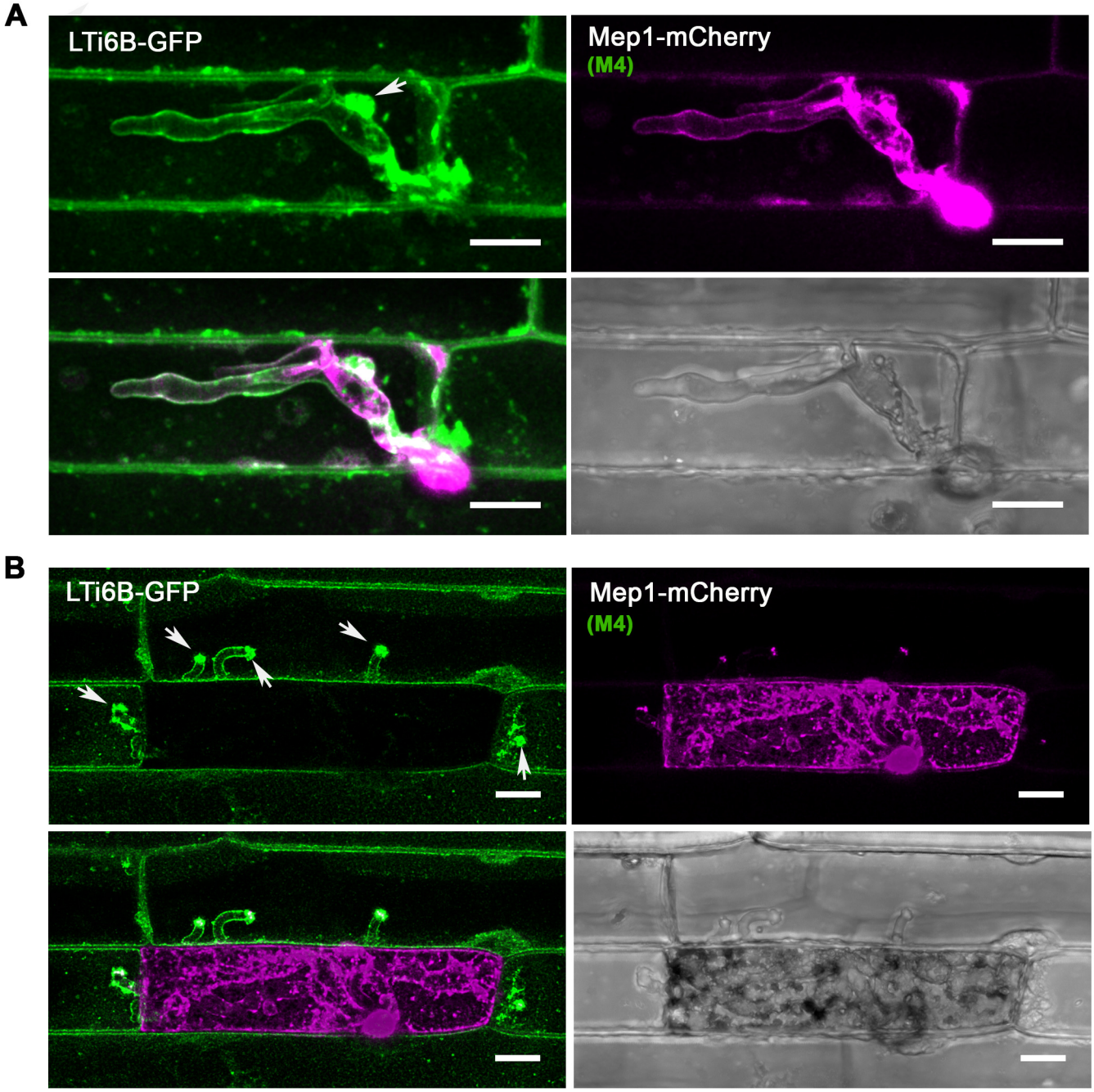

Figure 7. The rice plasma membrane is invaginated and accumulates at the Biotrophic Interfacial Complex (BIC) during plant infection.

Laser confocal micrographs of *M. oryzae* expressing Mep1-mCherry colonising epidermal leaf cells of a transgenic rice line expressing plasma membrane-localised LTi6B-GFP. Images were captured at 24 hpi **(A)** and 36 hpi **(B)**. The plant plasma membrane stays intact and invaginated at the early stages of plant infection. LTi6B fluorescence accumulates at the bright biotrophic interfacial complex, indicating the BIC is a plant membrane-rich structure. The fluorescence signal from secreted Mep1-mCherry is surrounded by the fluorescence signal of the rice cell plant plasma membrane marker LTi6B-GFP as the fungus invades new cells, but the initial epidermal cell occupied then loses viability and Mep1-mCherry fluorescence fills the rice cell. Scale bars = 10 um.

Figure 7

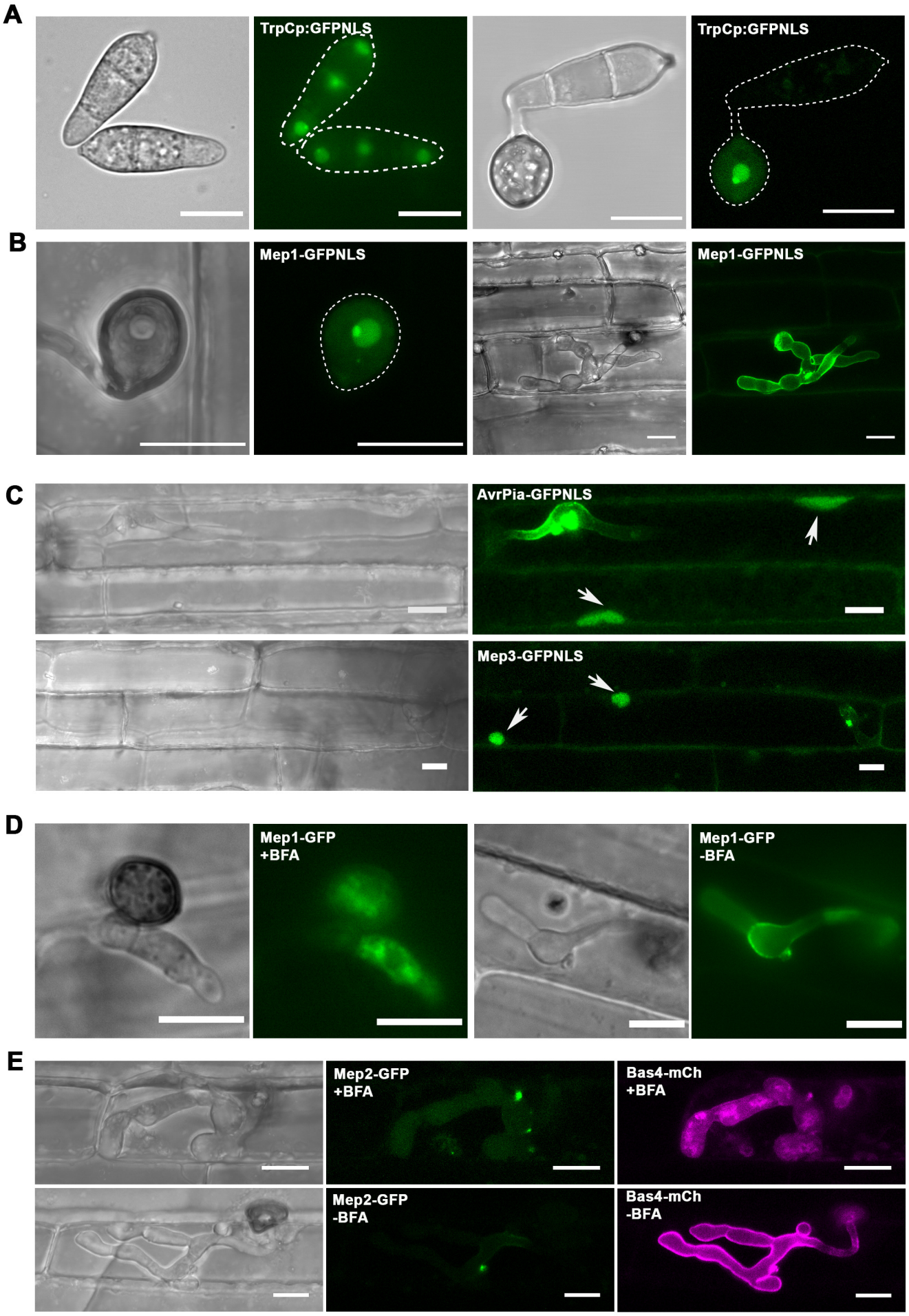
A
TrpCp:GFPNLS
TrpCp:GFPNLS
B
Mep1-GFPNLS
Mep1-GFPNLS
C
AvrPia-GFPNLS
Mep3-GFPNLS
D
Mep1-GFP
+BFA
Mep1-GFP
-BFA
E
Mep2-GFP
+BFA
Bas4-mCh
+BFA
Mep2-GFP
-BFA
Bas4-mCh
-BFA

Figure 8

Figure 8. Cytoplasmic Mep candidates, which accumulate at the BIC, are translocated into host cells.

(A) Cellular localisation of GFP with a nuclear localization signal (NLS) driven by the TrpC promoter in *M. oryzae*. The fluorescence signal in the nuclei and nucleoli of conidia and the appressorium. The outline of the fungus is depicted by a white dotted line. **(B)** Micrographs of Mep1-GFP^{NLS} inoculated onto rice leaf sheath and captured at 28 hpi. Fluorescence could be observed in the nucleus and nucleolus of the appressorium, but not in the fungus or plant cells. **(C)** Micrographs of AvrPia-GFP^{NLS} and BIC-accumulating Mep effector candidates showing delivery into both the invaded host cell and unoccupied neighbouring host cells. Arrows indicate plant nuclei. **(D)** Cellular localisation of Mep1-GFP in *M. oryzae* during biotrophic growth on epidermal rice cells. Brefeldin A (BFA) was applied at 20 hpi and 0.1% DMSO was used for the control treatment. Images were captured at 3-4 h post treatment. Mep1-GFP fluorescence showed accumulation within invasive hyphae and particularly in the BIC-associated cell **(E)** Micrographs of *M. oryzae* expressing Mep2-GFP and Bas4-mCherry during biotrophic growth on epidermal rice cells. BFA treatment was used to look at secretion of Mep2-GFP and Bas4-mCherry. Mep2-GFP fluorescence accumulated in the BIC in the presence or absence of BFA. By contrast, Bas4-mCherry fluorescence accumulated inside invasive hyphae. Scale bars = 10 µm.

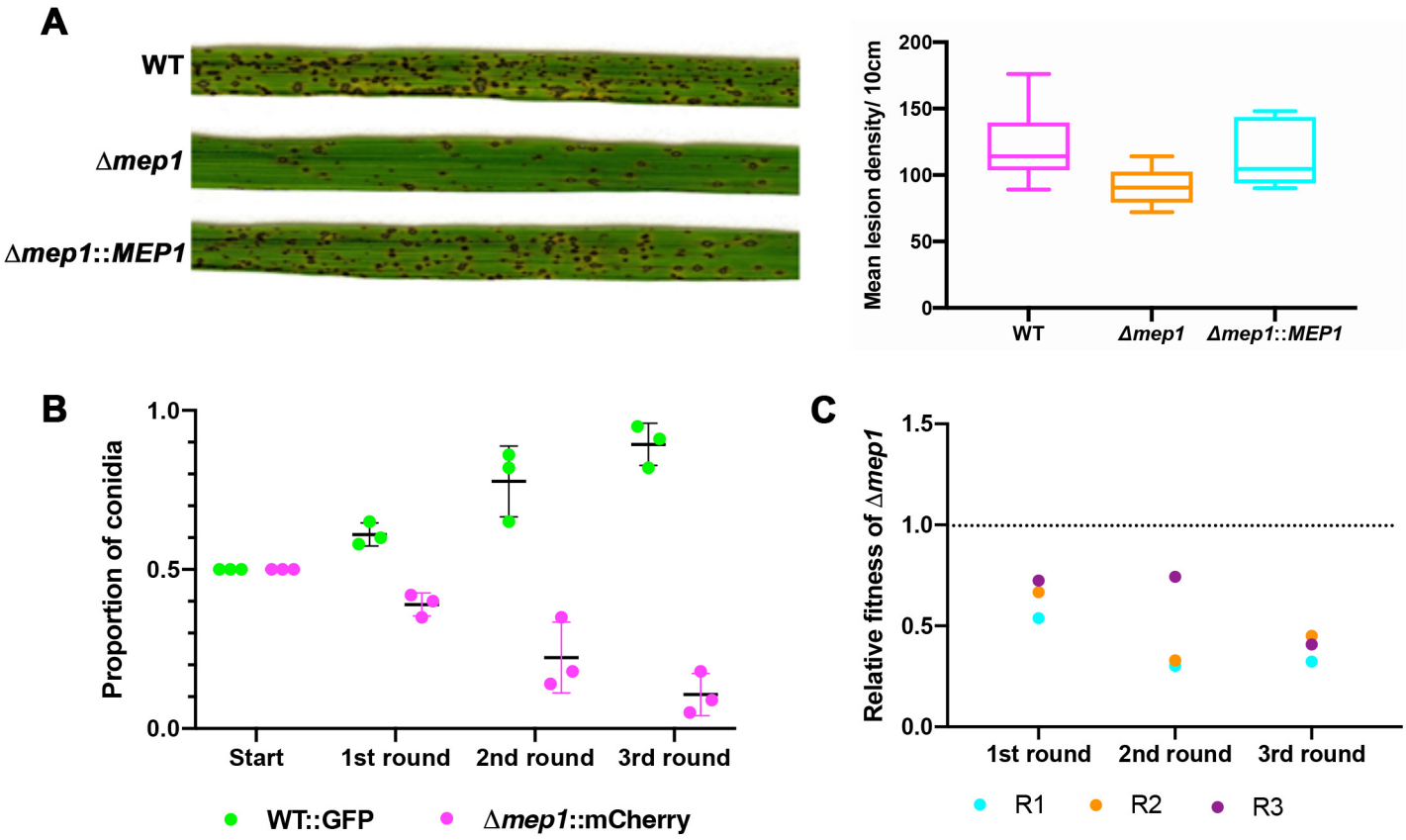

Figure 9. Mep1 contributes to pathogen fitness during plant infection.

(A) Conidial suspensions of equal concentration ($5x10^4$ spores mL^{-1}) from *M. oryzae* Guy11 or Δ*mep1* mutants were used to inoculate 21-day-old seedlings of the blast susceptible cultivar CO-39, and disease symptoms recorded after 5 dpi. The box plot shows the mean lesion density of seedlings infected with Guy11 and the Δ*mep1* mutant per unit area. (**B**) A relative fitness assay was carried out by mixing conidia in equal amounts (1:1) from Guy11 expressing GFP and Δ*mep1* mutant expressing mCherry. Spores were collected from disease lesions and used to inoculate new seedlings in the recovered proportions. A dot plot showing the proportion of WT::GFP and the Δ*mep1*::mCherry conidia recovered from each generation is shown. The Δ*mep1*::mCherry mutant was driven to near extinction in three generations **(C)** Relative fitness was calculated using the calculation $x_2(1-x_1)$ / x_1 $(1-x_2)$, where x1 is the initial frequency of Δ*mep1*::mCherry conidia and x2 the final frequency.

Figure 9

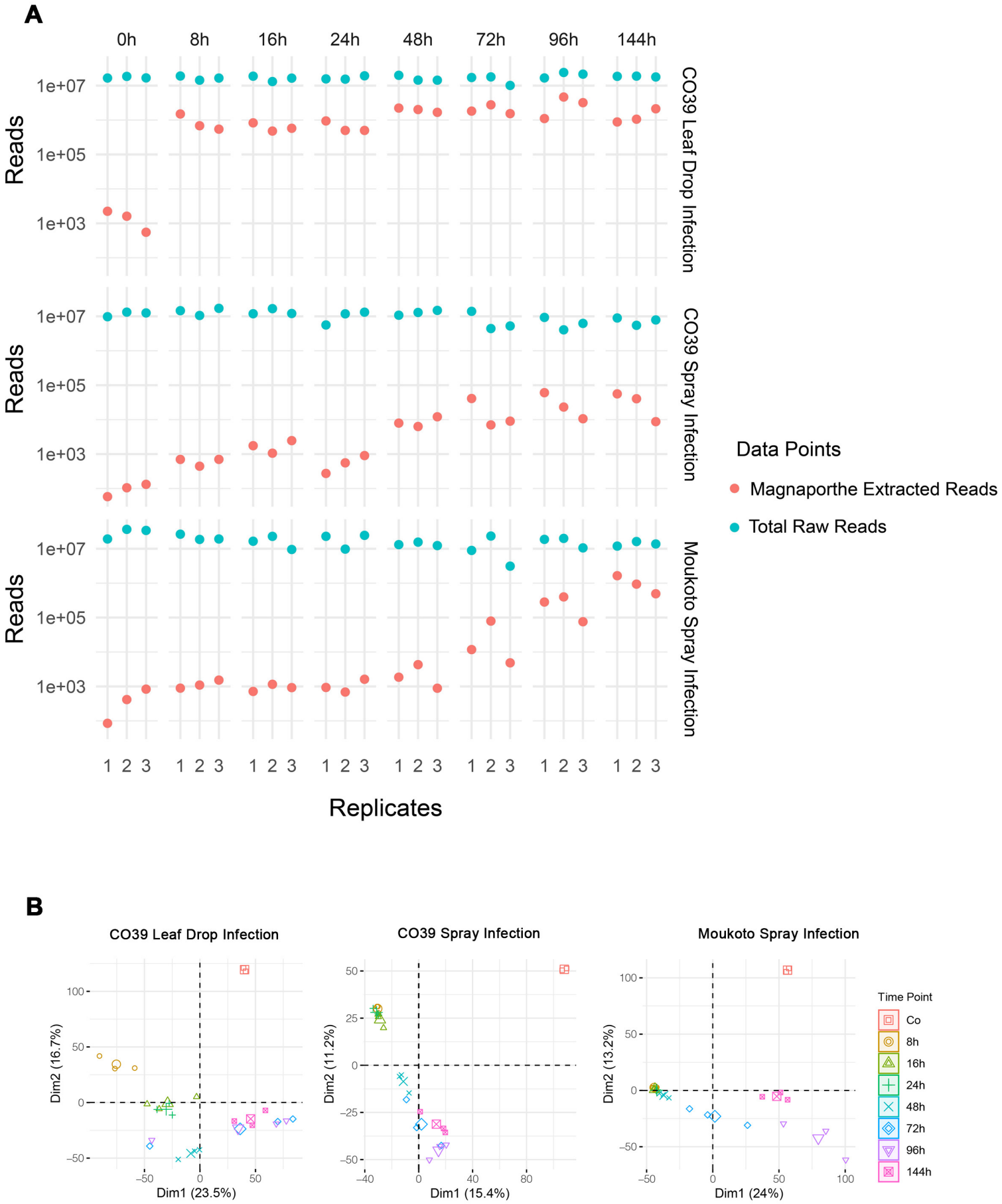

Supplemental Figure 1

Supplemental Figure 1. Assessment of the RNA-Seq Data Set of *M.oryzae* during rice infection.

(A) Graph showing comparison of total raw reads and *M. oryzae* extracted reads from each inoculation method and cultivar-strain combination. **(B)** Principal Component Analysis (PCA) of fungal reads from the three infection datasets; CO39 Leaf Drop Infection, CO39 Spray Infection and Moukoto Spray Infection. Three independent biological replicates were generated for each time point 0h, 8h 16h, 24h, 48h, 72h, 96h, 144h.

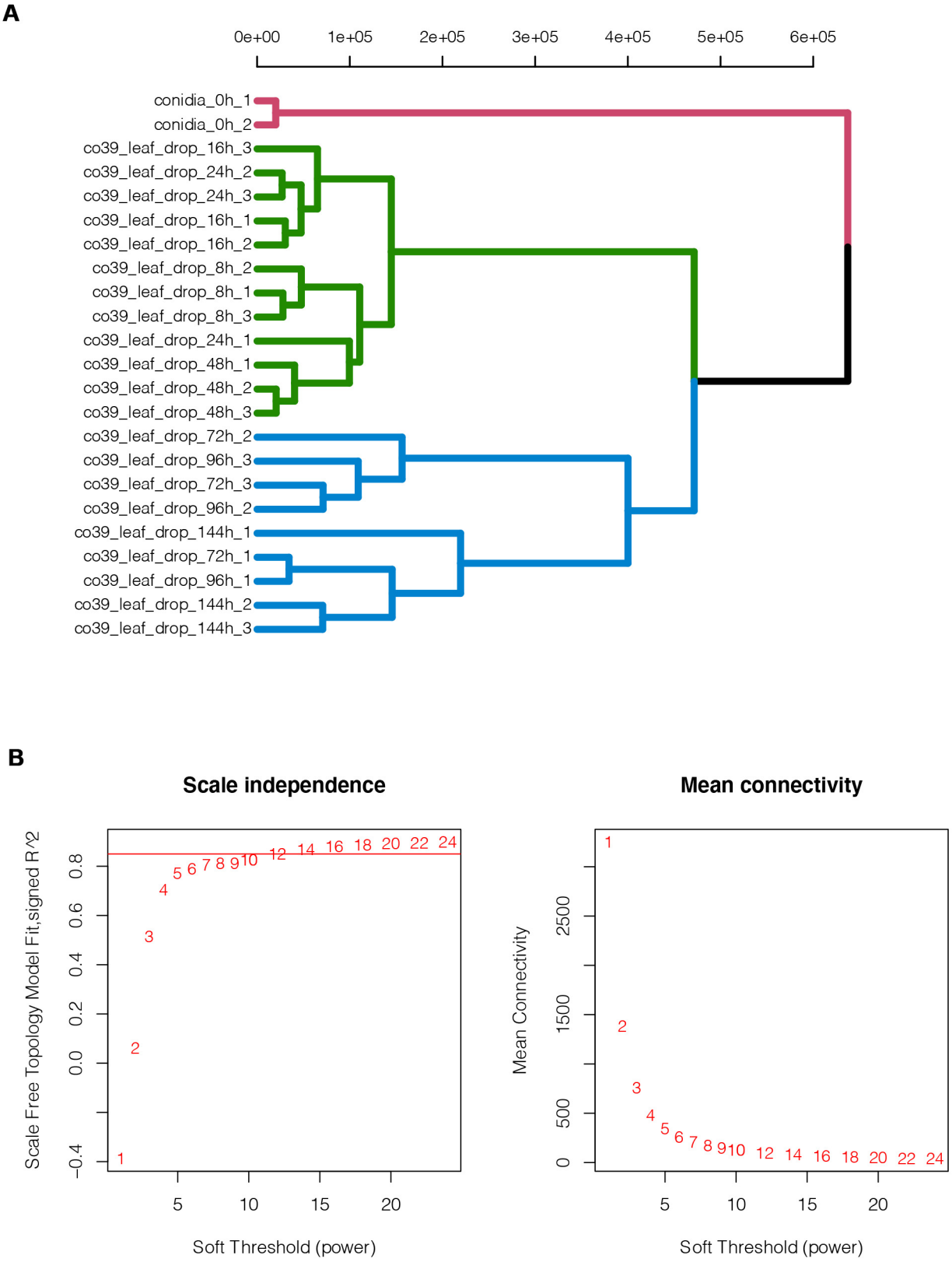

Supplemental Figure 2

Supplemental Figure 2. Sample clustering and the soft power analysis for WGCNA analysis.

(A) Sample cluster analysis of all infected rice RNA-seq data sets. Conidia RNA-seq data sets are significantly different to those from the infection time course (shown in red). RNA-Seq Data Sets from early time points of infection, 8h, 16h, 24h and 48h, all clustered into a single clade (shown in green) while later time points from 72h, 96h and 144h grouped together into a third clade (shown in blue). **(B)** Soft power analysis to obtain the optimised power number for WGCNA analysis. The cut-off threshold indicated that the total RNA-Seq Data Set from infected rice samples could be divided into 10 co-expression modules.

Supplemental Figure 3

Supplemental Figure 3. Biological process enrichment analysis of *M. oryzae* genes differentially expressed during plant infection.

M. oryzae differential gene expression during plant infection was evaluated by comparison to expression in conidial mRNA using Sleuth (Pimentel et al., 2017), identifying genes showing a log2 fold change > 1, and P-adj < 0.05. Diagram shows up-regulated gene functions (top and marked 'up' in legend) and down-regulated gene functions (bottom and marked 'd' in legend) during a time series of *M. oryzae* infection based on leaf drop inoculation of rice cultivar CO-39 by strain Guy11. GO enrichment analysis was carried out using the R package "mogo" (https://github.com/TeamMacLean/mogo).

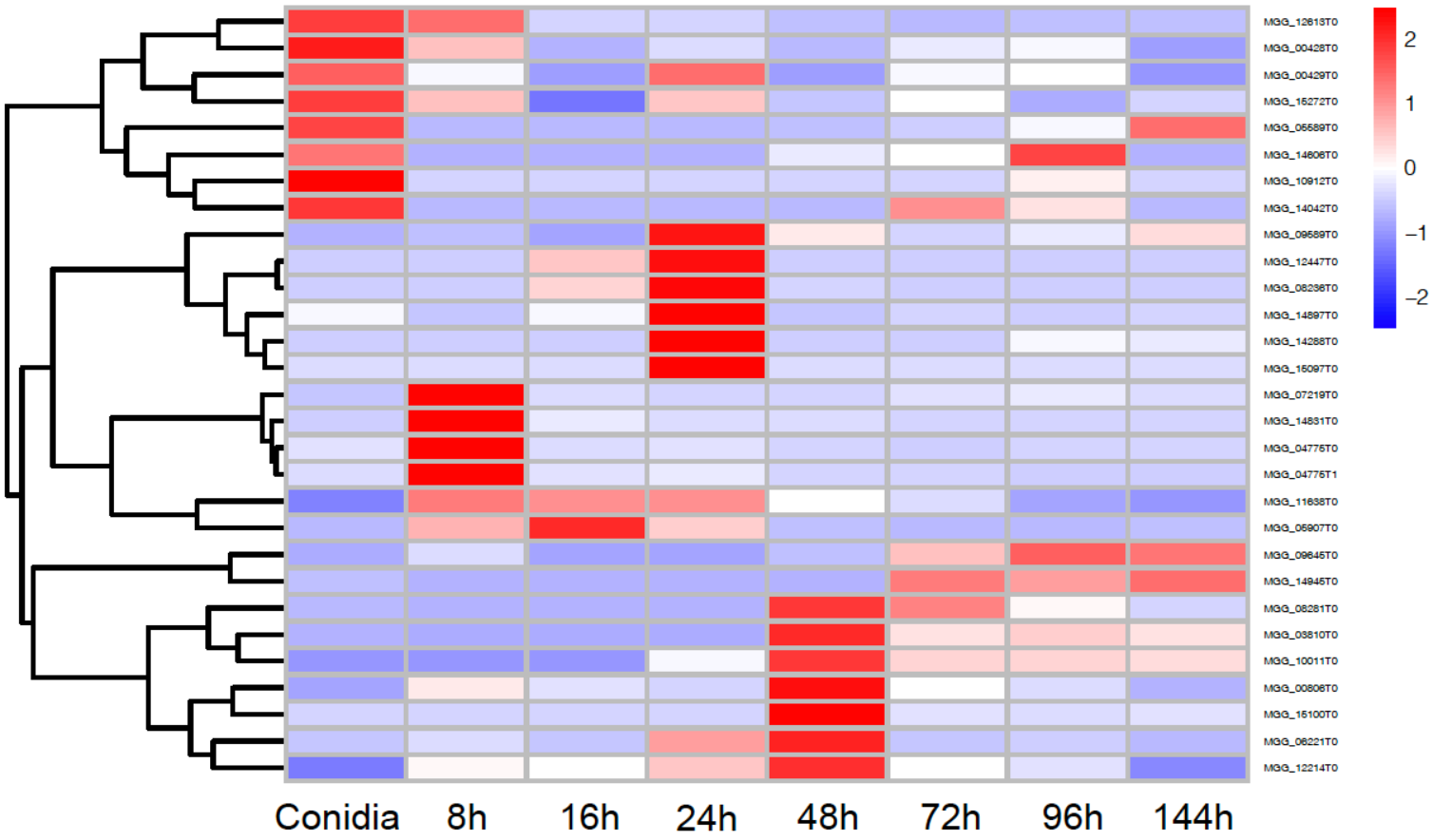

Supplemental Figure 4. Hierarchical clustering of the expression of *M. oryzae* genes predicted to encode polyketide synthase during plant infection.

Heat map showing the temporal pattern of the relative transcript abundance of 29 genes predicted to encode polyketide synthase during plant infection. Genome accession numbers are provided for each gene. Each gene is scaled to the mean TPM (transcript per kilobase million) value across all stages of infection-related-development and plant infection, with fold differences indicated according to the key.

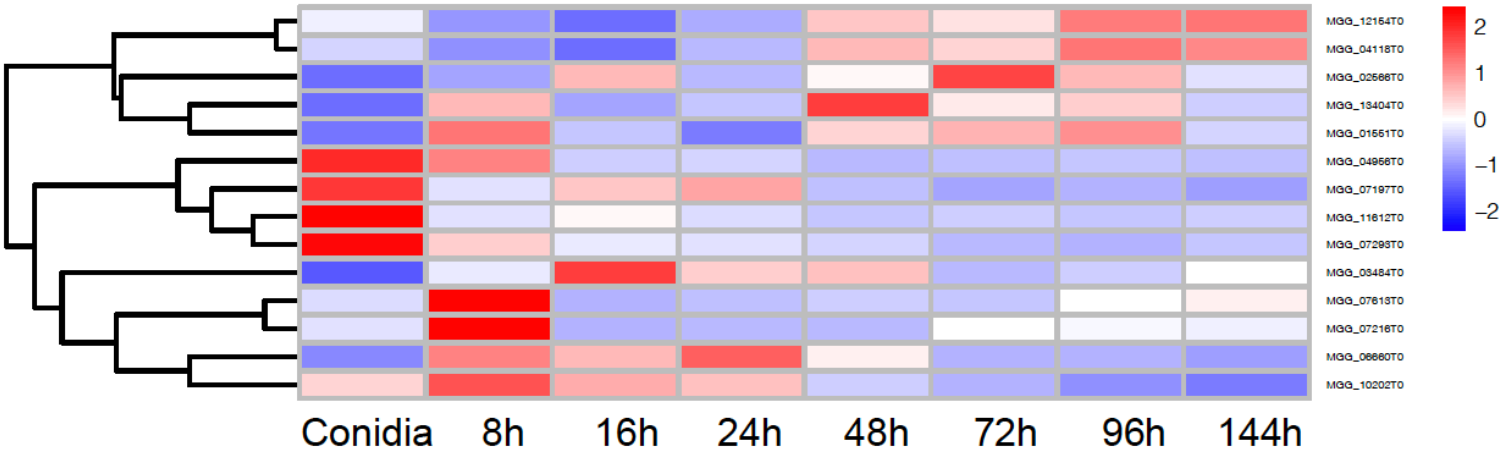

Supplemental Figure 5. Hierarchical clustering of *M. oryzae* genes predicted to encode fatty acid synthases during plant infection.

Heat map showing the temporal pattern of the relative transcript abundance of 14 genes predicted to encode fatty acid synthases during rice infection. TPM (transcript per kilobase million) value across all stages of infection-related-development and plant infection, with fold differences indicated according to the key.

Supplemental Figure 5

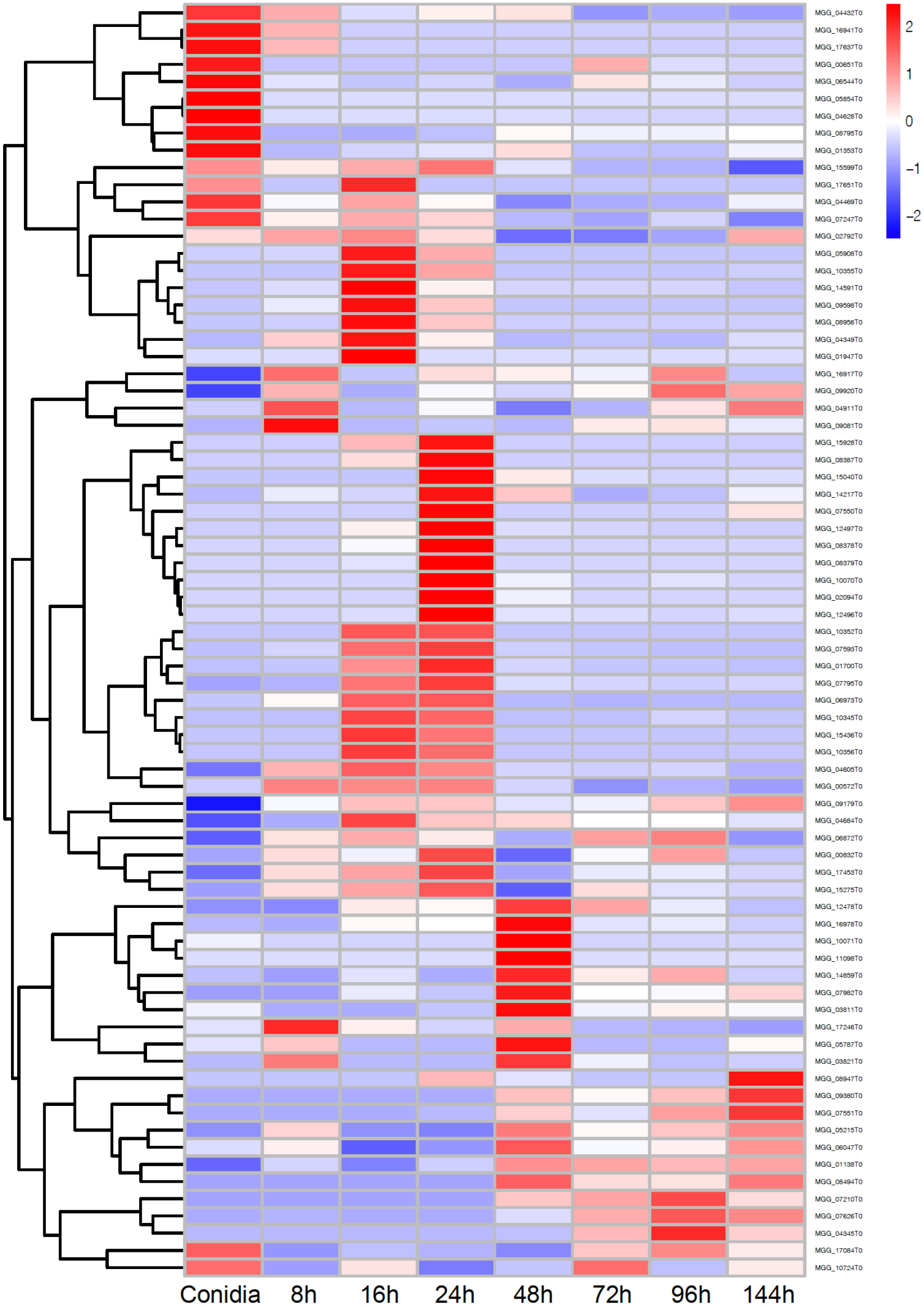

Supplemental Figure 6

Supplemental Figure 6. Hierarchical clustering of *M. oryzae* genes predicted to encode cytochrome P450 mono-oxygenases during plant infection.

Heat map showing the temporal pattern of the relative transcript abundance of 75 genes encoding cytochrome P450 mono-oxygenases during rice infection. TPM (transcript per kilobase million) value across all stages of infection-related-development and plant infection, with fold differences indicated according to the key.

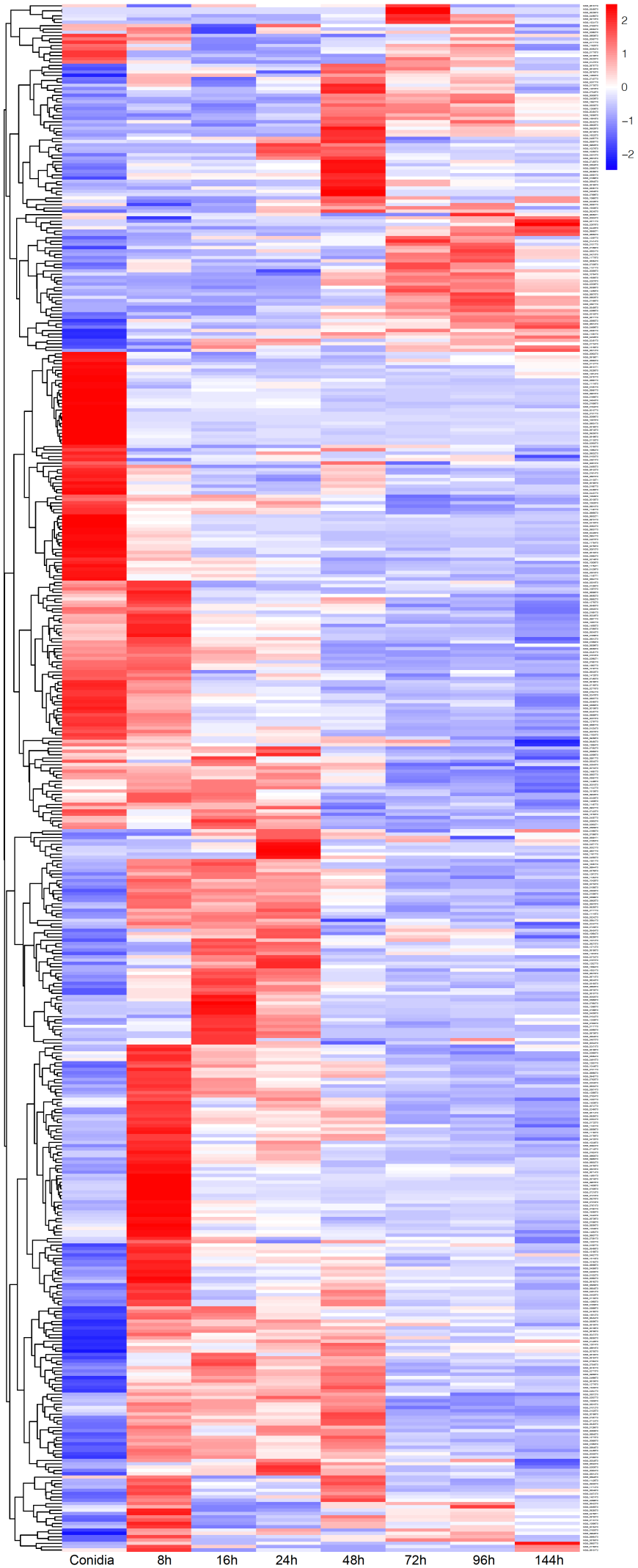

Supplemental Figure 7

Supplemental Figure 7. Hierarchical clustering of *M. oryzae* genes predicted to encode transcription factors during plant infection.

Heat map showing the temporal pattern of the relative transcript abundance of 495 genes predicted to encode transcription factors during rice infection. All putative transcription factors were extracted from the Fungal Transcription Factor Database (http://ftfd.snu.ac.kr/magnaporthe), a platform designed to identify transcription factor-encoding genes in fungi. TPM (transcript per kilobase million) value across all stages of infection-related-development and plant infection, with fold differences indicated according to the key.

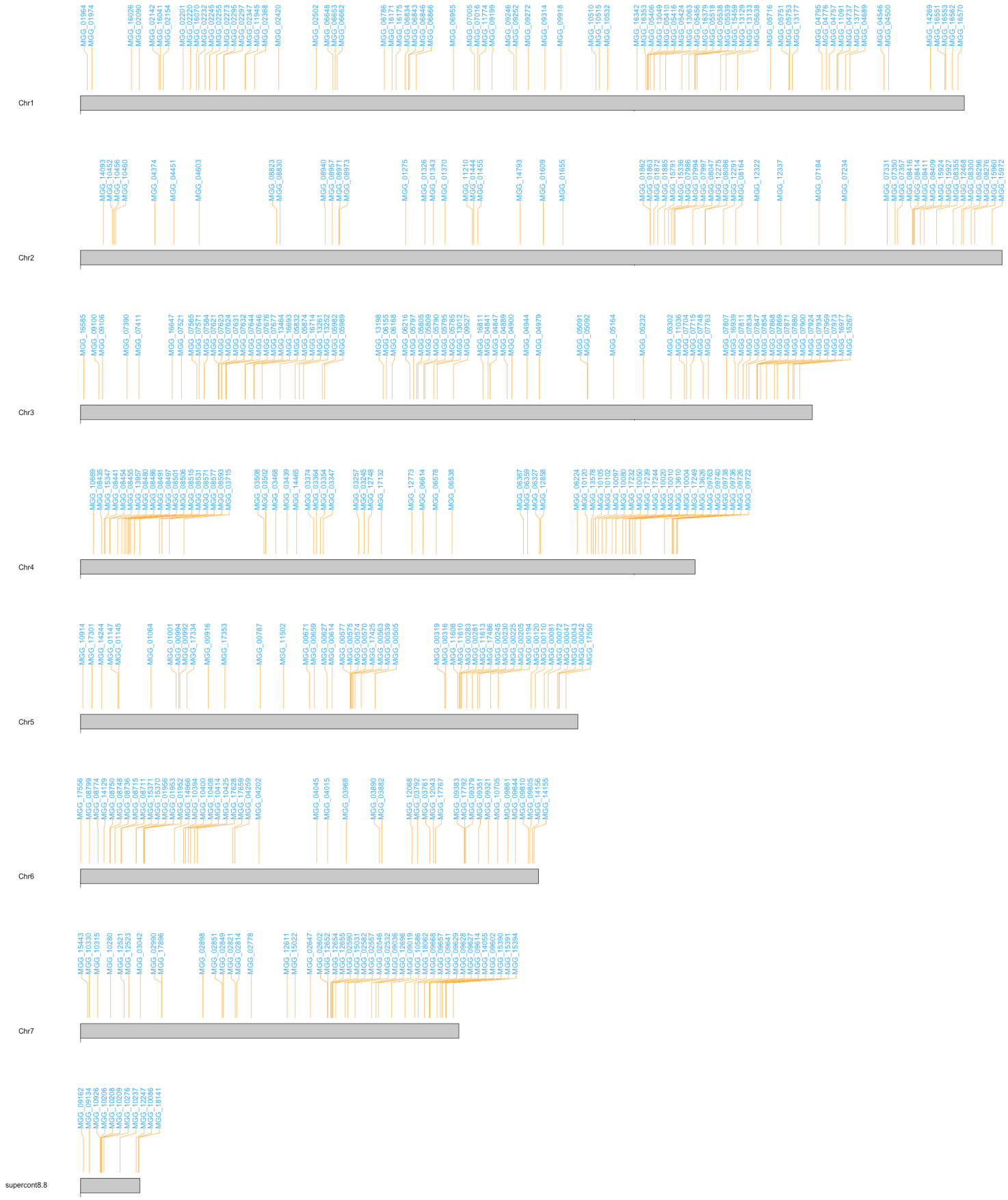

Supplemental Figure 8. Visualisation of the distribution of 863 *MEP* gene loci on the seven chromosomes of *M. oryzae*.

Genetic map showing the order and relative distribution of *MEP* loci among the seven chromosomes of *M. oryzae*. The positions were determined by analysis against the 70-15 reference genome (Dean et al., 2005).

Supplemental Figure 8

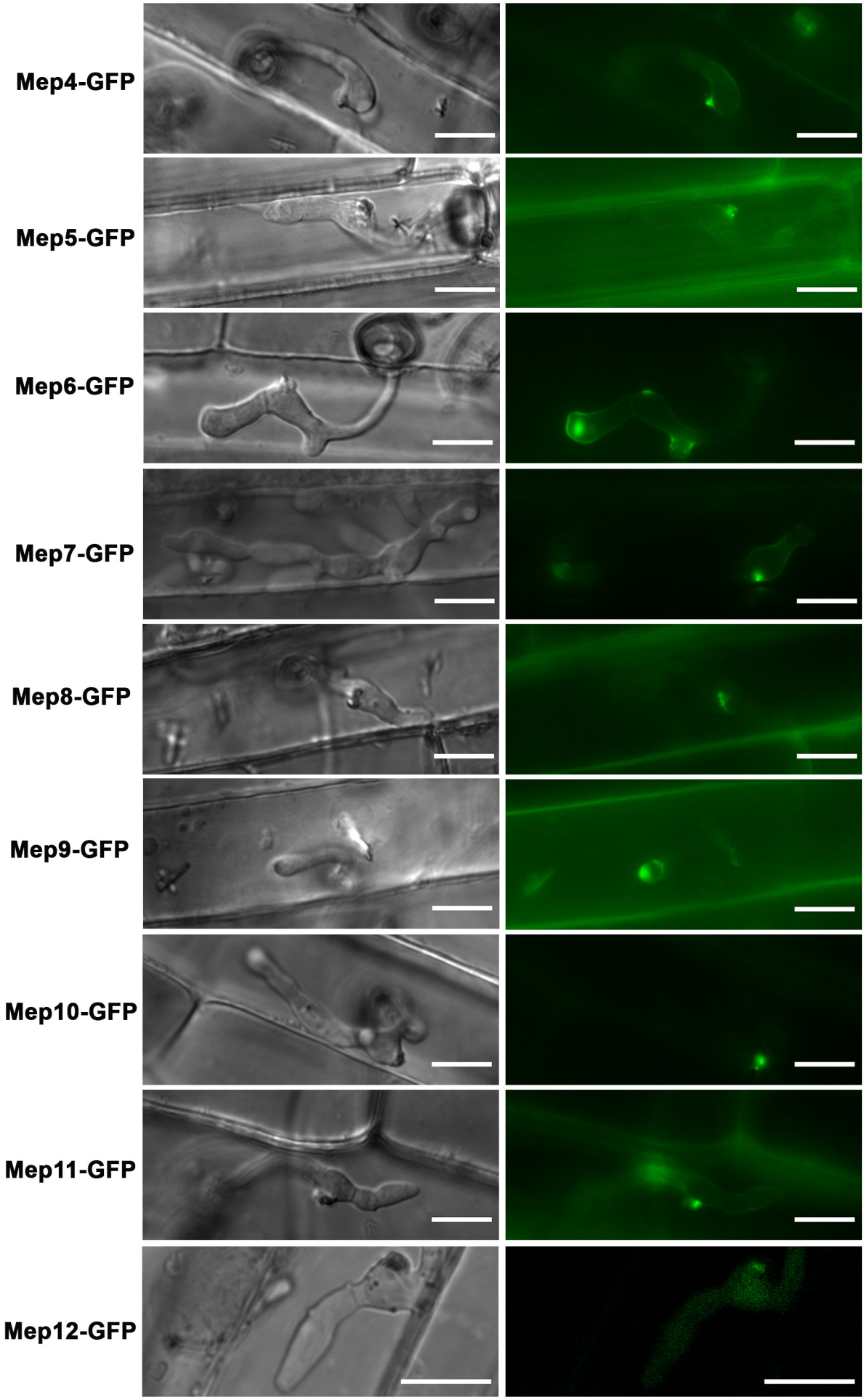

Supplemental Figure 9

Supplemental Figure 9. Cytoplasmically targeted Meps consistently localise to the BIC during biotrophic invasive growth of *M. oryzae*.

Micrographs showing the localisation of Mep4, Mep5, Mep6, Mep7, Mep8, Mep9, Mep10, Mep11 and Mep12 which were all C-terminally tagged with GFP, transformed and expressed in Guy11 and used to carry out infections of rice leaf sheath of cultivar CO39. Laser confocal images were captured at 22-28 hpi. A single large fluorescent punctum, the BIC, was always observed in the initially invaded epidermal cell. Scale bars = 10 μm.

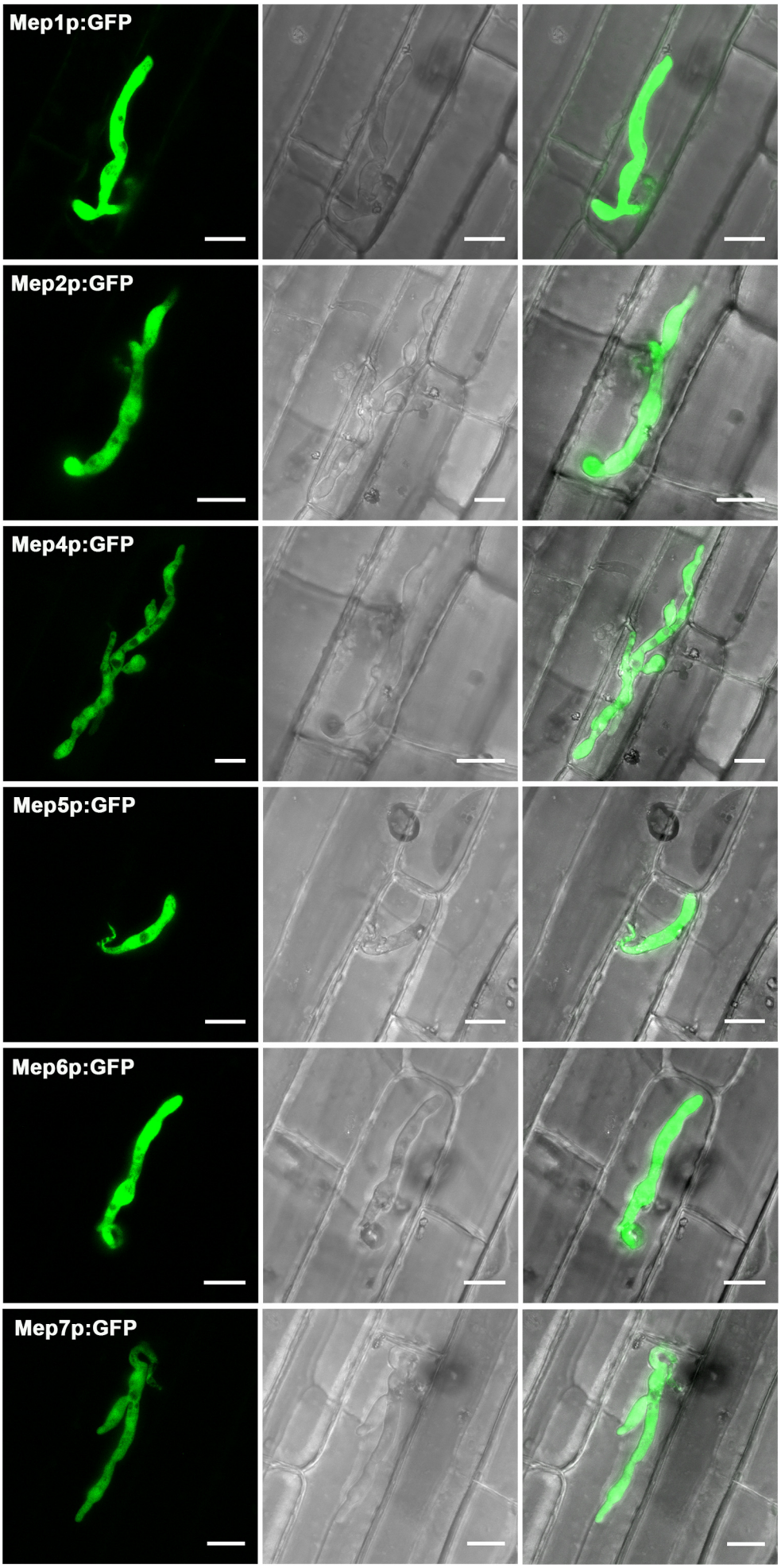

Supplemental Figure 10

Supplemental Figure 10. Assessment of the expression of Mep effector candidates during plant infection.

Micrographs showing the expression of cytoplasmic GFP driven by the promoters of Mep effector candidates during plant infection. Promoters of *MEP1, MEP2, MEP4, MEP5, MEP6* and *MEP7* were fused to GFP, transformed into Guy11 and single copy transformants selected. A strong fluorescence signal was specifically observed inside invasive hyphae during plant infection. Scale bars = 10 μm.

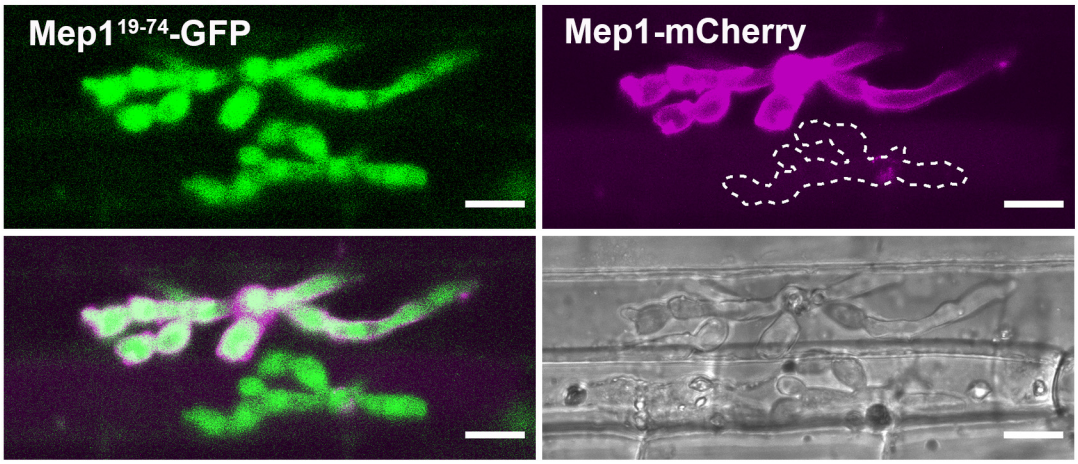

Supplemental Figure 11. Live-cell imaging of the secreted and non-secreted Mep1 protein variants during plant infection.

Micrographs showing invasive hyphae at two infection sites of *M. oryzae* Guy11 expressing Mep1$^{19-74}$-GFP and Mep1-mCherry. Two infection sites are present and can be observed by the GFP fluorescence signal from Mep1$^{19-74}$-GFP and by observation in the bright field channel. At one infection site, the green fluorescence from Mep1$^{19-74}$-GFP is uniformly enveloped by the magenta fluorescence from Mep1-mCherry. This is consistent with delivery of Mep1-mCherry into the apoplast between the fungal cell wall and extra-invasive hyphal membrane (EIHM). At the second infection site no Mep1-mCherry fluorescence could be observed. This suggests breakdown of the EIHM in the second infected cell in which Mep1-mCherry leaks into the whole cell, which loses viability. Laser confocal images were taken at 24 hpi. Scale bars = 10 um.

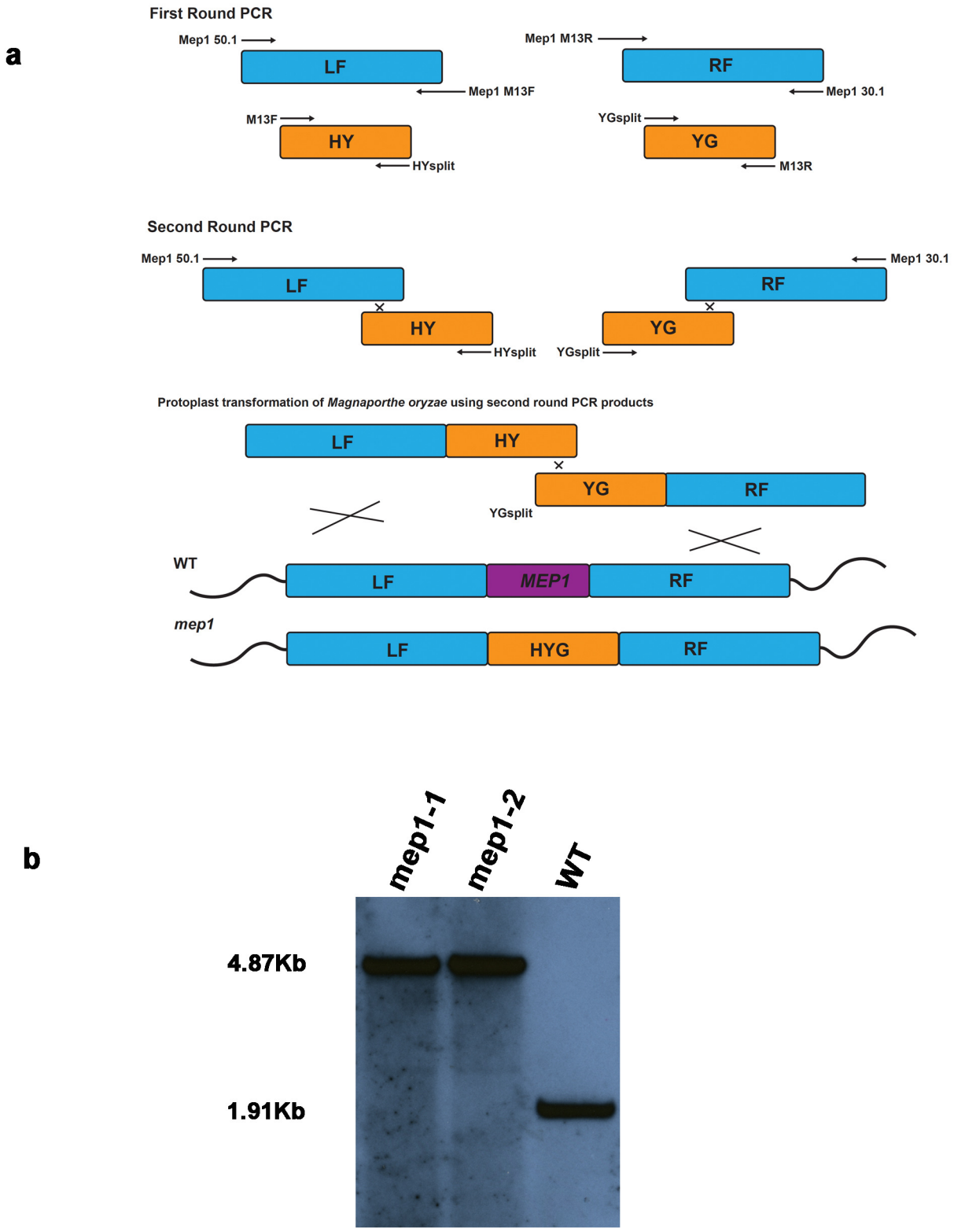

Supplemental Figure 12. Targeted *MEP1* gene deletion in the rice blast fungus *Magnaporthe oryzae*.

(A) Schematic representation of the *MEP1* gene deletion strategy using the split-marker strategy, as described in Methods. Two amplicons containing the left and right flanks of *MEP1* and each half of the hygromycin resistance gene cassette are used to transform Guy11. This results in three crossover events to generate a target gene replacement with re-synthesis of the whole hygromycin resistance cassette. **(B)** Southern blot to confirm targeted gene replacement of the *MEP1* gene. The same approach was used to generate gene replacement mutants for each *MEP* gene analysed in this study.

Supplemental Figure 12

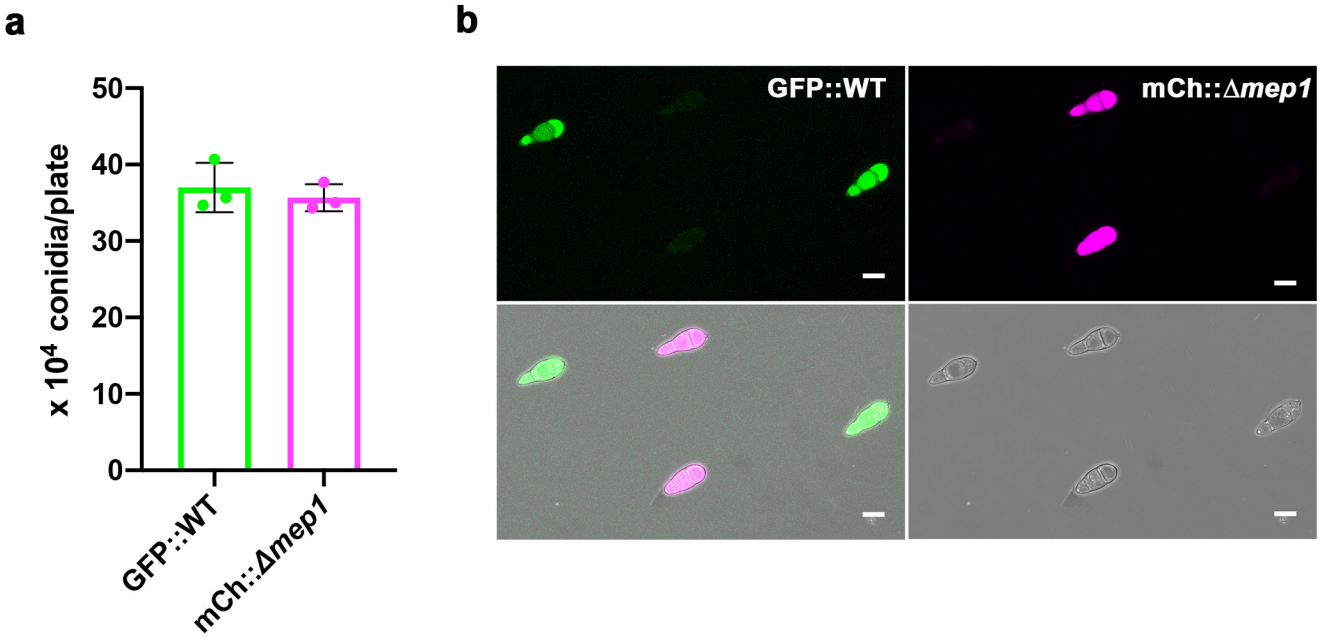

Supplemental Figure 13. Quantification of conidiogenesis from the Δ*mep1* mutant.

In order to be able to use a mixed infection fitness assay, it was essential to ensure that each *M. oryzae* strain sporulated with the same frequency **(A)** Conidia were collected from WT::TrpCp:GFP and Δ*mep1*::TrpCp:mCherry and counted using a haemocytometer. Conidiation was analysed by quantifying conidia harvested from 10 day-old CM plate cultures of *M. oryzae*. Bar charts show the mean and standard deviation. No significant difference ($P > 0.05$) in conidiation was observed in three biological replicates of the experiment. **(B)** Laser confocal micrographs showing conidia of WT::TrpCp:GFP and Δ*mep1*::TrpCP:mCherry, respectively.